Multiple Pulses in Nonlinear Optical Systems

by

Russell K. Jackson

M.S., University of North Carolina at Chapel Hill, 1997
B.S., Duke University, 1994

Thesis

Submitted in partial fulfillment of the requirements for
the degree of Doctor of Philosophy
in the Division of Applied Mathematics at Brown University

May 2003

Abstract of "Multiple Pulses in Nonlinear Optical Systems," by Russell K. Jackson, Ph.D., Brown University, May 2003

In the first part of this thesis, we consider a system of two Schrödinger equations coupled together through the nonlinearity; models of this sort have been developed to describe the effects of birefringence in an optical fiber as well as the incoherent interaction of two optical beams in a slab. Mathematically, localized pulses in a fiber and beams in a slab are considered as standing waves. Such waves are important as information carriers — and the profiles of these waves and their stability upon perturbation are of great interest. We describe a family of multi–component pulses, as well as multi–component N–pulses, that bifurcate from a simple one–component stationary wave as a system parameter is increased. We also develop numerical and analytical tools to analyze the stability of these waves. It is shown that the bifurcating multi–component pulses are stable for a range of parameters near the bifurcation point and a geometric mechanism is provided that can spur an eventual instability. A related criterion is used to show that all of the bifurcating multi–component N–pulses are unstable.

In the second part of this thesis, we consider a model for pulse propagation in the regime of strong dispersion management; this model takes the form of a Schrödinger equation with a nonlocal nonlinearity. We approximate and study dispersion managed solitons using their characterization as minima of an averaged variational principle. This approach helps to explain the persistence of the dispersion managed soliton in the regime of negative residual dispersion and the mechanism for its disappearance as the residual dispersion decreases further. We also decribe the discovery of a bisoliton that has implications for increased data transmission rates and more advanced coding schemes.

© Copyright

by

Russell K. Jackson

2003

This dissertation by Russell K. Jackson is accepted in its present form by
the Division of Applied Mathematics as satisfying the
dissertation requirement for the degree of
Doctor of Philosophy

Date_____ _____

Christopher K.R.T. Jones, Director

Recommended to the Graduate Council

Date_____ _____

Tobias Schäfer, Reader

Date_____ _____

Vadim Zharnitsky, Reader

Approved by the Graduate Council

Date_____ _____

Peder J. Estrup

Dean of the Graduate School and Research

The Vita of Russell K. Jackson

Russell Kenneth Jackson was born on the 10th of September, 1972 in Washington, D.C. He grew up in the southeastern United States, eventually completing high school at the North Carolina School of Science and Mathematics in Durham, North Carolina. Upon graduation in 1990, he moved three blocks down the street to attend college at Duke University (Trinity College), supported by a North Carolina High School Mathematics Contest Scholarship. He graduated Magna Cum Laude in 1994, receiving a Bachelor of Science degree in Mathematics and a Julia Dale Prize for Excellence in Mathematics.

He began his graduate career, moving a full ten miles further to the Mathematics Department at the University of North Carolina, Chapel Hill. There he completed a Master's project titled "Iterated function systems and a measure on Julia sets," under the direction of Karl Petersen, and received a Master of Science degree in 1997.

In the Fall of 1997, he finally left his hot and humid home and moved on to the cold northeast, arriving at Brown University's Division of Applied Mathematics. He began work on his doctoral research in 1998 and during the Summer of 2001 served as an intern in the Mathematical Sciences Division of Bell Laboratories, Lucent Technologies, under the supervision of Vadim Zharnitsky. He has been awarded a National Science Foundation Mathematical Sciences Postdoctoral Research Fellowship, and will begin a Research Instructorship at Boston University in the Fall of 2002.

Acknowledgments

My first and most heartfelt thanks go to my thesis advisor Chris Jones. His skillful guidance and persistent support have made this research work not only possible, but a true pleasure.

A special thanks goes also to the readers on my thesis committee, Tobias Schäfer and Vadim Zharnitsky; their insight and comments have been a great asset. I am also very grateful to the many others who have shared an interest in this work and have helped me to move forward: especially Shunsaku Nii, Todd Kapitula, Keith Promislow, Michael Weinstein, Björn Sandstede, Alice Yew and Alan Champneys.

And, of course, none of this would have been possible without the support and refreshing perspectives of my family and friends — most especially the love and good humor of my wife Froggi. This one's for you, my sunshine!

Contents

Acknowledgments **v**

I Pulses in Nonlinearly Coupled Schrödinger Equations **1**

1 Introduction **2**

2 On the existence of stationary waves **8**

2.1 A numerical investigation 17

2.2 An analytic study of alternating multipulses 29

2.3 Degeneracy of the multi–component pulse and Plücker coordinates 40

3 On the stability of stationary waves **50**

3.1 The Evans function 57

3.2 Numerical implementation 59

3.3 A motivating example 69

3.4 The single–component pulse $q_u(x)$ 79

3.5 The bifurcating pulse $q_{|0,i\rangle}(x)$. 84

3.6 N–pulses 100

II Pulses in the Gabitov–Turitsyn Equation **106**

4 Introduction **107**

5 Approximate pulses via a variational principle **111**

5.1 Governing equations and the numerical method 111

5.2 The dispersion managed soliton 118

5.3 The bisoliton 131

Part I

Pulses in Nonlinearly Coupled Schrödinger Equations

Chapter 1

Introduction

The nonlinear Schrödinger (NLS) equation has received significant attention as a model for pulse propagation in varying optical contexts. In optical fibers, it can describe the travel of a temporally localized pulse, possibly broadening due to chromatic dispersion. In a photorefractive slab, it describes a spatially localized beam, possibly broadening because of diffraction. Under the right circumstances, the broadening or widening seen in these cases can be counteracted exactly by the nonlinearity of the material properties. In certain cases, a solitary wave (called a *soliton*) is formed. For the cubic NLS equation, the evolution of such initial conditions can be calculated explicitly using the Inverse Scattering Transform and it can be shown that the wave is stable, see Zakharov and Shabat [1], Ablowitz and Segur [2].

Whether such a wave survives the inclusion of additional effects is always of great interest. Such additional terms might model higher order nonlinear effects such as the Raman effect, the Brillouin effect or self–steepening, saturation of the nonlinearity, attenuation and periodic amplification, birefringence, dispersion management or even random effects,

see for instance [3]. The first question in these cases is whether a solution like the original NLS soliton persists for the perturbed equations (and perhaps whether or not trains of such pulses also exist). If such solutions do exist, then the follow–up question of stability arises. Will initial conditions close to the pulse solution evolve similarly to the pulse or will small variations destroy the wave?

Another important extension is the inclusion of two or more fields interacting within the same medium. Birefringence (models accounting for the two polarizations of light simultaneously within a fiber) requires such a model. Other phenomena that force the consideration of multiple fields include systems incorporating Wavelength Division Multiplexing (WDM) or models for all–optical switching. In the first part of this thesis, we will consider a system of the form

$$\begin{array}{ccccccccc} iu_t & + & \frac{1}{2}u_{xx} & + & h_1(|u|^2,|w|^2)u & - & u & = & 0 \\ iw_t & + & \frac{1}{2}w_{xx} & + & h_2(|u|^2,|w|^2)w & - & rw & = & 0, \end{array} \tag{1.1}$$

where $0 < r < 1$ is a normalized propagation constant and $h_1(\cdot)$ and $h_2(\cdot)$ model the material properties. This general form for $h_1(\cdot)$ and $h_2(\cdot)$ encompasses models for several different phenomena. For example, Haelterman and Sheppard's model [4] for birefringence in optical fibers can be written in this form; as well as Ostrovskaya and Kivshar's model [5] for incoherent beam interaction in a biased photorefractive crystal. We denote the evolution variable by "t", although depending on the model, this variable may not actually be time.

Stationary waves of this system are real–valued, pulse–like solutions that do not vary with t. As such, they may be considered as homoclinic orbits – nontrivial intersections

between the global stable and unstable manifolds of the origin – in a system of ordinary differential equations given by

$$\begin{array}{rcrcrcl} \frac{1}{2}u_{xx} & + & h_1(|u|^2,|w|^2)u & - & u & = & 0 \\ \frac{1}{2}w_{xx} & + & h_2(|u|^2,|w|^2)w & - & rw & = & 0 \end{array} \tag{1.2}$$

which may also be written as a four–dimensional first–order system. There are various stationary waves present in this system, depending upon the parameter r. For any value of $0 < r < 1$ there are two elementary solutions: a fast solution $q_u(x) = (U(x), 0)$ and a slow solution $q_w(x) = (0, W(x))$ (which depends upon the parameter r). We call the solution $q_u(x)$ "fast" for two reasons: first, the propagation constant 1 is larger than the constant r of the other solution, and second, the tails decay to 0 at a faster rate than those of the "slow" solution. Depending upon the peculiarities of the phase space, we might expect other more complicated solutions to be found nearby for various special values of r. For instance, when $r = 0$, the slow pulse ceases to exist and the origin has a pair of zero eigenvalues. This is one potential bifurcation value. At the other extreme, when $r = 1$, the problem displays a resonance in which all of the eigenvalues at the origin have the same magnitude. This is a second possible bifurcation value, and has been studied by Yew, Sandstede and Jones [6]. Slightly more subtle is the possibility of intermediate bifurcation values: parameters r^* at which the fast stationary wave solution $q_u(x)$ is *degenerate*, i.e., the global stable and unstable manifolds of the origin are tangent to one another along the pulse. This is the scenario that we will consider in the first part of this thesis.

We use a simple shooting method for various values of the parameter r to approximate pulses in the above equations. Numerically, we see a rich variety of stationary waves in

this system. Nearby the parameters r^* mentioned above, we see multi–component pulses with a small second component (that looks like a guided mode of the first component) bifurcating from $q_u(x)$. Additionally, we also see families of multipulses that look like widely spaced concatenated copies of the bifurcating multi–component pulses. With these numerically generated pulses in mind, we give a proof of the existence of alternating N–pulses for $r^* < r < 1$, where r^* is any point of degeneracy as described above, under fairly general conditions.

One reason these multi–component solutions are of such great interest is that they appear to be stable for a range of parameters near r^*, see Ostrovskaya et al. [7]. As such, this provides the possibility of stable pulses that have multiple peaks in their intensity profile. It had long been believed that all such optical pulses would prove to be unstable.

We use a numerical implementation of the Evans function to investigate the location of eigenvalues for these pulses. Indeed we verify the numerical result of Ostrovskaya et al. that the multi–component solitons have spectrum lying entirely on the imaginary axis for a range of the parameter r beyond the bifurcation point r^*.

As r increases, Ostrovskaya et al. [7] observe a pair of eigenvalues for the multi–component pulse that bifurcate from the end of the essential spectrum into the gap on the imaginary axis, eventually passing through the origin and onto the real axis, at which point they generate an instability. In one case, Ostrovskaya et al. predict the onset of this instability using the Vakhitov–Kolokolov stability criterion (also called the Weinstein criterion [8]). However, other pulses show instabilities that are not predicted by this condition. A primary goal of this thesis is to understand the origin of these eigenvalues and the mechanism by which they generate this delayed instability.

To this end, we will first consider a toy problem in which a series of eigenvalues bifurcate from the branch point of the essential spectrum as a parameter is changed. Such a problem is

$$Y' = \left(\begin{bmatrix} 0 & 1 \\ \lambda & 0 \end{bmatrix} + \begin{bmatrix} 0 & 0 \\ \chi_{[-\mu,0]}(x) & 0 \end{bmatrix} \right) Y. \tag{1.3}$$

For this simple problem, we can compute the Evans function $E_\mu(\lambda)$ explicitly and can even continue this function across the essential spectrum to locate zeros of an extended Evans function. In fact, we can extend the Evans function to an analytic function on a two sheeted Riemann surface. This allows us to pinpoint not only eigenvalues, but the location of potential eigenvalues which are seen as zeros of the extended Evans function on a two–sheeted Riemann surface. Of particular note is that the eigenvalues that eventually emerge through the branch points of the essential spectrum in this example are not originally embedded within the essential spectrum, but are zeros of the extended Evans function on the second Riemann sheet. Indeed, we see an infinite family of these zeros and observe the mechanism by which they may become eigenvalues for increasing μ.

The eigenvalue problem for a standing wave of equation (1.2) with respect to the full coupled PDE (1.1) is, of course, much more complicated than the toy problem above. However, for the fast elementary solution $(U(x), 0)$, the eigenvalue problem decouples into two simpler problems: one is a one–dimensional nonlinear Schrödinger equation – for usual functions $h_1(\cdot)$ the spectrum of this operator should be well understood; the second is an eigenvalue problem which can be reduced to a Sturm–Liouville problem much like the toy problem (1.3), except with the fast pulse $U(x)$ itself as potential. Thus we can isolate

eigenvalues (and potential eigenvalues) at a bifurcation point $r = r^*$. We then show the following as we follow the bifurcating multi–component pulse for increasing r to better understand the mechanism for instability:

1. The bifurcating multi–component pulse cannot have any positive real eigenvalues for some range of the parameter r above r^*.

2. The multi–component pulse itself may pass through a degeneracy as r is increased further. This can be detected using the Plücker coordinates to follow the tangent spaces of the stable and unstable manifolds in an auxiliary system.

3. Using the numerical Evans function, we verify that the onset of instability of the higher order mode in Ostrovskaya and Kivshar's problem corresponds to the moment of degeneracy of the pulse.

4. Using the Maslov index and an instability criterion as in Jones [9] or Grillakis [10], we relate the winding of the tangent space of the stable manifold of the pulse to the number of positive eigenvalues on the real axis. In this context, it is clear that the passage through degeneracy changes the Maslov index of the pulse and therefore changes the number of eigenvalues expected on the positive real axis. Additionally, this criterion allows us to conclude that all true N–pulses accompanying the bifurcation are unstable.

In this way we have tied the stability characteristics of the multi–component pulse to the topological properties of the pulse itself. This should go a long way toward demystifying a mechanism for the unexpected delayed instability of these multi–component pulses.

Chapter 2

On the existence of stationary waves

In models of physical phenomena, clues concerning the evolution of an initial state can be gleaned from the identification of coherent structures within that system — structures that either serve to organize the overall flow or contain information about the asymptotic behavior of typical orbits.

In systems modeled by partial differential equations (PDEs), these structures will often be nonlinear waves. As individual solutions (or families of solutions) that never change their shape and propagate in a fixed direction, these nonlinear waves serve as information carriers in a system. They provide permanent structures in the phase space and may evolve simply by spinning (standing waves), by translating in a fixed direction (traveling waves) or even by never moving at all (stationary waves). The importance of these waves in physical systems is often a function of their stability; how does a wave behave when a small

perturbation is introduced either to the initial data or to the governing equations? Waves that are not stable in a mathematical sense will not be realizable in a physical system, as imperfections in the system may destroy the wave. The fundamental mathematical challenge is then to develop techniques to find these nonlinear waves and determine their stability.

Complicated physical systems are often governed by multiple evolution equations coupled together. These higher dimensional systems pose problems which do not arise in simpler low dimensional models, where analysis can often be reduced to flow on an annulus or a Möbius band, see Sandstede [11] or Chow, Liu and Yi [12]. In this section, we identify and analyze a particular bifurcation occurring in nonlinearly coupled Schrödinger equations which leads to multi–component and multi–hump solutions.

The nonlinear Schrödinger equation provides a model for many different phenomena in the field of optics. It describes temporally localized pulses that serve as information carriers sending streams of zeros and ones down a fiber. It also models the spatially localized beams in a photorefractive slab that provide a possible method for realizing all–optical switching. When more than one field is present, for instance the two copropagating polarizations present in birefringent fibers or two incoherent beams in a slab, the model will take the form of a system of coupled Schrödinger equations.

The system.

We consider the following system:

$$\begin{array}{ccccccccc} iu_t & + & \frac{1}{2}u_{xx} & + & h_1(|u|^2,|w|^2)u & - & u & = & 0 \\ iw_t & + & \frac{1}{2}w_{xx} & + & h_2(|u|^2,|w|^2)w & - & rw & = & 0, \end{array}$$

where $0 \leq r \leq 1$ is a normalized propagation constant and h_1 and h_2 describe the material properties, which depend upon the situation being modeled. In the models we will consider, we assume that the material properties vary only through the intensity of the fields and the coupling between the fields is strictly through the nonlinear terms, hence we write the nonlinear terms as $h_1(|u|^2, |w|^2)u$ and $h_2(|u|^2, |w|^2)w$. Moreover, we assume that these equations have a Hamiltonian structure, and thus we could write them as

$$\begin{aligned} h_1(|u|^2, |w|^2)u &= \partial H/\partial u \\ h_2(|u|^2, |w|^2)w &= \partial H/\partial w. \end{aligned}$$

Two important models that display this structure can be found in

1. Haeltermann and Sheppard [4], where

$$H = \frac{1-B}{8}u^4 + \frac{1+B}{4}u^2w^2 + \frac{1-B}{8}w^4, \qquad \text{and}$$

2. Kivshar and Ostrovskaya [5], where

$$H = \frac{1}{S^2}\left(-\ln(1 + S(u^2 + w^2)) + S(u^2 + w^2)\right).$$

A standing wave is a real–valued solution of a PDE, decaying as $x \to \pm\infty$, that is independent of t. As such, a standing wave can be interpreted as a homoclinic orbit of

the following system of coupled ordinary differential equations:

$$\begin{array}{rcrcrcl} \frac{1}{2}u_{xx} & + & h_1(|u|^2,|w|^2)u & - & u & = & 0 \\ \frac{1}{2}w_{xx} & + & h_2(|u|^2,|w|^2)w & - & rw & = & 0. \end{array}$$

which we further write as the four dimensional first order system

$$\begin{array}{rcrcr} u' & = & p_u & & \\ w' & = & p_w & & \\ p_u' & = & -2h_1(|u|^2,|w|^2)u & + & 2u \\ p_w' & = & -2h_2(|u|^2,|w|^2)w & + & 2rw. \end{array} \tag{2.1}$$

For convenience, we sometimes abbreviate this system as simply

$$v' = f(v)$$

where $v \in \mathbf{R}^4$ and $f : \mathbf{R}^4 \to \mathbf{R}^4$.

Properties of the ODE.

The assumptions above lead to several nice properties of the ordinary differential equations found in equation (2.1). We will list these properties here.

Property 1. The system (2.1) is Hamiltonian, i.e., there is a function $H(u, w, p_u, p_w)$

such that

$$\begin{aligned} u' &= -\frac{\partial H}{\partial p_u} \\ w' &= -\frac{\partial H}{\partial p_w} \\ p_u' &= \frac{\partial H}{\partial u} \\ p_w' &= \frac{\partial H}{\partial w}. \end{aligned}$$

Property 2. The system (2.1) is time-reversible, i.e., there exists an involution $R : \mathbf{R}^4 \to \mathbf{R}^4$ with $R^2 = I$ such that $f(R(u, w, p_u, p_w)) = -R(f(u, w, p_u, p_w))$. In particular, R acts as $R(u, w, p_u, p_w) = (u, w, -p_u, -p_w)$.

Property 3. There are additional symmetries S_1 and S_2 such that $f(S_i(u, w, p_u, p_w)) = S_i f(u, w, p_u, p_w)$. These are $S_1(u, w, p_u, p_w) = (-u, w, -p_u, p_w)$ and $S_2(u, w, p_u, p_w) = (u, -w, p_u, -p_w)$.

It follows from Property 3 that the two–dimensional subspaces $U = \{(u, w, p_u, p_w) | w = p_w = 0\}$ and $W = \{(u, w, p_u, p_w) | u = p_u = 0\}$ are invariant. These are the subspaces corresponding to one of the two fields being identically zero, in which case the system reduces to a simple Hamiltonian vector field in a plane. In the subspace U, there is a symmetric pair of homoclinic orbits: we call the solution with positive u–part $q_u(x)$; the other solution is then $S_1 q_u(x)$. Note that these solutions are independent of the parameter r. Likewise, when $r > 0$, there is a symmetric pair of homoclinic orbits in W that can be written as $q_w(x)$ and $S_2 q_w(x)$.

Here we also take note of several important properties of the solutions $q_u(x)$ and $S_1 q_u(x)$.

Property 4. The elementary pulses $q_u(x)$ and $S_1 q_u(x)$ in U are in orbit–flip configuration. That is, they approach the origin from a direction other than the one associated with the eigenvalues of smallest real part.

Property 5. Depending upon the functions h_1 and h_2, for particular values of the parameter r between 0 and 1, the pulses $q_u(x)$ and $S_1 q_u(x)$ in the subspace U may be degenerate, i.e., $\dim(T_{q_u(x)} W^u(0) \cap T_{q_u(x)} W^s(0)) > 1$.

Property 4 follows easily because the linearization of the vector field at the origin has eigenvalues $\{-1, -\sqrt{r}, \sqrt{r}, 1\}$ and the invariant subspace U is spanned by the eigenvectors associated with ± 1. Because Property 5 is a property of the tangent spaces about a pulse, such parameter values can be found by studying the linearization about either of the pulses $q_u(x)$ or $S_1 q_u(x)$ in question. We elaborate below.

Degeneracy and Sturm–Liouville.

We write the solution $q_u(x)$ in component form as $(U(x), 0, U'(x), 0)$. Linearizing equation (2.1) about the pulse $q_u(x)$ yields

$$\begin{aligned} u' &= p_u \\ w' &= p_w \\ p_u' &= 2(1 - h_1(U^2(x), 0) - 2U^2(x) D_1 h_1(U^2(x), 0))u \\ p_w' &= 2(r - h_2(U^2(x), 0))w. \end{aligned} \tag{2.2}$$

This decouples into the two smaller systems

$$\begin{cases} u' &= p_u \\ p_u' &= 2(1 - h_1(U^2(x), 0) - 2U^2(x) D_1 h_1(U^2(x), 0))u \end{cases} \tag{2.3}$$

$$\begin{cases} w' &= p_w \\ p_w' &= 2(r - h_2(U^2(x), 0))w. \end{cases} \tag{2.4}$$

The first system (2.3) captures the trivial intersection of the tangent spaces induced by the existence of a homoclinic orbit. This is seen as the bounded solution $(U'(x), 0, U''(x), 0)$. The degeneracy described in Property 5 can then be interpreted in terms of a simultaneous bounded solution of the second system (2.4). This is a Sturm–Liouville problem, the analysis of which is well known – for completeness and for comparison in later sections we include a geometric analysis here. We simplify the system (2.4) for consideration in two ways. First, since these equations are linear, we projectivize the flow, which allows us to consider an equivalent one dimensional problem. Second, since we are interested in the behavior of orbits as $x \to \pm\infty$, we compactify the phase space. In this way, the bounded solutions we seek can be considered as connecting orbits between the appropriate points on opposite ends of a cylinder. We projectivize the system by introducing the radial and angular variables

$$\begin{aligned} \rho^2 &= w^2 + p_w^2 \\ \theta &= \tan^{-1}\left(\tfrac{p_w}{w}\right). \end{aligned}$$

It is a simple exercise to show that this yields the equivalent system

$$\begin{aligned} \rho' &= \tfrac{1}{2}\,(1+2(r-h_2(U^2(x),0)))\ \sin(2\theta)\ \rho \\ \theta' &= 2\ (r-h_2(U^2(x),0))\ \cos^2(\theta)-\sin^2(\theta). \end{aligned} \tag{2.5}$$

Note especially that the equation for θ is independent of ρ. We can therefore consider the second equation of (2.5) as a flow on the real projective space $\mathbf{R}P^1 \times \mathbf{R}$.

Next, in order to clarify the asymptotic behavior, we use Terman's convention and set

$$x = \frac{1}{2\kappa}\ln\left(\frac{1+\tau}{1-\tau}\right)$$

where κ is chosen appropriately so that

$$U_c^2(\tau) = U^2\left(\frac{1}{2\kappa}\ln\left(\frac{1+\tau}{1-\tau}\right)\right)$$

can be smoothly extended from the open interval $(-1,1)$ to its closure. Hence we have

$$\begin{aligned} \theta' &= 2(r-h_2(U_c^2(\tau),0))\cos^2(\theta)\ -\ \sin^2(\theta) \\ \tau' &= \kappa(1-\tau^2) \end{aligned} \tag{2.6}$$

which is a flow on $\mathbf{R}P^1 \times [-1,1]$.

The spaces $\tau=-1$ and $\tau=+1$ are now invariant and carry the asymptotic flows. In these spaces we simply have

$$\begin{aligned} \theta' &= 2r\cos^2(\theta)-\sin^2(\theta) \\ \tau' &= 0. \end{aligned}$$

For $r > 0$, this equation has two fixed points: $\theta_+ = +\tan^{-1}(\sqrt{2r})$ and $\theta_- = -\tan^{-1}(\sqrt{2r})$. The unstable subspace in the original problem corresponds to the attracting fixed point in the projectivized problem $\theta = \theta_+$. The stable subspace corresponds to the repelling fixed point $\theta = \theta_-$. Solutions of the linearized equation (2.4) that decay as $x \to -\infty$ correspond to solutions of (2.6) that tend to $(\theta_+, -1) \in \mathbf{R}P^1 \times (-1, 1]$ as $x \to -\infty$. Likewise, solutions of the linearized equation (2.4) that decay as $x \to +\infty$ correspond to solutions of (2.6) that tend to $(\theta_-, +1) \in \mathbf{R}P^1 \times [-1, 1)$ as $x \to +\infty$. And hence a bounded solution of (2.4) corresponds to an orbit of (2.6) connecting $(\theta_+, -1)$ and $(\theta_-, +1)$.

We then have the following shooting problem. As $r > 0$ varies, we follow the solution that approaches $(\theta_+, -1)$ as $x \to -\infty$. This solution will wind around the cylinder for $\tau \in (-1, 1)$, and for particular values of r it may meet up exactly with $(\theta_-, +1)$ as $x \to +\infty$. We can count the number of these connecting values exactly by invoking a monotonicity argument. In particular, consider two solutions $\theta_{r_1}(x)$ and $\theta_{r_2}(x)$ which approach $(\theta_+, -1)$ as $x \to -\infty$ for different values of the parameter r. The following result can be deduced easily.

Lemma 2.1. For each x, if $r_1 < r_2$, then $\theta_{r_1}(x) < \theta_{r_2}(x)$.

Proof. First, since $\theta_+ = +\tan^{-1}(\sqrt{2r})$ and $\tan^{-1}(\cdot)$ is a monotonically increasing function, the result clearly follows for $x \to -\infty$. Second, we let $\alpha(x) = \theta_{r_1}(x) - \theta_{r_2}(x)$. Suppose that for some x that $\alpha(x) = 0$. At such a point we would have $\alpha'(x) = 2(r_1 - r_2) < 0$. Since $\alpha(-\infty) < 0$ and $\alpha'(x) < 0$ if $\alpha(x) = 0$, it follows that $\alpha(x) < 0$ for all x. In particular, $\theta_{r_1}(x) < \theta_{r_2}(x)$ for all x. $\square$

Also, for r large, there is no winding. In particular, we have the following lemma.

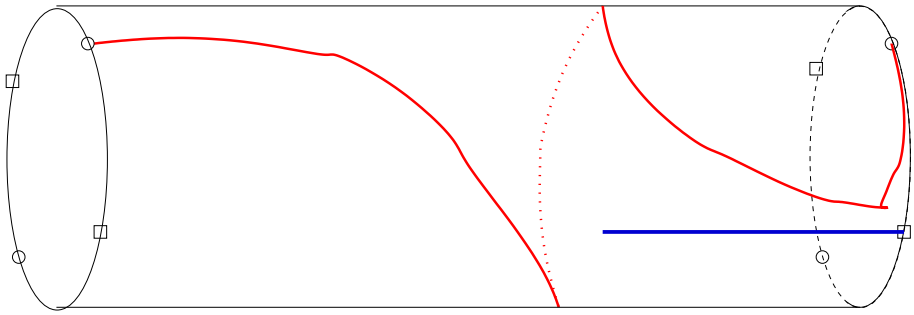

Figure 2.1: Degeneracy of the pulse $q_u(x)$ can be reduced to a Sturm–Liouville problem, where a connecting orbit between the global unstable manifold at $\tau = -1$ and the global stable manifold at $\tau = +1$ for a given value of r indicates a degeneracy of the pulse.

Lemma 2.2. For r sufficiently large, $0 < \theta_r(x) < \pi/2$ for all x.

Proof. Let $r > \max\{h_2((U_c^2(\tau), 0)) \mid \tau \in [-1, 1]\}$. If $\theta = \pi/2$, then $\theta' = -1 < 0$. On the other hand, if $\theta = 0$, then $\theta' = 2(r - h_2((U_c^2(\tau), 0))) > 0$. Hence for r large, θ remains bounded between 0 and $\pi/2$. □

Since there is no winding for r large, and $\theta(x)$ changes monotonically in r, the number of winds associated with the center manifold at $r = 0$ gives an exact count of the number of points of degeneracy between $r = 0$ and r large (for instance $r = 1$). See Figure 2.1.

2.1 A numerical investigation

Before we move to a rigorous proof of the various additional stationary waves which may occur in a system with the above properties, we will first use numerical shooting methods in order to gain some intuition and to visualize the waves that are present. There are two closely related ways to shoot for pulses that respect the system's reversibility (Property 2), and both reduce to a search along a one–dimensional curve of initial conditions.

1. First, for small ϵ and fixed r, we could choose approximate conditions in the tail of the

pulse of the form $\epsilon(\cos(\theta), \sin(\theta), \sqrt{2}\cos(\theta), \sqrt{2r}\sin(\theta))$. Such an initial condition is $O(\epsilon^2)$ close to the unstable manifold. We then numerically approximate the solution through this point, and when it passes through an appropriate space (for instance, $\Sigma_u = \{(u, w, p_u, p_w) \mid u = 0\}$ or $\Sigma_{p_u} = \{(u, w, p_u, p_w) \mid p_u = 0\}$) we check whether or not the pulse is additionally within $\mathrm{Fix}\,(R)$ (particularly, if either w or p_w is also zero). If we can find two values of θ nearby one another for which the corresponding values of w (or p_w) within Σ_u (or Σ_{p_u}) are of opposite sign, then we can isolate a stationary wave in this interval.

2. Conversely, we can choose an initial condition in $\mathrm{Fix}\,(R)$, with one of the three possible conditions $\{(u, w, p_u, p_w) | p_u = 0, w = 0\}$, $\{(u, w, p_u, p_w) | p_u = 0, p_w = 0\}$ and $\{(u, w, p_u, p_w) \mid u = 0, p_w = 0\}$. Since any homoclinic orbit must have Hamiltonian $H = 0$, we consider $\mathrm{Fix}\,R \cap \{H = 0\}$ to provide a one–dimensional curve of initial conditions. Note that the fourth possibility $\{(u, w, p_u, p_w) \mid u = 0, w = 0\}$ is forbidden since $\{(u, w, p_u, p_w) \mid u = 0, w = 0\} \cap \{H = 0\} = \{0, 0, 0, 0\}$. We can shoot from these initial conditions at the stable manifold of the origin. If we can find nearby initial conditions along this curve for which the associated solutions are kicked out on opposite sides of the stable manifold, then we can isolate a stationary wave in this interval.

Using this second method, we explore the Ostrovskaya–Kivshar problem for varying r values and fixed saturability constant $s = 0.8$. For this value of s there are two points of degeneracy in the interval $0 < r < 1$.

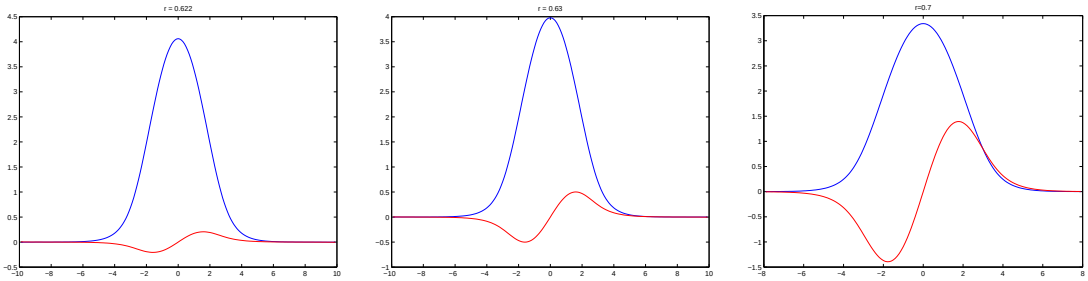

Figure 2.2: For $r > r_1$, there is a simple multi–component pulse bifurcating from the single–component pulse $q_u(x)$. As r increases the w component increases in magnitude.

First of all, considering the Sturm–Liouville argument above, we expect a simple multi–component pulse to bifurcate from the elementary pulse in U at each of the degenerate r values. For $r > r_1 \approx 0.621$, we shoot from the space $\{(u, w, p_u, p_w)|p_u = 0, w = 0\}$ and indeed find such a pulse, as pictured in Figure 2.2. Following the notation of Ostrovskaya and Kivshar [5], we call this pulse $q_{|0,1\rangle}(x)$. For r near r_1, this pulse looks like the original elementary solution $q_u(x)$ with the addition of a small, but nontrivial w component. As r gets closer to 1, this solution approaches several widely separated copies of the so–called "circularly–polarized pulse" with equal u and w components. Similarly, for $r > r_2 \approx 0.193$, we shoot from the space $\{(u, w, p_u, p_w) \mid p_u = 0, p_w = 0\}$ and find a similar pulse, shown in Figure 2.3. We call this pulse $q_{|0,2\rangle}(x)$. As r approaches 1, this solution appears to approach widely separated overlaid copies of the elementary pulses $q_w(x + x_0)$, $q_u(x)$ and $q_w(x - x_0)$.

Cascades of multiple pulses.

Without any further structure, the bifurcation diagram near a point of degeneracy unfolds like a pitchfork, see for instance Knobloch [13]. Because of the orbit–flip configuration assumed in Property 4, however, we expect a richer family of homoclinic solutions

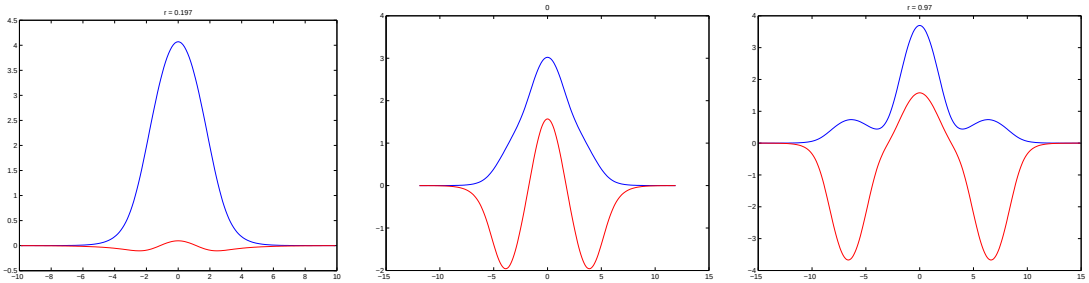

Figure 2.3: For $r > r_2$, there is a simple multi–component pulse, bifurcating from the single–component pulse $q_u(x)$.

in this case. For the sake of specificity, we consider the Ostrovskaya–Kivshar problem with $s = 0.8$ and $r = 0.7$. This r value is slightly beyond the bifurcation value $r = r_1$ and well beyond $r = r_2$. We will first look for pulses using initial conditions in the space $\{(u, w, p_u, p_w) \mid p_u = 0, w = 0\}$; this is the space that gives us the simple pulse associated with r_1.

Shooting from $\{(u, w, p_u, p_w) \mid p_u = 0, w = 0\}$.

For a given value of u, a value $p_w(u)$ in this space is specified by the Hamiltonian constraint; in particular

$$p_w = \sqrt{-\frac{1}{2}u^2 + \frac{25}{8}\ln(1 + 0.8u^2)}.$$

The simple multi–component pulse associated with the bifurcation point $r = r_1$ intersects this space at $(u, p_w) = (3.3414, 1.2616)$ – this is already a fair distance from the single component pulse at $(u, p_w) = (4.0777, 0)$. As the shooting parameter u is increased from the value $u = 3.3414$, the multi–component 1–pulse is broken and we see a cascade of pulses with increasing numbers of oscillations in u – these may be considered as multi–

pulses in which the u–component is alternating. Increasing u from the 1–pulse value, we see a 5–pulse, then a 9–pulse, and hypothesize that there are $4n+1$–pulses for all n as we increase u, until eventually the solution shooting from (u, p_w) gains the appearance of a periodic wave. Then, increasing u further, we see the reverse cascade which moves through the $4n+3$–pulses for decreasing n until it terminates at $u = 3.7339$ with the alternating 3–pulse.

In addition to the pulses with alternating u–component, for $u < 3.3414$, a cascade of pulses that are non–alternating in the u–component appears. Decreasing u from the value where the 1–pulse is found, we move through the non–alternating $2n+1$–pulses for increasing n. As the shooting value u shrinks further, we unwrap the $2n$–pulses for decreasing n, terminating at the 2-pulse when $u = 0.4232$. These multi–pulses intersect the space $\{(u, w, p_u, p_w) | p_u = 0, w = 0\}$ between the actual bodies of the individual pulses themselves. There are also pulses (for instance the up–down–down–up pulse in the figure) which are not strictly alternating or non–alternating.

Shooting from $\{(u, w, p_u, p_w) \mid u = 0, p_w = 0\}$.

The remaining alternating pulses associated with the bifurcation point $r = r_1$ can be found shooting from the space $\{(u, w, p_u, p_w) \mid u = 0, p_w = 0\}$. Given a value for w within this space, the p_u value is given by

$$p_u = \sqrt{\left(2r - \frac{5}{2}\right) u^2 + \frac{25}{8} \ln(1 + 0.8u^2)}.$$

The alternating 2–pulse is found to intersect this space when $(w, p_u) = (0.7023, 0.7049)$. Decreasing w in this space, we see increasing oscillations in the resulting pulses and slide

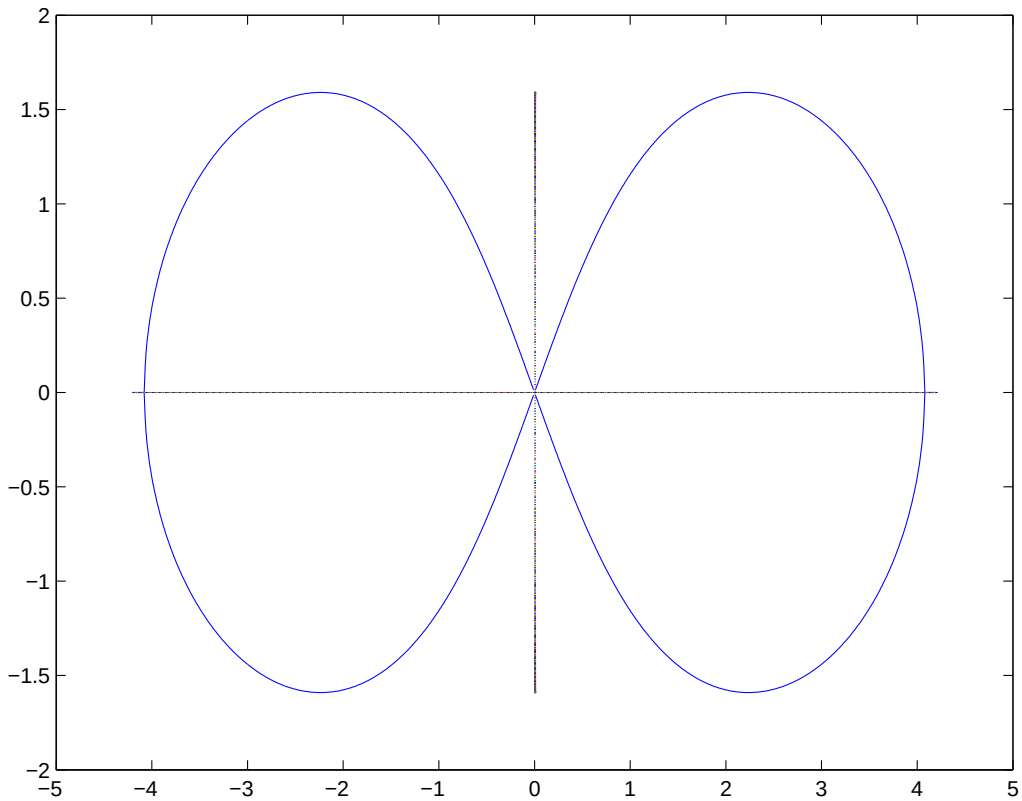

Figure 2.4: The section $\{(u, w, p_u, p_w) | p_u = 0, w = 0\}$ intersects several families of pulses.

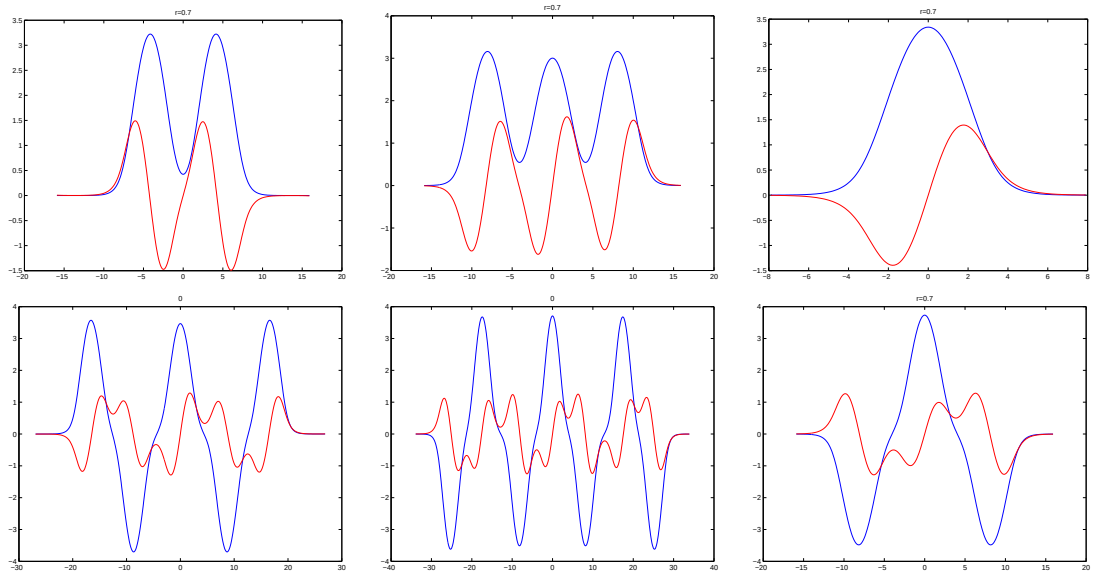

Figure 2.5: Pulses meeting the section $\{(u, w, p_u, p_w) \mid p_u = 0, w = 0\}$.

through the alternating $4n + 2$–pulses. As w is decreased further, we then unwrap the alternating $4n$–pulses, terminating in the alternating 4–pulse when $w = 0.0948$.

In a similar fashion, alternating pulses associated with the other bifurcation point $r = r_2$ can be seen in this space. Since this bifurcation point is farther away, these pulses intersect this space at much larger values of the shooting parameter w. However, the cascade forms in the same way, with the $4n$–pulses appearing for $w < 1.9717$, where the 4–pulse itself is, and the $4n+2$ pulses appearing in sequence beyond the value $w = 1.4827$, where the 2-pulse intersects this space.

Shooting from $\{(u, w, p_u, p_w) \mid p_u = 0, p_w = 0\}$.

The multi–component pulse associated with $r = r_2$ is even in both u and w and can be found shooting from the space $\{(u, w, p_u, p_w) | p_u = 0, p_w = 0\}$. Given a value for w, the

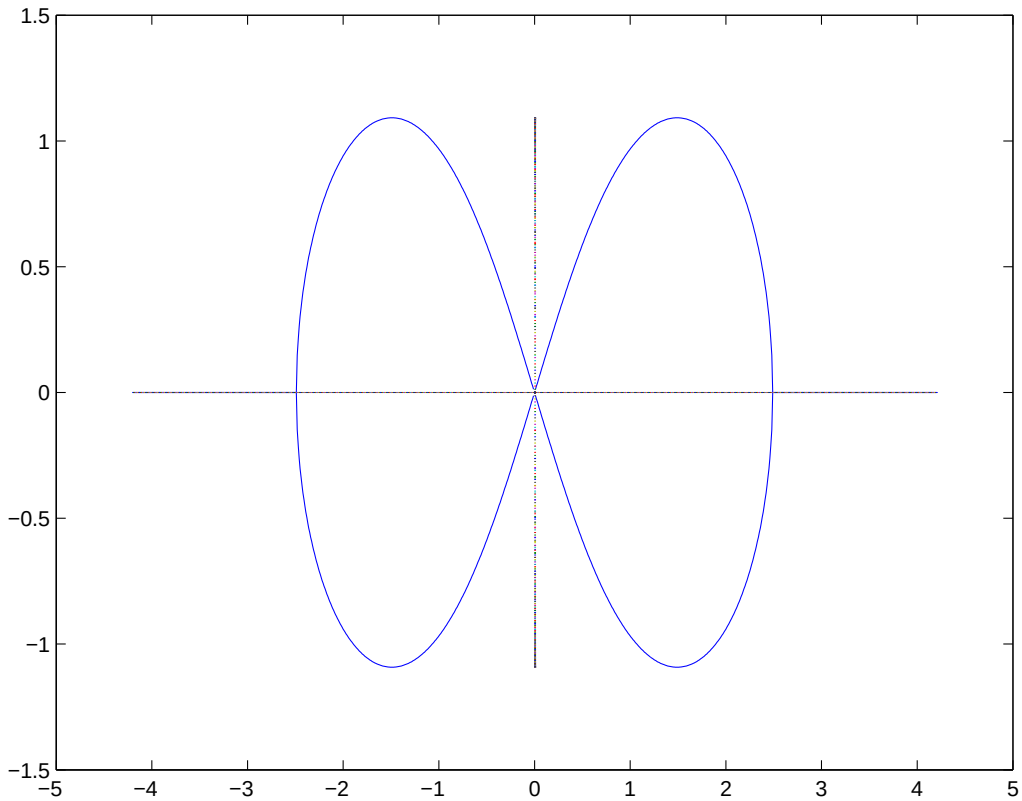

Figure 2.6: The section $\{(u, w, p_u, p_w) \mid u = 0, p_w = 0\}$ intersects several families of pulses.

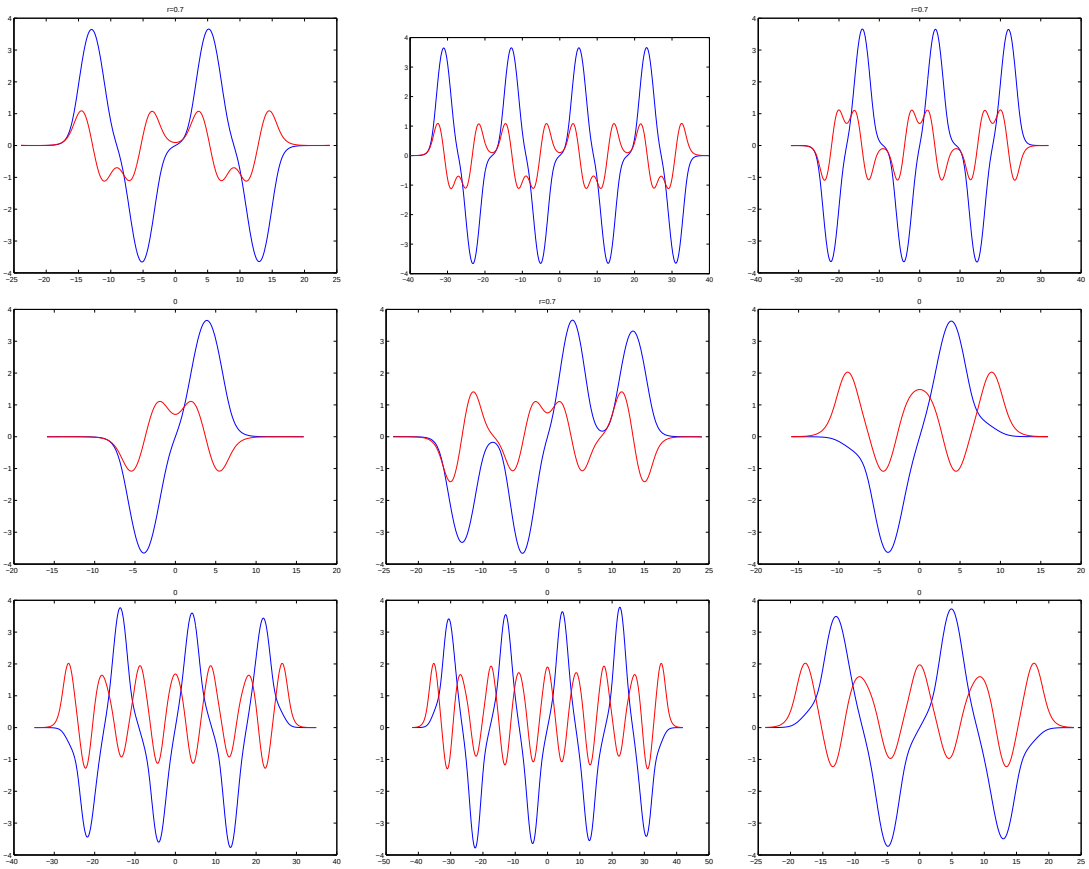

Figure 2.7: Pulses meeting the section $\{(u, w, p_u, p_w) \mid u = 0, p_w = 0\}$.

associated u–value can be determined by solving

$$0 = -\left(\frac{1}{s} - 1\right) u^2 - \left(\frac{1}{s} - r\right) w^2 + \frac{1}{s^2} \ln(1 + s(u^2 + w^2))$$

implicitly. This multi–component 1–pulse is found with $(u, w) = (3.0223, 1.5711)$. We expect the same structure of cascading multipulses found for the $r = r_1$ bifurcation. However, perhaps because this pulse is farther removed from its bifurcation value, the structure appears more complicated. Increasing u from 3.0223, we do find a nice alternating 5–pulse and an alternating 9–pulse. We find a second more awkward looking 5–pulse nearby, however, and the only 3–pulse present is between the multi–component 1–pulse and the 5–pulses. It is as though the two expected cascades have folded over upon themselves! In fact, examining this space for $r = 0.25$, closer to the bifurcation value at $r = r_2$ reveals the expected cascades.

A precursor to the bifurcating pulse.

The numerics above focus primarily on the many exotic pulses which appear after passing through a point of degeneracy like $r = r_1$ or $r = r_2$. Before the degeneracy, the winding of the linearized w–component is insufficient to produce a bounded 1–pulse with nonzero w–component. However, it is possible that some manner of multipulse might still exist that compensates for the insufficient winding by traversing another loop and then returning via the stable or unstable manifold of this second loop. Indeed, this appears to be the case. For $r < 0.622$, we shoot from the space $\{(u, w, p_u, p_w) \mid p_u = 0, w = 0\}$, where the multi–component pulse will arise for $r > 0.622$. Numerically, we find a pulse that resembles $-q_w(x + T) + q_u(x) + q_w(x - T)$.

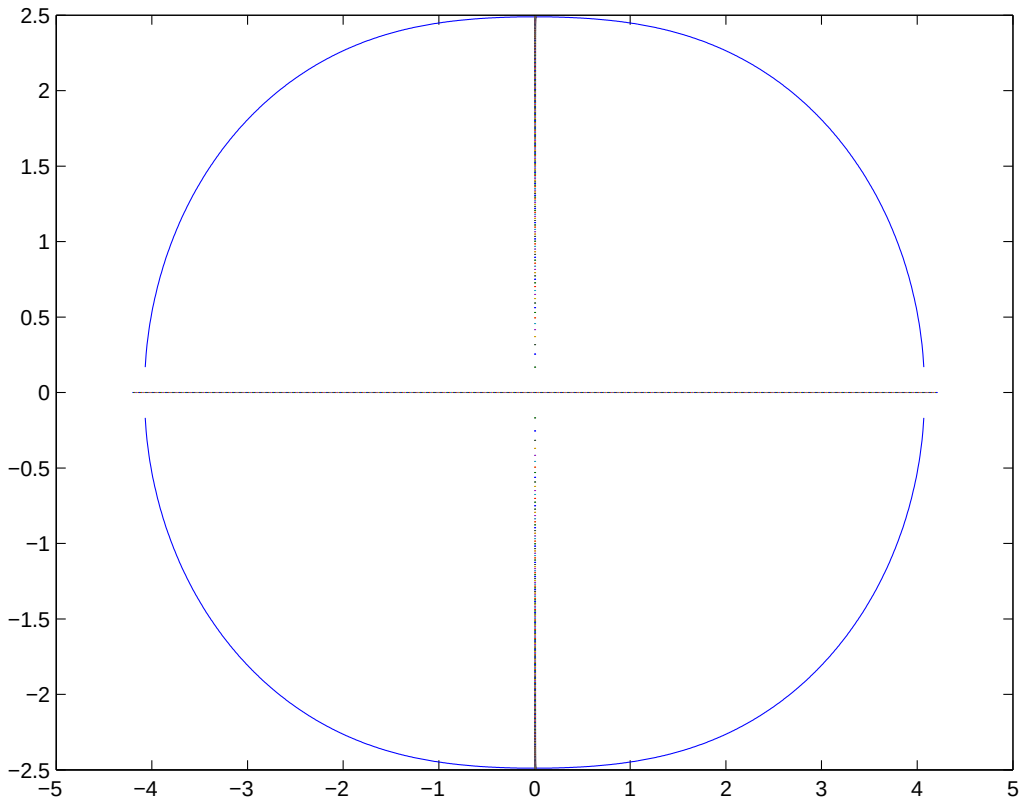

Figure 2.8: The section $\{(u, w, p_u, p_w) | u = 0, p_w = 0\}$ intersects several families of pulses.

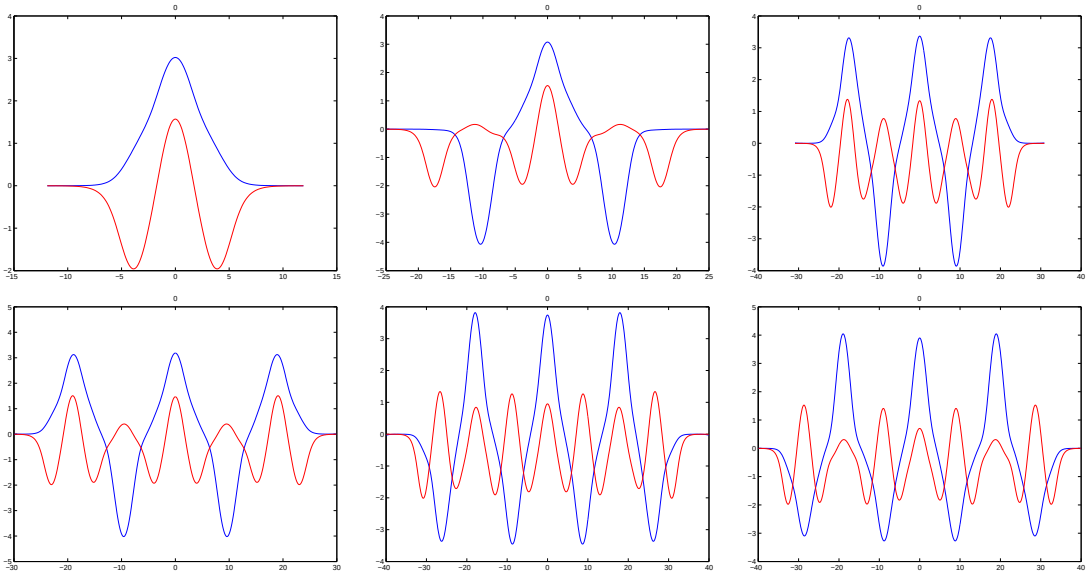

Figure 2.9: Pulses meeting the section $\{(u, w, p_u, p_w)|u = 0, w = 0\}$.

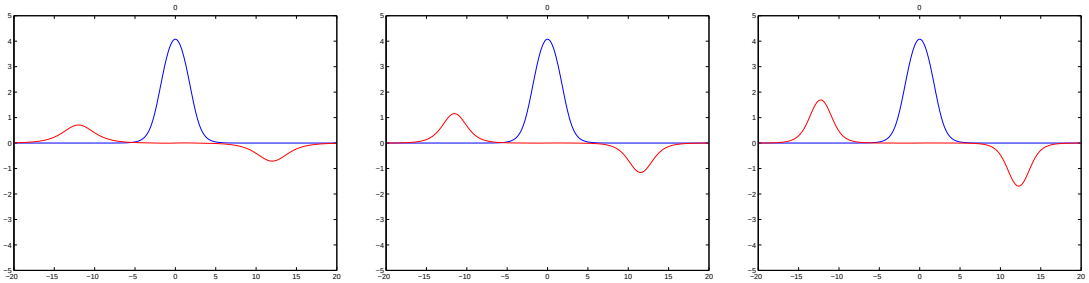

Figure 2.10: Precursors to the multi–component pulse for $r = 0.20$,$r = 0.40$ and $r = 0.60$.

2.2 An analytic study of alternating multipulses

There are a variety of methods available for studying bifurcations of homoclinic orbits in such a system. The usual geometric method involves assuming that the flow can be linearized about the origin and considering the "near" and "far" maps induced by the flow between sections set up in this linearized region. This method has been used successfully to analyze various bifurcations, for instance the orbit–flip as well as the inclination–flip, see Nii [14], Homburg, Kokubu and Krupa [15] or Homburg and Krauskopf [16]. A more analytic method which avoids the linearization assumption is the homoclinic Lyapunov–Schmidt method, also called the Hale–Lin–Sandstede method (and in either case abbreviated as the HLS method). In this method, piecewise continuous solutions are defined between sections with jumps only allowed in a specified direction within these sections. Homoclinic orbits correspond to solutions where the jumps are all set to be 0. Despite the increased generality of the HLS method, the geometric mechanisms for multipulse production are often hidden behind detailed remainder estimates. Analyses of this type can be seen for various bifurcations in Sandstede [17], Yew [18], Sandstede, Jones and Alexander [19], Knobloch [13] or van Gils, Krupa and Tchistiakov [20].

We will use the geometric method to study the bifurcation to be described in this section. Because the governing equations are Hamiltonian, it is certainly reasonable to expect that the flow will be linearizable in a neighborhood of the origin, see Moser [21] or Devaney [22] for examples in which the equilibrium is of saddle–focus type. At any rate, we assume the existence of a linear coordinate system near the origin.

The theorem and analysis below require only the five properties of the ordinary differ-

ential equations and the elementary solutions listed previously. With these in mind, we have the following theorem:

Theorem 2.3. Suppose that the ordinary differential equation $v' = f(v)$ satisfies Properties 1–5, is linearizable in a neighborhood of the origin, and the single component solution $q_u(x)$ is degenerate at a point r^*. Then there exists a multi–component pulse bifurcating from $q_u(x)$ for $r > r^*$. Additionally, for all $N \geq 2$ there exist N–pulse solutions that are alternating in the u component. These N–pulse solutions are not necessarily unique.

Proof. This theorem will be proven by construction. This construction will vary depending upon whether $r^* < 1/4$ or $r^* \geq 1/4$, but the result holds in either case. We fix a parameter value $r = r^* + \epsilon$, where ϵ is chosen to be sufficiently small; in particular, if $r^* < 1/4$, then $r < 1/4$.

The sections Σ_{in}, Σ_{out}, $S_1\Sigma_{in}$, $S_1\Sigma_{out}$.

First, by assumption, we can consider a linear coordinate system in a neighborhood of the origin. This system can be written as

$$\begin{aligned} v'_{ss} &= -\sqrt{2}\, v_{ss} \\ v'_s &= -\sqrt{2r}\, v_s \\ v'_u &= \sqrt{2r}\, v_u \\ v'_{uu} &= \sqrt{2}\, v_{uu}. \end{aligned}$$

We renormalize inside the region where this coordinate system is available, so that the

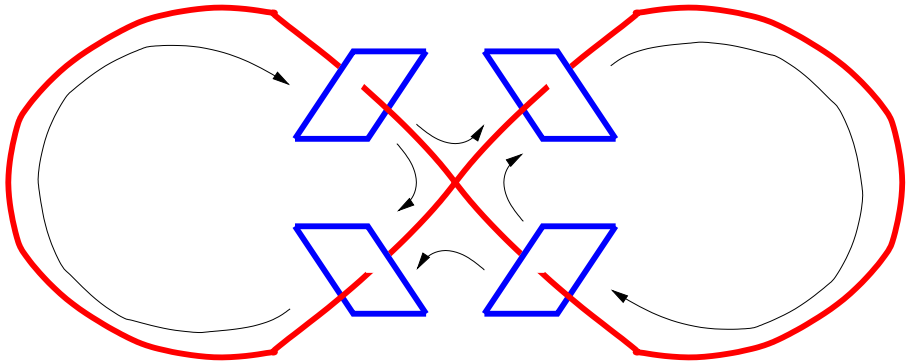

Figure 2.11: The sections Σ_{in}, $S_1\Sigma_{in}$, Σ_{out} and $S_1\Sigma_{out}$ are set up perpendicular to the homoclinic orbits $q_u(x)$ and $S_1 q_u(x)$. The maps Φ_{near} and $S_1\Phi_{near}$ define the local flow between these sections, while Φ_{far} and $S_1\Phi_{far}$ are diffeomorphisms which define the global flow.

unit box is in the interior of this region. Define the sections Σ_{in} and Σ_{out} as

$$\Sigma_{in} = \{(v_{ss}, v_s, v_u, v_{uu}) \mid v_{ss} = 1\}$$

and

$$\Sigma_{out} = \{(v_{ss}, v_s, v_u, v_{uu}) \mid v_{uu} = 1\}.$$

Notice that because the pulse $q_u(x)$ is in orbit–flip configuration (Property 4), these three dimensional sections are normal to the homoclinic orbit $q_u(x)$ and intersect $q_u(x)$ at the points $(1, 0, 0, 0)$ and $(0, 0, 0, 1)$. The homoclinic orbit $S_1 q_u(x)$ meets the sections $S_1\Sigma_{in}$ and $S_1\Sigma_{out}$ similarly. See Figure 2.11.

Reduction of dimension via the Hamiltonian.

Any homoclinic orbit approaching the origin as $x \to \pm\infty$ must lie on the same level set of the Hamiltonian as the origin itself, i.e. $H = 0$. In the linear coordinates near the

origin, the Hamiltonian reduces to

$$H(v_{ss}, v_s, v_u, v_{uu}) = 4v_{ss}v_{uu} + 4rv_sv_u.$$

Considering the intersection of the sets $\Sigma_{in} \cap \{H = 0\}$ and $\Sigma_{out} \cap \{H = 0\}$, we can restrict our attention to a two dimensional manifold within Σ_{in} and Σ_{out}. In particular, given v_s and v_u in Σ_{in} (Σ_{out}), $v_{ss}(v_{uu}) = -rv_sv_u$. We can therefore consider the maps $\Phi_{far} : \Sigma_{out} \to \Sigma_{in}$ and $\Phi_{near} : \Sigma_{in} \to \Sigma_{out}$ as maps from $\mathbf{R}^2 = (v_u, v_s)$ into itself.

Degeneracy, reversibility and the "far" map.

At the parameter value r^*, the homoclinic orbit $q_u(x)$ is degenerate (via Property 5). In particular, Φ_{far} takes the v_u–axis in Σ_{out} (i.e. the unstable manifold) to a curve that is tangent at the origin to the v_s–axis in Σ_{in} (the stable manifold). Conversely, Φ_{far}^{-1} takes the v_s–axis in Σ_{in} to a curve that is tangent at the origin to the v_u–axis in Σ_{out}. A key observation is that, because of the reversibility (Property 2), if $\Phi_{far} : (v_1, v_2) \to (w_1, w_2)$ then $\Phi_{far}^{-1} : (v_2, v_1) \to (w_2, w_1)$. Hence the curves $\Phi_{far}(W^u(0) \cap \Sigma_{out})$ and $\Phi_{far}^{-1}(W^s(0) \cap \Sigma_{in})$ are reflections of one another about the line $v_s = v_u$ (as are the lines $W^u(0) \cap \Sigma_{out}$ and $W^s(0) \cap \Sigma_{in}$ themselves).

For $r = r^* + \epsilon$, we have

$$\Phi_{far}(v_s, v_u) = \pm \begin{bmatrix} \mu & -(1-\mu^2)^{1/2} \\ (1-\mu^2)^{1/2} & \mu \end{bmatrix} \begin{bmatrix} v_s \\ v_u \end{bmatrix} + O(||(v_s, v_u)||^3).$$

All of the second order error terms vanish because of the symmetry assumption of Property 3. The parameter $\mu \to 0$ as $\epsilon \to 0$ in this bifurcation and assuming the generic

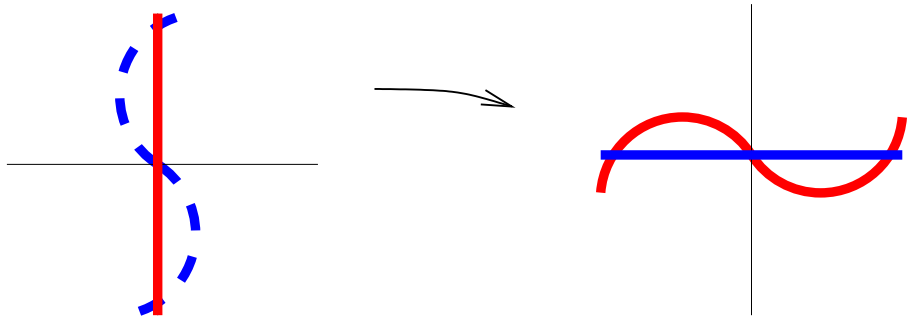

Figure 2.12: The map Φ_{far}. Φ_{far} takes the local unstable subspace (in red) to a "cubic–like" curve, while Φ_{far}^{-1} acts identically on the local stable subspace (in blue).

condition that $D_{222}\Phi_{far}^2(0,0) > 0$, there is a nontrivial intersection in Σ_{out} of the v_u–axis and $\Phi_{far}^{-1}(\text{Span}\,(v_s))$. This intersection represents the multi–component one–pulse of the theorem.

Of primary importance to the search for multipulses is the following observation: even though there is no clear reason to believe that Φ_{far} is an area preserving map, it is still true that it takes the region bounded between the v_u–axis and $\Phi_{far}^{-1}(\text{Span}\,(v_s))$ in Σ_{out} to its reflection in Σ_{in} bounded by $\Phi_{far}(\text{Span}\,(v_u))$ and the v_s–axis. Thus, the reversibility provides a "quasi"-area preservation. See Figure 2.12.

Orbit flip configuration and the "near" map.

Before we search for multipulses in earnest, we need to consider the behavior of the map $\Phi_{near} : \Sigma_{in} \to \Sigma_{out} \cup S_1\Sigma_{out}$. First, observe that whether Φ_{near} takes an initial condition to Σ_{out} or $S_1\Sigma_{out}$ is determined solely by the value of v_{uu} associated with (v_s, v_u) in Σ_{in}. If $v_{uu} = rv_uv_s > 0$, then $\Phi_{near} : \Sigma_{in} \to \Sigma_{out}$. Likewise, if $v_{uu} = rv_uv_s < 0$, then $\Phi_{near} : \Sigma_{in} \to S_1\Sigma_{out}$. (If $v_{uu} = 0$, then $(v_s, v_u) \in W^s_{loc}(0)$ and the evolution of such a point approaches the origin as $x \to \infty$.)

Using the linearized system and the Hamiltonian (Property 1), one can quickly deter-

mine the behavior of the map Φ_{near}. In particular, given $(v_s, v_u) \in \Sigma_{in}$ (where $v_{ss} = 1$), the value of v_{uu} is explicitly determined. Since $|v_{uu}| = 1$ in either exit slice Σ_{out} or $S_1\Sigma_{out}$, the elapsed time T between the slices is determined to be

$$\begin{aligned}
1 &= |v_{uu}|e^{\sqrt{2}T} \\
|v_{uu}|^{-1} &= e^{\sqrt{2}T} \\
-\ln|v_{uu}| &= \sqrt{2}T \\
T &= -\ln|v_{uu}|/\sqrt{2} \\
T &= -\ln|rv_sv_u|/\sqrt{2}.
\end{aligned}$$

Φ_{near} is then given by

$$\begin{aligned}
\Phi_{near}(v_s, v_u) &= \left(v_s e^{-\sqrt{2r}T}, v_u e^{\sqrt{2r}T}\right) \\
&= \left(v_s e^{\sqrt{r}\ln|rv_sv_u|}, v_u e^{-\sqrt{r}\ln|rv_sv_u|}\right) \\
&= \left(v_s(r|v_s|\ |v_u|)^{\sqrt{r}}, v_u(r|v_s|\ |v_u|)^{-\sqrt{r}}\right).
\end{aligned}$$

The first thing to notice about this map is that unlike the map Φ_{far}, Φ_{near} is truly area preserving – a quick calculation shows that Div $(\Phi_{near}) = 0$. Secondly, the qualitative behavior of Φ_{near} varies depending upon whether or not the bifurcation point r^* satisfies $\sqrt{r^*} < 1/2$. In particular, consider how the map Φ_{near} acts on a curve approaching the origin: for small x, $\Phi_{near} : (x, ax) \to \left((ar)^{\sqrt{r}}x^{1+2\sqrt{r}}, (ar)^{1-\sqrt{r}}x^{1-2\sqrt{r}}\right)$. So, if $\sqrt{r^*} < 1/2$, then for r near r^* this curve is taken to a curve also approaching the origin, but now tangent to the v_u–axis at the origin. However, if $\sqrt{r^*} \geq 1/2$, then for $r > r^*$, the curve is mapped to a curve approaching infinity along the v_u–axis. (Of course, the linear coordinate system does not extend out to infinity.) Likewise, a curve intersecting the v_s–axis in a

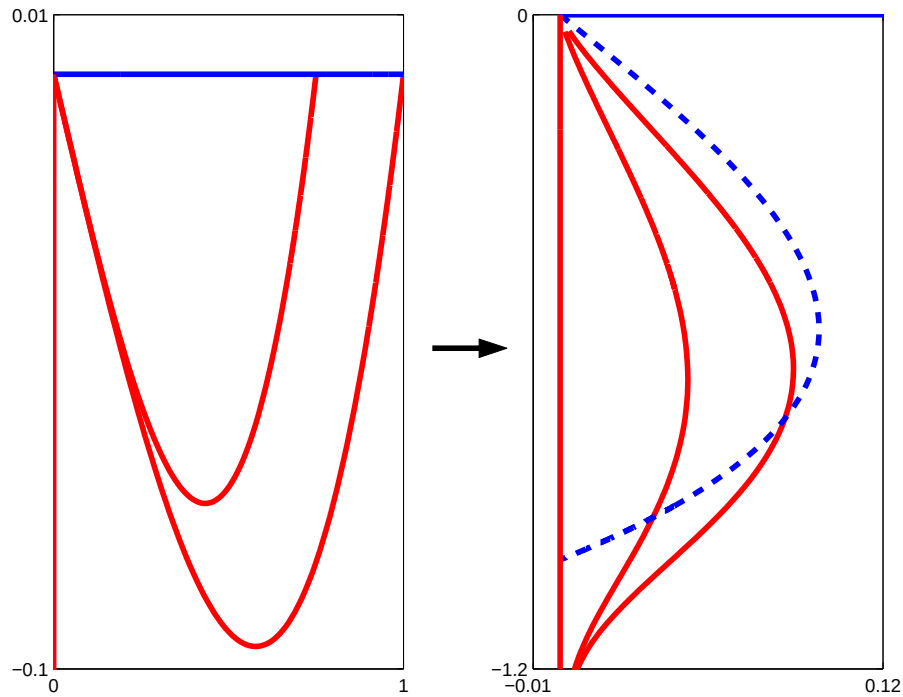

Figure 2.13: The map Φ_{near}. Φ_{near} acts in a different manner depending on the value of r. For $\sqrt{r} > 1/2$, "cubic–like" curves are taken to unbounded curves.

point other than the origin will be taken to a curve tangent to the v_s–axis at the origin if $\sqrt{r} < 1/2$, and it will be taken to a curve tangent to the v_u–axis if $\sqrt{r} \geq 1/2$. See Figures 2.13 and 2.14.

This then leads to two cases for the bifurcation analysis.

Bifurcation analysis.

Of primary interest in the search for multipulses is the evolution of small "cubic–like" curves in the section Σ_{in}. First we define the closed region Ω in Σ_{in} as the bounded area between the v_s–axis and $\Phi_{far}(\text{Span}\,(v_u))$, i.e. between the local stable manifold $W^s(0)$ and the global unstable manifold $W^u(0)$ continued along the homoclinic orbit $q_u(x)$. A "cubic–like" curve γ is a curve in Ω which intersects the v_s–axis at the origin and two nearby points, symmetric about the origin, recalling Property 3. In particular, the boundary

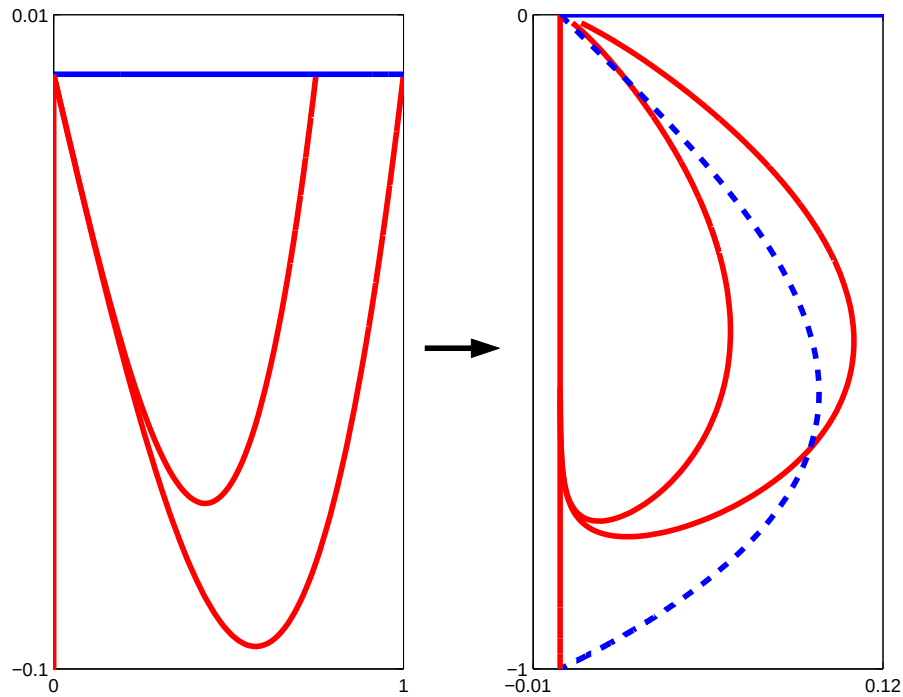

Figure 2.14: The map Φ_{near}. Φ_{near} acts in a different manner depending on the value of r. For $\sqrt{r} < 1/2$, "cubic–like" curves are taken to closed curves.

$\Phi_{far}(\text{Span}\,(v_u))$ is such a curve. For simplicity, we consider only the simply connected component of Ω in the fourth quadrant — the component in the second quadrant is equivalent. In each case, we will show that the image $\Phi_{far} \circ \Phi_{near}(\gamma)$ also contains a "cubic–like" curve.

Case 1. $\sqrt{r} > 1/2$.

Let γ_0 be a "cubic–like" curve in Ω. As noted above, when $\sqrt{r} > 1/2$, Φ_{near} takes the end of γ_0 near the origin to an unbounded curve in $S_1\Sigma_{out}$ asymptotic to the v_u–axis at $-\infty$. Likewise, it takes the end of γ_0 near the nonzero intersection point with the v_s–axis to a curve in $S_1\Sigma_{out}$ which is tangent to the v_u–axis at the origin and enters the interior of $-\Phi_{far}^{-1}(\Omega)$ in $S_1\Sigma_{out}$. Therefore, there must be a nontrivial intersection in $S_1\Sigma_{out}$ of $\Phi_{near}(\gamma_0)$ and $-\Phi_{far}^{-1}(\Omega)$. We call the portion of $\Phi_{near}(\gamma_0)$ between the origin and the first

intersection $\gamma_{1/2}$. The map Φ_{far} then takes $\gamma_{1/2}$ to another "cubic–like" curve in $S_1\Sigma_{in}$, and this curve is clearly in $S_1\Omega$. We call this curve γ_1.

If we take Λ_0 to be $\Phi_{far}(\text{Span}\,(v_u))$ itself, i.e. the continuation of the unstable manifold of the origin, then the intersection of Λ_1 with the v_s–axis in $S_1\Sigma_{in}$ represents the 2–pulse. Continuing recursively, we find an alternating N–pulse for all N.

Case 2. $\sqrt{r} < 1/2$.

This case follows similarly, except here the curve $\Phi_{near}(\gamma_0)$ is a closed bounded curve. The map Φ_{near} takes the portion of γ_0 near the origin to a curve approaching the origin tangent to the v_u–axis in $S_1\Sigma_{out}$; the portion of γ_0 near the nontrivial intersection is taken to a curve in $S_1\Sigma_{out}$ approaching the origin tangent to the v_s–axis. Since the first portion of $\Phi_{near}(\gamma_0)$ is inside $-\Phi_{far}^{-1}\Omega$ and the return portion is outside $-\Phi_{far}^{-1}\Omega$, there must again be a first nontrivial intersection with the boundary and we again call the portion of $\Phi_{near}(\gamma_0)$ interior to $-\Phi_{far}^{-1}\Omega$ between the origin and the first intersection $\gamma_{1/2}$. The map Φ_{far} again takes $\gamma_{1/2}$ to another "cubic–like" curve γ_1 in $S_1\Sigma_{in}$, and this curve is clearly in $S_1\Omega$.

The two cases vary primarily in the manner in which the curve $\gamma_{1/2}$ is produced — the preimage of $\gamma_{1/2}$ comes from different ends of γ_0 in each case.

Multipulses!

We take our initial cubic curve γ_0 to be the global unstable manifold $W^u(0)$ in Σ_{in} as continued along $q_u(x)$, i.e. $\Phi_{far}(\text{Span}\,(v_u))$. Then the intersection of γ_1 with the local stable manifold $W^u(0)$ in $S_1\Sigma_{in}$, represents an alternating 2–pulse. Now, $\gamma_1 \subset W^u(0)$ and taking it as our initial "cubic–like curve", we get a curve $\gamma_2 \subset \Sigma_{in}$ whose nontrivial intersection indicates the existence of an alternating 3-pulse. An induction argument then

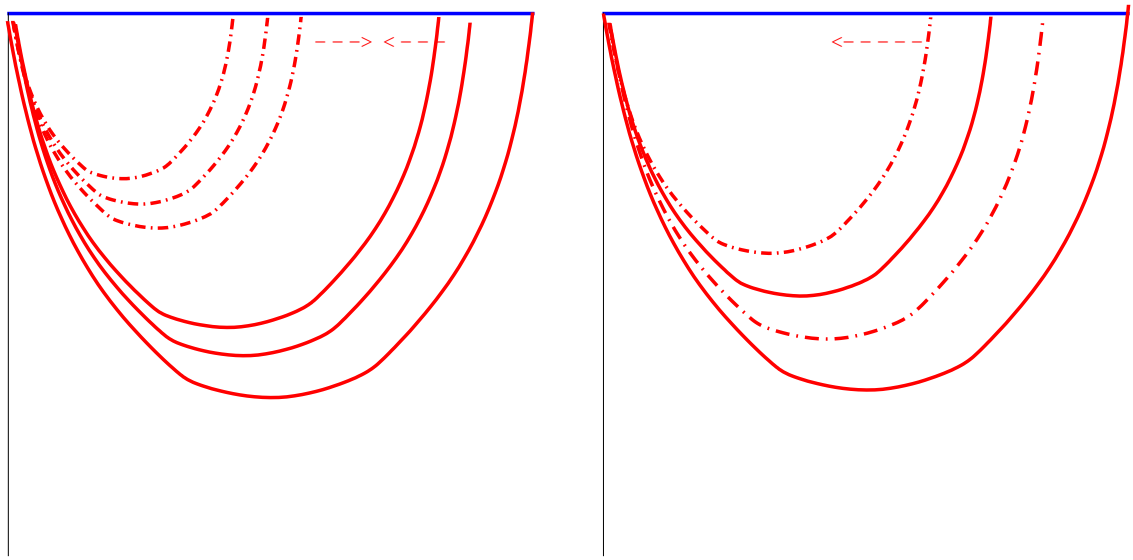

Figure 2.15: The image of a "cubic–like" curve under the map $\Phi_{far} \circ \Phi_{near}$ contains a "cubic–like" curve. The intersections of iterates of $\Phi_{far} \circ \Phi_{near}$ with the local stable manifold are indicators of multipulses. The iteration with $\sqrt{r} > 1/2$ is shown on the left; $\sqrt{r} < 1/2$ is on the right. Solid curves indicate iterates which are in Σ_{in} while the dashed curves are in $S_1\Sigma_{in}$.

yields the existence of an alternating N–pulse for all N. See Figure 2.15.

This ends the proof of the existence of multipulses. □

A remark on (non)uniqueness.

It is certainly possible that the image $\Phi_{near}(\gamma)$ of a "cubic–like" curve intersects $-\Phi_{far}^{-1}\Omega$ in more than one point — this would lead to multiple N–pulses for the corresponding value of N. In particular, suppose that the parameter r^* at which the pulse $q_u(x)$ is degenerate in near $1/4$. If we allow r^* to vary with the system parameters, then as $\sqrt{r^*}$ passes through the value $1/2$, a pitchfork bifurcation is destroyed which produces at least 3 points of intersection for an interval of r^* values on one side of $\sqrt{r^*} = 1/2$. For the 2–pulse, only the central point of intersection corresponds to a pulse which respects the reversibility; the other two 2–pulses are reflections of one another through the reversibility

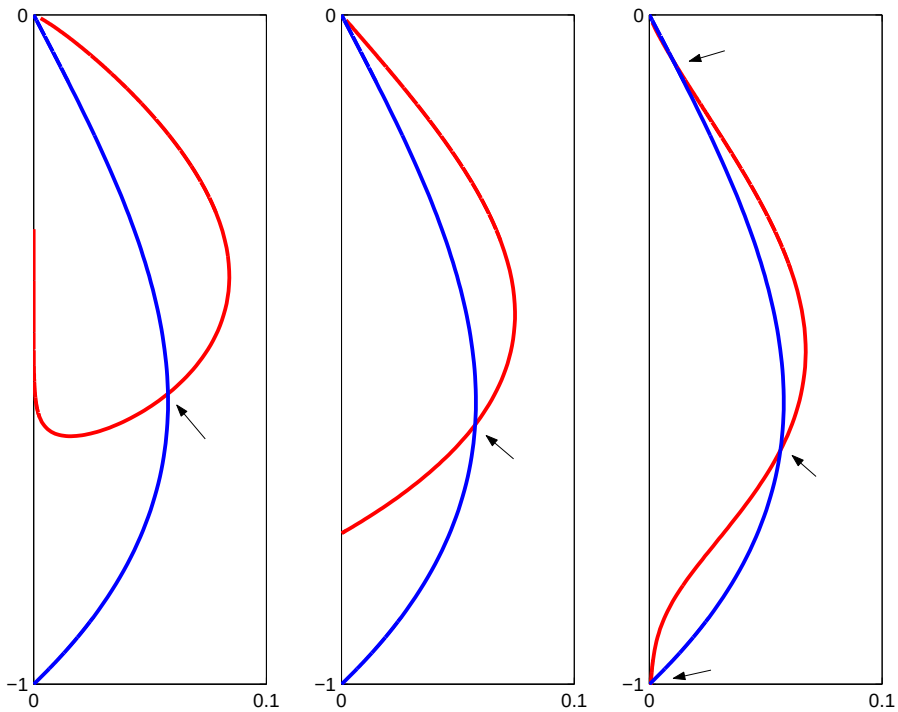

Figure 2.16: The map Φ_{near} and non-uniqueness of multipulses. There is a pitchfork bifurcation of intersection points in Φ_{near} which is destroyed as $\sqrt{r^*}$ passes through $1/2$.

involution. See Figure 2.16.

2.3 Degeneracy of the multi–component pulse and Plücker coordinates

The key to the bifurcation of multi–component pulses was the notion of degeneracy, sometimes called a *homoclinic–flip*. A solution is said to be degenerate if the stable and the unstable manifold have a two dimensional tangency along the solution. The simple form of the single–component pulse $q_u(x)$ led to a decoupling of the equation of variations, and in that case such a degeneracy could be understood in terms of a Sturm–Liouville problem – a classical problem whose analysis is well understood. However, the variational equation for the resulting multi–component pulses does not decouple in this way and hence it becomes more difficult to detect these simple degeneracies of a pulse.

We write the equation of variations as follows:

$$v' = \left[\begin{array}{cc|c} \multicolumn{2}{c|}{0_{2\times 2}} & I_{2\times 2} \\ \hline 2 - f_u(\cdot) & -f_c(\cdot) & \\ & & 0_{2\times 2} \\ -f_c(\cdot) & 2r - f_w(\cdot) & \end{array}\right] v. \tag{2.7}$$

In order to more easily follow the two dimensional subspaces (the tangent spaces to the global stable and unstable manifolds), we move to the Grassmannian of two dimensional planes in $\mathbf{R}^4$, G_2^4. The subspaces of interest in $\mathbf{R}^4$ correspond to points in G_2^4, so following these subspaces is akin to simply following an orbit in this new space. For this calculation, we make use of the exterior power space $\Lambda^2(\mathbf{R}^4)$ – we will delve into the intricacies of this space more deeply in Section 3.1. This space is six dimensional and we can explicitly

derive the system in $\Lambda^2(\mathbf{R}^4)$ induced by the linear system (2.7):

$$\begin{aligned}
P'_{12} &= P_{14} - P_{23} \\
P'_{13} &= -f_c(\cdot)P_{12} \\
P'_{24} &= f_c(\cdot)P_{12} \\
P'_{14} &= P_{34} + (2r - f_w(\cdot))P_{12} \\
P'_{23} &= -P_{34} - (2 - f_u(\cdot))P_{12} \\
P'_{34} &= (2 - f_u(\cdot))P_{14} - (2r - f_w(\cdot))P_{23} + f_c(\cdot)\left(P_{13} - P_{24}\right).
\end{aligned} \tag{2.8}$$

Not every set of coefficients P_{ij} corresponds to a point in G_2^4. The set of numbers P_{ij} are the Plücker coordinates if the following *Grassmannian condition* is satisfied:

$$P_{12}P_{34} - P_{13}P_{24} + P_{14}P_{23} = 0. \tag{2.9}$$

A quick calculation indeed shows that

$$(P_{12}P_{34} - P_{13}P_{24} + P_{14}P_{23})' = 0.$$

Additionally, because (2.7) is Hamiltonian, the system also preserves Lagrangian planes, $\Lambda(2)$. This invariance is given by the following *Lagrangian condition*:

$$P_{13} + P_{24} = 0. \tag{2.10}$$

An even quicker calculation shows that

$$(P_{13} + P_{24})' = 0$$

and hence both the Lagrangian and the Grassmannian conditions will continue to be satisfied as x evolves, if only the initial conditions satisfy them.

In (2.7) the asymptotic system has positive eigenvalues $\sqrt{2}$ and $\sqrt{2r}$, hence in (2.8) the largest positive eigenvalue for the asymptotic system is $\sqrt{2} + \sqrt{2r}$. The associated eigenvector is $v_{uu} = (1, 0, 0, \sqrt{2r}, -\sqrt{2}, 2\sqrt{r})$. Similarly, there is a negative eigenvalue $-\sqrt{2} - \sqrt{2r}$ with associated eigenvector $v_{ss} = (1, 0, 0, -\sqrt{2r}, +\sqrt{2}, 2\sqrt{r})$. The vector v_{uu} is the point in Plücker coordinates that corresponds to the unstable subspace of the asymptotic system, and we wish to evolve forward a solution $P^u(x) = (P^u_{12}(x), P^u_{13}(x), P^u_{24}(x), P^u_{14}(x), P^u_{23}(x), P^u_{34}(x))$ that is asymptotic to v_{uu} as $x \to -\infty$. Likewise, v_{ss} corresponds to the stable subspace of the asymptotic system, and we wish to evolve backward a second solution $P^s(x) = (P^s_{12}(x), P^s_{13}(x), P^s_{24}(x), P^s_{14}(x), P^s_{23}(x), P^s_{34}(x))$ that is asymptotic to v_{ss} as $x \to +\infty$. Of interest is the manner in which the two spaces corresponding to the vectors $P^u(x)$ and $P^s(x)$ intersect.

Because of the symmetries of the pulses described in the previous chapter, we expect that the points $P^u(x)$ and $P^s(-x)$ in G^4_2 will be very closely related. This relationship is described in the following lemma.

Lemma 2.4. Suppose $(U(x), W(x), U'(x), W'(x))$ is a stationary wave as found in the previous chapter.

1. If $U(x)$ and $W(x)$ are both even, then

$$(P^s_{12}(x), P^s_{13}(-x), P^s_{24}(-x), P^s_{14}(-x), P^s_{23}(-x), P^s_{34}(-x))$$
$$= \pm(P^u_{12}(x), -P^u_{13}(x), -P^u_{24}(x), -P^u_{14}(x), -P^u_{23}(x), P^u_{34}(x)).$$

2. If either $U(x)$ and $W(x)$ is odd while the other is even, then

$$(P^s_{12}(x), P^s_{13}(-x), P^s_{24}(-x), P^s_{14}(-x), P^s_{23}(-x), P^s_{34}(-x))$$
$$= \pm(-P^u_{12}(x), -P^u_{13}(x), -P^u_{24}(x), P^u_{14}(x), P^u_{23}(x), -P^u_{34}(x)).$$

Proof. This lemma follows easily by considering the reversibility involution (which takes $P'_{ij}(x) \to -1^{\sigma(ij)}P'_{ij}(x)$, where $\sigma(ij)$ is the number of elements of the pair $\{i, j\}$ that are also in the set $\{3, 4\}$), as well as the symmetries of the pulse (which affect the sign of the cross term $f_c(\cdot)$). □

This characterization will significantly ease the detection of degeneracies for symmetric pulses. Particularly, if we make our calculations at $x = 0$, once we calculate $P^u(0)$, we get $P^s(0)$ for free by simply flipping the appropriate signs.

This leads immediately to the following characterization for the degeneracy of a pulse.

Proposition 2.5. Consider a stationary wave $(U(x), W(x), U'(x), W'(x))$.

1. If both $U(x)$ and $W(x)$ are even, then the stationary wave is degenerate if and only if either

$$P^u_{12}(0) = P^u_{34}(0) = 0$$

or

$$P^u_{13}(0) = P^u_{24}(0) = P^u_{14}(0) = P^u_{23}(0) = 0.$$

2. If either $U(x)$ or $W(x)$ is even while the other is odd, then the stationary wave is degenerate if and only if

$$P^u_{14}(0) = P^u_{23}(0) = 0$$

or

$$P^u_{12}(0) = P^u_{13}(0) = P^u_{24}(0) = P^u_{34}(0) = 0.$$

Proof. This proposition may not be as immediately apparent as it first seems, because different sets of coordinates could conceivably span the same plane in $\mathbf{R}^4$. However, since one of the components $P^u_{ij}(0)$ must be nonzero, we can easily write down two independent vectors that span the unstable subspace specified by $P^u(0)$ (and the related vectors that span $P^s(0)$). For example, if $P^u_{12}(0) \neq 0$ then

$$TW^u(0) = \text{Span}\,\{(0, P^u_{12}(0), P^u_{13}(0), P^u_{14}(0))\ ,\ (P^u_{12}(0), 0, -P^u_{23}(0), -P^u_{24}(0))\}.$$

If the pulse is degenerate, then we must have

$$(0, P^u_{12}(0), P^u_{13}(0), P^u_{14}(0)) = \pm(0, P^s_{12}(0), P^s_{13}(0), P^s_{14}(0))$$

and

$$(P^u_{12}(0), 0, -P^u_{23}(0), -P^u_{24}(0)) = \pm(P^s_{12}(0), 0, -P^s_{23}(0), -P^s_{24}(0)).$$

These requirements force the equalities above. □

The condition that two (or even four) components be simultaneously zero is not ridiculously singular in this case. In addition to the Grassmannian and Lagrangian conditions, there are other properties that ease our way.

First of all, because $P^u(x)$ and $P^s(x)$ represent the tangent spaces along a homoclinic orbit, these spaces must have at least a one–dimensional intersection. This forces the condition that $P^u(x) \wedge P^s(x) = 0$. At $x = 0$ this again takes a simplified form.

Lemma 2.6. Suppose $(U(x), W(x), U'(x), W'(x))$ is a stationary wave as found in the previous chapter.

1. If $U(x)$ and $W(x)$ are both even, then

$$P^u_{12}(0)P^u_{34}(0) + P^u_{13}(0)P^u_{24}(0) - P^u_{14}(0)P^u_{23}(0) = 0.$$

2. If either $U(x)$ or $W(x)$ is odd while the other is even, then

$$P^u_{12}(0)P^u_{34}(0) - P^u_{13}(0)P^u_{24}(0) - P^u_{14}(0)P^u_{23}(0) = 0.$$

Proof. In light of the discussion above, the proof of these conditions is a simple calculation. □

Each of these resembles the Grassmannian condition (2.9), and in combination with it

forces a decoupling of the two conditions. For instance, in the first case we then have

$$P^u_{12}(0)P^u_{34}(0) = 0$$

and

$$P^u_{13}(0)P^u_{24}(0) - P^u_{14}(0)P^u_{23}(0) = 0.$$

Automatically, either $P^u_{12}(0)$ or $P^u_{34}(0)$ is equal to zero. Also if any one of the second four coefficients is equal to zero then at least three of them are, since $P^u_{13}(0)$ and P^u_{24} must both be zero as they are related through the Lagrangian condition.

A final condition comes about by considering the Hamiltonian H of the system.

Lemma 2.7. The stable and unstable manifolds are both contained within the level set $\{H = 0\}$. Any vector v tangent to either of these manifolds must therefore satisfy

$$v \cdot \nabla H((U(0), W(0), U'(0), W'(0))) = 0.$$

Degeneracy of the pulse $q_{|0,2\rangle}(x)$.

Here we follow the multi–component wave $q_{|0,2\rangle}(x)$ for which the w–component has two zeros in the Ostrovskaya–Kivshar problem with $s = 0.8$. At $r = 0.45$ we have

$$P^u(0) = (0.0000, -0.0676, 0.0676, 0.0946, -0.0484, -0.9897),$$

where the vector has been normalized to unity. And by the time $r = 0.51$, we have

$$P^u(0) = (0.0000, 0.0396, -0.0396, -0.0608, 0.0258, -0.9962),$$

see Figure 2.17. As the sign of $P^u_{13}(0), P^u_{24}(0), P^u_{14}(0)$ and $P^u_{23}(0)$ have all changed in this interval, we posit that they all went through zero simultaneously and that the pulse therefore passed through a degeneracy. Indeed, consider the value of r for which $P^u_{23}(0) = 0$. We immediately have $P^u_{13}(0) = P^u_{24}(0) = 0$ by the lemmas above. All that remains is to show that $P^u_{14} = 0$. This follows from the Hamiltonian condition since, for $P^u_{34}(0) \neq 0$, we require

$$(-P^u_{13}(0), -P^u_{23}(0), 0, P^u_{34}(0)) \cdot (\partial H/\partial u, \partial H/\partial w, 0, 0) = 0$$

and

$$(P^u_{14}(0), P^u_{24}(0), P^u_{34}(0), 0) \cdot (\partial H/\partial u, \partial H/\partial w, 0, 0) = 0.$$

Since $P^u_{24}(0) = 0$, the second equality then requires $P^u_{14}(0)\partial H/\partial u = 0$ and, in particular, $P^u_{14}(0) = 0$. We can therefore conclude that the multi–component pulse $q_{|0,2\rangle}(x)$ has a point of degeneracy between $r = 0.45$ and $r = 0.51$.

Bifurcation from the degenerate multi–component pulse.

As was the case in the previous chapter, when a stationary wave passes through degeneracy, we expect a bifurcation of other stationary waves. In this case, we expect a pair of nonsymmetric solutions to bifurcate from this stationary wave. The more exotic multipulses are not present in this case because the multi–component pulses $q_{|0,i\rangle}(x)$ are not in orbit–flip configuration.

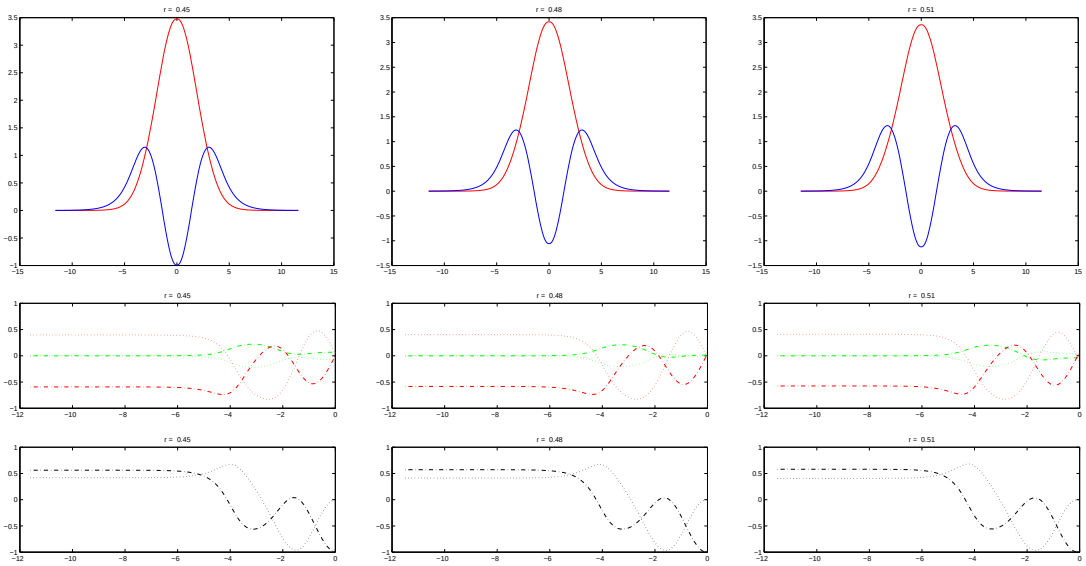

Figure 2.17: Above is the multi–component pulse $q_{|0,2\rangle}(x)$ for varying r, in particular, $r = 0.45, 0.48, 0.51$, from left to right. The lower graphs show the evolution of the six Plücker variables which coordinatize the tangent space to the stable manifold along the pulse. $P_{13}(x), P_{24}(x), P_{14}(x)$ and $P_{23}(x)$ are shown in the upper graph, while $P_{12}(x)$ and $P_{34}(x)$ are below. As the parameter r increases, the Plücker coordinates $P_{13}(0), P_{24}(0), P_{14}(0)$ and $P_{23}(0)$ all go through zero simultaneously, signaling a degeneracy of this multimode pulse.

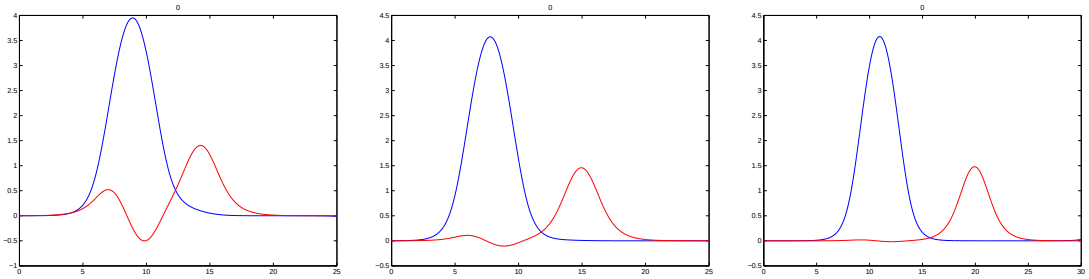

Figure 2.18: There is a pair of nonsymmetric multi–component pulses that bifurcate from the symmetric multi–component pulse when it becomes degenerate. Shown in this figure is one of those pulses for $r = 0.50$, $r = 0.52$ and $r = 0.5275$. (The other is simply its reflection in the vertical plane.)

Because we are now looking for nonsymmetric waves, we must expand upon the shooting methods used in the first chapter in order to see these waves numerically. We will use a hybrid method in which we specify decay conditions in the tail of the pulse of the form $\epsilon(\cos(\theta), \sin(\theta), \sqrt{2}\cos(\theta), \sqrt{2r}\sin(\theta))$. As we adjust θ, we then find two values of θ for which the evolved solutions are kicked out on opposite sides of the stable manifold, and therefore isolate a stationary wave in this interval. Repeatedly bisecting this interval allows us to converge to the stationary wave.

Using this method, we find the expected asymmetric waves. As r is increased from the bifurcation point, this pulse quickly converges to another "precursor" of the multimode pulse which bifurcates from the elementary pulse $q_u(x)$ at $r = r_1 \approx 0.621$. This pulse has the appearance of a pulse $q_u(x + T)$ concatenated with the pulse $q_w(x)$. See Figure 2.18.

Chapter 3

On the stability of stationary waves

In physical systems, the stability of waves is often as important as (and perhaps more interesting than) the problem of existence. If a pulse is not stable, then any noise in the system or a single imperfection in the initial data can cause the pulse to degrade. Stable pulses then correspond to pulses that are physically realizable. In this section we will develop tools to assess the stability of the pulses found in the previous section.

It has been suggested by Ostrovskaya et al. [7] that the multimode 1–pulses found in the previous chapter are stable for a range of the parameter r beyond the bifurcation value r^*. In particular, as r moves away from the bifurcation point, the corresponding 1–pulse may remain stable even after the total intensity profile develops a multi–humped structure. We wish to more deeply understand this stability and the mechanism which eventually causes instability as the parameter value is increased.

To begin, we consider any stationary wave given by $(U(x), W(x))$ for the equation

$$\begin{array}{ccccccccc} iu_t & + & \frac{1}{2}u_{xx} & + & h_1\left(|u|^2, |w|^2\right) u & - & u & = & 0 \\ iw_t & + & \frac{1}{2}w_{xx} & + & h_2\left(|u|^2, |w|^2\right) w & - & r\,w & = & 0. \end{array}$$

A stationary wave is a real-valued t–independent solution of this equation with tails decaying as $x \to \pm\infty$.

To proceed in the analysis of solutions of these equations, we first decompose the equation above into real and imaginary parts. Let $u = u_r + iu_i$ and $w = w_r + iw_i$. Then the governing equations may be rewritten as the real–valued system

$$\begin{array}{ccccccccc} (u_r)_t & + & \frac{1}{2}(u_i)_{xx} & + & h_1\left(u_r^2 + u_i^2, w_r^2 + w_i^2\right) u_i & - & u_i & = & 0 \\ (w_r)_t & + & \frac{1}{2}(w_i)_{xx} & + & h_2\left(u_r^2 + u_i^2, w_r^2 + w_i^2\right) w_i & - & r\,w_i & = & 0 \\ (u_i)_t & - & \frac{1}{2}(u_r)_{xx} & - & h_1\left(u_r^2 + u_i^2, w_r^2 + w_i^2\right) u_r & + & u_r & = & 0 \\ (w_i)_t & - & \frac{1}{2}(w_r)_{xx} & - & h_2\left(u_r^2 + u_i^2, w_r^2 + w_i^2\right) w_r & + & r\,w_r & = & 0. \end{array}$$

Since we wish to study the stability of stationary waves in this system, we are interested in the behavior of solutions that are small perturbations of a given stationary wave $(U(x), W(x))$. Since the stationary wave is real–valued, we can then write this as

$$\begin{bmatrix} u_r \\ w_r \\ u_i \\ w_i \end{bmatrix} = \begin{bmatrix} U \\ W \\ 0 \\ 0 \end{bmatrix} + \epsilon \begin{bmatrix} p_1 \\ p_2 \\ q_1 \\ q_2 \end{bmatrix}.$$

We linearize formally by letting $\epsilon \to 0$, and arrive at the linear system

$$
\begin{array}{ccccccccccc}
(p_1)_t & + & \frac{1}{2}(q_1)_{xx} & + & h_1(\cdot)\, q_1 & & & - & q_1 & = & 0 \\
(p_2)_t & + & \frac{1}{2}(q_2)_{xx} & + & h_2(\cdot)\, q_2 & & & - & r\, q_2 & = & 0 \\
(q_1)_t & - & \frac{1}{2}(p_1)_{xx} & - & h_1(\cdot)\, p_1 - 2U^2 D_1 h_1(\cdot)\, p_1 - 2UW D_2 h_1(\cdot)\, p_2 & & & + & p_1 & = & 0 \\
(q_2)_t & - & \frac{1}{2}(p_2)_{xx} & - & h_2(\cdot)\, p_2 - 2UW D_1 h_2(\cdot)\, p_1 - 2W^2 D_2 h_2(\cdot)\, p_2 & & & + & r\, p_2 & = & 0,
\end{array}
$$

where the character $\cdot$ replaces U^2, W^2 simply for typographical space considerations. Setting

$$
\begin{aligned}
L_- &= \tfrac{1}{2}\tfrac{d^2}{dx^2} + \begin{bmatrix} h_1(\cdot) & 0 \\ 0 & h_2(\cdot) \end{bmatrix} + \begin{bmatrix} 1 & 0 \\ 0 & r \end{bmatrix} \\
L_+ &= \tfrac{1}{2}\tfrac{d^2}{dx^2} + \begin{bmatrix} h_1(\cdot) & 0 \\ 0 & h_2(\cdot) \end{bmatrix} + \begin{bmatrix} 2U^2 D_1 h_1(\cdot) & 2UW D_2 h_1(\cdot) \\ 2UW D_1 h_2(\cdot) & 2W^2 D_2 h_2(\cdot) \end{bmatrix} + \begin{bmatrix} 1 & 0 \\ 0 & r \end{bmatrix}
\end{aligned}
$$

the linearized equation can be rewritten as

$$
\begin{bmatrix} p_1 \\ p_2 \\ q_1 \\ q_2 \end{bmatrix}_t = \begin{bmatrix} 0_{2\times 2} & -L_- \\ L_+ & 0_{2\times 2} \end{bmatrix} \begin{bmatrix} p_1 \\ p_2 \\ q_1 \\ q_2 \end{bmatrix}.
$$

Writing $v(x,t) = (p_1, p_2, q_1, q_2)$, we study instability by searching for solutions of this equation of the form $v(x,t) = v(x)e^{\lambda t}$ where $v(x)$ is a bounded function with decaying

tails and λ is a complex scalar. Of interest then are the eigenvalue equations

$$
\begin{aligned}
L_- \begin{bmatrix} q_1 \\ q_2 \end{bmatrix} &= -\lambda \begin{bmatrix} p_1 \\ p_2 \end{bmatrix} \\
L_+ \begin{bmatrix} p_1 \\ p_2 \end{bmatrix} &= \lambda \begin{bmatrix} q_1 \\ q_2 \end{bmatrix}.
\end{aligned}
$$

Explicitly, this is the system

$$
\begin{aligned}
\tfrac{1}{2}(p_1)_{xx} &= \lambda q_1 - h_1(\cdot)p_1 - 2U^2 D_1 h_1(\cdot)p_1 - 2UW D_2 h_1(\cdot)p_2 + p_1 \\
\tfrac{1}{2}(p_2)_{xx} &= \lambda q_2 - h_2(\cdot)p_2 - 2UW D_1 h_2(\cdot)p_1 - 2W^2 D_2 h_2(\cdot)p_2 + r\, p_2 \\
\tfrac{1}{2}(q_1)_{xx} &= -\lambda p_1 - h_1(\cdot)q_1 + q_1 \\
\tfrac{1}{2}(q_2)_{xx} &= -\lambda p_2 - h_2(\cdot)q_2 + r\, q_2.
\end{aligned}
$$

Letting $(v_1, v_2, v_3, v_4) = (p_1, p_2, q_1, q_2)$ and introducing the variables $v_5, \ldots, v_8$ as the derivatives with respect to x of $v_1, \ldots, v_4$, respectively, we can write this as an eight dimensional system of first order equations

$$
v' = \left[\begin{array}{c|c} 0_{4\times 4} & I_{4\times 4} \\ \hline 2\Lambda_{4\times 4} & 0_{4\times 4} \end{array}\right] v \tag{3.1}
$$

where $\Lambda_{4\times 4}$ is given by

$$\left[\begin{array}{cc|cc} 1-h_1(\cdot)-2U^2D_1h_1(\cdot) & -2UWD_2h_1(\cdot) & \lambda & 0 \\ -2UWD_1h_2(\cdot) & r-h_2(\cdot)-2W^2D_2h_2(\cdot) & 0 & \lambda \\ \hline -\lambda & 0 & 1-h_1(\cdot) & 0 \\ 0 & -\lambda & 0 & r-h_2(\cdot) \end{array}\right].$$

This formulation emphasizes the differing dependence on the real and imaginary parts of the solutions. It is sometimes also convenient to reorder the variables in order to better visualize the separate roles of the two pulse components. To this end, by reordering the components of the vector v, the matrix $\Lambda_{4\times 4}$ could alternatively be written as

$$\left[\begin{array}{cc|cc} 1-h_1(\cdot)-2U^2D_1h_1(\cdot) & \lambda & -2UWD_2h_1(\cdot) & 0 \\ -\lambda & 1-h_1(\cdot) & 0 & 0 \\ \hline -2UWD_1h_2(\cdot) & 0 & r-h_2(\cdot)-2W^2D_2h_2(\cdot) & \lambda \\ 0 & 0 & -\lambda & r-h_2(\cdot) \end{array}\right].$$

When one of the pulse components is zero, the cross terms disappear and this system is easily seen to decouple into a pair of four dimensional systems.

For either formulation, if there is a bounded solution $v(x)$ of this system associated with an eigenvalue λ with $\mathrm{Re}\,(\lambda) > 0$, then $v(x)e^{\lambda z}$ is an unstable mode of the linear equation. Moreover, this eigenvalue problem has a four–fold symmetry; i.e., if λ is an eigenvalue of this system, then so are $\bar{\lambda}$, $-\lambda$, and $-\bar{\lambda}$, where $^{-}$ denotes complex conjugation. Hence, the only chance a pulse has to be stable is for its entire spectrum to be confined to the imaginary axis.

This is the eigenvalue problem we wish to analyze for the pulses described in the previous section. Before we begin this analysis in earnest, we will build up some numerical machinery and study in full a lower dimensional example which displays a mechanism for the delayed bifurcation of eigenvalues from the essential spectrum. With this in hand, we will prove results for the three different cases:

1. **The single component pulse $q_u(x)$.** We can completely describe the spectrum in this case – and it is completely contained on the imaginary axis.

2. **The symmetric multi–component pulses $q_{|0,i\rangle}(x)$.** The initial stability for bifurcating multi–component pulses is easily explained since we know the initial configuration of eigenvalues at the bifurcation point via the results for the single component pulse. We describe a mechanism for instability using the notion of degeneracy – this is the same condition that brought about the bifurcation of multimode pulses originally. A quick check of the Maslov index in the variational equation then allows us to conclude instability for these pulses beyond such a degeneracy, using the criterion of Jones [9] or Grillakis [10].

3. **Nonsymmetric multi–component pulses.** Recall that when the symmetric multi–component pulses $q_{|0,i\rangle}(x)$ pass through a degeneracy, there is a bifurcation of nonsymmetric multi–component pulses. In many different models (see Jones [10], Aschbacher et al. [23]), it is the case that beyond such a bifurcation, the symmetric wave is unstable and the nonsymmetric waves are stable. In this case also, the instability criterion provides the possibility of stability for these waves.

4. **Multi–component N–pulses.** A primary difficulty for N–pulses is keeping track

of the myriad eigenvalues near the origin. The instability criterion of Jones [9] and Grillakis [10] is again a valuable tool, and it turns out that all N–pulses that look like N concatenated copies of the single pulse $q_{|0,i\rangle}(x)$ are unstable. This is a result of properties of the bifurcating pulse $q_{|0,i\rangle}(x)$ itself, even before consideration of the exponentially small eigenvalues near zero resulting from the glueing.

3.1 The Evans function

The usual approach to analyzing the stability of a nonlinear wave is to use the linearization of the governing equation about the wave in question. The proof of stability is then two–pronged. First, it must be shown that using only the linear information is sufficient to conclude stability in the full nonlinear problem. With this proved, one must then work to actually analyze the linear equations. In question is whether the appropriate linear operator has any spectrum in the right half of the complex plane.

A powerful tool in the latter pursuit is the Evans function. The Evans function is an analytic function on the complex plane whose zeros coincide with the eigenvalues of the nonlinear wave — and the order of the zero equals the multiplicity of the eigenvalue. Therefore, if it can be proved that the Evans function has no zeros in the right half plane, the wave will be stable. Below we describe in detail the Evans function and the steps in its computation.

Background and definition of the Evans function.

First we shall outline the fundamental ideas. For now we consider a somewhat generic N–dimensional linear equation

$$Y' = A(\lambda, x)Y = (A_0(\lambda) + R(\lambda, x))\, Y$$

which represents a linear eigenvalue problem (such as the one in the previous section) written as a first order system — the parameter λ is a prospective eigenvalue. The matrix $A_0(\lambda)$ describes the asymptotic behavior of the system while the matrix $R(\lambda, x)$ captures the transient behavior and decays exponentially as $|x| \to \infty$. If λ is not in the

essential spectrum, then the matrix $A_0(\lambda)$ does not have any purely imaginary eigenvalues and the eigenvalues of $A_0(\lambda)$ can be separated into two groups according to the signs of their real parts. Suppose that there are k eigenvalues with negative real part and $N-k$ eigenvalues with positive real part. It is then possible to find k linearly independent solutions $Y_1(\lambda,x),\ldots,Y_k(\lambda,x)$ that decay as $x\to-\infty$ and $N-k$ linearly independent solutions $Y_{k+1}(\lambda,x),\ldots,Y_N(\lambda,x)$ that decay as $x\to+\infty$. For any $x\in\mathbf{R}$, it is then possible to define subspaces $E^u(\lambda,x)=\operatorname{Span}\{Y_1(\lambda,x),\ldots,Y_k(\lambda,x)\}$ and $E^s(\lambda,x)=\operatorname{Span}\{Y_{k+1}(\lambda,x),\ldots,Y_N(\lambda,x)\}$. For any given value of x, the spaces E^u and E^s contain all of the initial conditions that decay as $x\to-\infty$ and $x\to+\infty$, respectively. Since an eigenfunction must decay both as $x\to-\infty$ and as $x\to+\infty$, λ is an eigenvalue if and only if there is a nontrivial intersection between the two subspaces $E^u(\lambda,x)$ and $E^s(\lambda,x)$ for some (and hence for any) x. As such, the Evans function may be defined as

$$E(\lambda)=Y_1(\lambda,0)\wedge\cdots\wedge Y_N(\lambda,0).$$

The Evans function then provides a measure of how far the vectors $Y_1(\lambda,0),\ldots,Y_N(\lambda,0)$ are from being linearly dependent. And if $E(\lambda)=0$, then these vectors are no longer linearly independent and hence there is an eigenfunction that decays as $x\to\pm\infty$. Therefore, for λ outside the essential spectrum, the Evans function $E(\lambda)$ is zero if and only if λ is an eigenvalue.

3.2 Numerical implementation

The theoretical properties of the Evans function are detailed in Alexander, Gardner and Jones [24], while many issues which come up in the numerical implementation are addressed in the thesis of Brin [25].

Because our current interest is in nonlinear Schrödinger-type equations, we will adopt the convention that the total dimension of the space is $2n$ and that for λ not in the essential spectrum, the number of eigenvalues of the asymptotic matrix $A_0(\lambda)$ with positive real part is the same as the number of eigenvalues with negative real part, i.e. $k = n$. Because we are not so much interested in particular solutions of this system, but rather the evolution of the entire n-dimensional subspaces $E^u(\lambda, x)$ and $E^s(\lambda, x)$, it is natural to move our consideration from simple flows in $\mathbf{R}^{2n}$ to flows on the Grassmannian space $G_n(\mathbb{C}^{2n})$. The Plücker coordinates on the space of exterior powers $\Lambda^n\mathbb{C}^{2n}$ provide a basis for this computation.

Preliminaries of $\Lambda^n\mathbb{C}^{2n}$.

In moving to the space of exterior powers, a primary computational difficulty is bypassed. In order to compute the Evans function as described above, two sets of n linearly independent solutions with appropriate decay at $+\infty$ or $-\infty$ must be computed. However, the fastest growing mode quickly dominates the numerics, leading to a "numerical" linear dependence as the n independent solutions approach multiples of the single solution with the largest eigenvalue.

However, in the associated system on $\Lambda^n\mathbb{C}^{2n}$, the eigenvalues are given by summing the various combinations of n eigenvalues of the original system (a quick proof of this fact

will be given below). In this space, the set $E^u(\lambda, x)$ is an eigenvector associated with the largest positive eigenvalue (the sum of all the positive eigenvalues of the original system). Likewise, $E^s(\lambda, x)$ is the eigenvector associated with the negative eigenvalue of largest magnitude. Hence, these spaces are easy to track numerically.

We can describe elements of the space $\Lambda^n \mathbb{C}^{2n}$ with the use of the wedge product $\wedge$. The $\wedge$ can be defined on $\underbrace{\mathbb{C}^{2n} \times \cdots \times \mathbb{C}^{2n}}_{n \text{ times}}$ by enforcing n-multilinearity and antisymmetry. If $v_1, \ldots, v_n, w_1$ and w_2 are vectors in $\mathbb{C}^{2n}$ and α is a scalar in $\mathbb{C}$, then these properties may be defined as follows:

i. n-multilinearity

$$\begin{aligned} & v_1 \wedge \cdots \wedge v_{i-1} \wedge (w_1 + \alpha w_2) \wedge v_{i+1} \wedge \cdots \wedge v_n \\ & = v_1 \wedge \cdots v_{i-1} \wedge w_1 \wedge v_{i+1} \wedge \cdots \wedge v_n \\ & \quad + \alpha\, v_1 \wedge \cdots \wedge v_{i-1} \wedge w_2 \wedge v_{i+1} \wedge \cdots \wedge v_n. \end{aligned}$$

ii. antisymmetry

$$\begin{aligned} & v_1 \wedge \cdots \wedge v_{i-1} \wedge v_i \wedge v_{i+1} \wedge v_{i+2} \wedge \cdots \wedge v_n \\ & = -v_1 \wedge \cdots v_{i-1} \wedge v_{i+1} \wedge v_i \wedge v_{i+2} \wedge \cdots \wedge v_n. \end{aligned}$$

In particular, antisymmetry implies that if any two vectors among $v_1, \ldots, v_n$ are equal, then $v_1 \wedge \cdots \wedge v_n = 0$; this is sometimes even taken as the definition for antisymmetry. If the vectors $e_1, \ldots, e_{2n}$ represent the usual basis for $\mathbb{C}^{2n}$, then the basis for $\Lambda^n \mathbb{C}^{2n}$ will be

generated by

$$\{e_{i_1} \wedge e_{i_2} \wedge \cdots \wedge e_{i_n} | 1 \leq i_1 < i_2 < \cdots < i_n \leq 2n\}$$

and an arbitrary element of $\Lambda^n \mathbb{C}^{2n}$ will look like

$$v = \sum_{1 \leq i_1 < i_2 < \cdots < i_n \leq 2n} v_{i_1 i_2 \cdots i_n} \; e_{i_1} \wedge e_{i_2} \wedge \cdots \wedge e_{i_n}.$$

Given n vectors $v^1, \ldots, v^n \in \mathbb{C}^{2n}$, the associated n-form may be computed

$$\begin{aligned}
& v^1 \wedge \cdots \wedge v^n \\
&= \left(\sum_{i_1=1}^{2n} v^1_{i_1} \; e_{i_1} \right) \wedge \cdots \wedge \left(\sum_{i_n=1}^{2n} v^n_{i_n} \; e_{i_n} \right) \\
&= \sum_{i_1=1}^{2n} \cdots \sum_{i_n=1}^{2n} v^1_{i_1} \; e_{i_1} \wedge \cdots \wedge v^n_{i_n} \; e_{i_n} \\
&= \sum_{i_1=1}^{2n} \cdots \sum_{i_n=1}^{2n} (v^1_{i_1} \cdots v^n_{i_n}) \; e_{i_1} \wedge \cdots \wedge e_{i_n} \\
&= \sum_{i_1=1}^{n} \sum_{i_2=i_1+1}^{n+1} \cdots \sum_{i_n=i_{n-1}+1}^{2n} V_{i_1 i_2 \cdots i_n} \; e_{i_1} \wedge \cdots \wedge e_{i_n}
\end{aligned}$$

where

$$V_{i_1 i_2 \cdots i_n} = \det \begin{bmatrix} v^1_{i_1} & v^2_{i_1} & \cdots & v^n_{i_1} \\ v^1_{i_2} & v^2_{i_2} & \cdots & v^n_{i_2} \\ \vdots & \vdots & \ddots & \vdots \\ v^1_{i_n} & v^2_{i_n} & \cdots & v^n_{i_n} \end{bmatrix}.$$

We are then interested in the evolution of the $\binom{2n}{n}$ coefficients $V_{i_1 i_2 \cdots i_n}$. To derive the

appropriate evolution equation, we note that if $Y_1, \ldots, Y_n$ are solutions of the original ODE, then $Y = Y_1 \wedge \cdots \wedge Y_n$ should be a solution of the appropriate system in $\Lambda^n(\mathbb{C}^{2n})$. And Y will satisfy the linear ODE

$$\begin{aligned} Y' &= \textstyle\sum_{i=1}^n Y_1 \wedge \cdots \wedge Y_{i-1} \wedge Y_i' \wedge Y_{i+1} \wedge \cdots \wedge Y_n \\ &= \textstyle\sum_{i=1}^n Y_1 \wedge \cdots \wedge Y_{i-1} \wedge A(\lambda, x) Y_i \wedge Y_{i+1} \wedge \cdots \wedge Y_n. \end{aligned}$$

These relationships then define a $\binom{2n}{n} \times \binom{2n}{n}$ matrix $\tilde{A}(\lambda, x)$ so that

$$Y' = \tilde{A}(\lambda, x) Y.$$

This is the system that we solve numerically. Just as we wrote the original system in terms of its transient and asymptotic parts, we may also decompose $\tilde{A}(\lambda, x)$ as $\tilde{A}(\lambda, x) = \tilde{A}_0(\lambda) + \tilde{R}(\lambda, x)$. The promised result concerning the eigenvalues of $\tilde{A}_0$ is proved here.

Lemma 3.1. Suppose $\tilde{A}_0$ is a $2n \times 2n$ matrix with eigenvalues $\mu_1, \ldots, \mu_{2n}$ and associated eigenvectors $V_1, \ldots, V_{2n}$. Then the eigenvalues and eigenvectors of $\tilde{A}_0$ are given by $\mu_{i_1} + \cdots + \mu_{i_n}$ and $V_{i_1} \wedge \cdots \wedge V_{i_n}$ for $1 \leq i_1 < i_2 < \cdots < i_n \leq 2n$.

Proof. Let the indices $1 \leq i_1 < i_2 < \cdots < i_n \leq 2n$ be given. Then

$$\begin{aligned}
&\tilde{A}_0(V_{i_1} \wedge \cdots \wedge V_{i_n}) \\
&\quad = \sum_{j=1}^{n} Y_{i_1} \wedge \cdots \wedge Y_{i_{j-1}} \wedge A_0 Y_{i_j} \wedge Y_{i_{j+1}} \wedge \cdots \wedge Y_{i_n} \\
&\quad = \sum_{j=1}^{n} Y_{i_1} \wedge \cdots \wedge Y_{i_{j-1}} \wedge \mu_{i_j} Y_{i_j} \wedge Y_{i_{j+1}} \wedge \cdots \wedge Y_{i_n} \\
&\quad = \left(\sum_{j=1}^{n} \mu_{i_j} \right) Y_{i_1} \wedge \cdots \wedge Y_{i_n}.
\end{aligned}$$

□

The numerical algorithm.

For λ outside of the essential spectrum, the numerical algorithm consists of the following steps:

1. Choosing the appropriate asymptotic conditions.

2. Translating into wedge space.

3. Evolving forward and backward in wedge space.

4. Calculating the Evans function $E(\lambda)$ at $x = 0$.

Step 1: Choosing the asymptotic conditions.

Since we have an explicit representation of the matrix $A_0(\lambda)$, we can often derive exact expressions for the eigenvalues and their associated eigenvectors. This will be the case in all of our examples and we can easily choose expressions for the eigenvectors of $A_0(\lambda)$ which are analytic in λ. If no such exact formulas are available, Brin and

Zumbrun [26] have developed a nice scheme for numerically computing analytic asymptotic conditions. In any connected component of $\mathbb{C}$ disjoint from the essential spectrum, we can then analytically define eigenvalues $\mu_1(\lambda), \ldots, \mu_n(\lambda), \mu_{n+1}(\lambda), \ldots, \mu_{2n}(\lambda)$ of $A_0(\lambda)$. And because we avoid the essential spectrum, the signs of the real parts of each eigenvalue $\mu_i(\lambda)$ cannot change with λ. We therefore dictate that $\mu_1(\lambda), \ldots, \mu_n(\lambda)$ have positive real parts and $\mu_{n+1}(\lambda), \ldots, \mu_{2n}(\lambda)$ have negative real parts inside $\mathbb{C} \setminus \sigma_{ess}$.

Step 2: Translating into wedge space.

Both the initial conditions and the evolution equations must be translated into Plücker coordinates on the wedge product space. For smaller dimensional problems this can be done by hand. For example, if $n = 2$ and $k = 1$, then the translation to 1–forms is merely the identity; if $n = 4$ and $k = 2$, the we move to a wedge product space $\Lambda^2\mathbb{C}^4$ which is six dimensional. However, our primary example has $n = 8$ and $k = 4$, leading to the seventy dimensional space $\Lambda^4\mathbb{C}^8$. Here, it helps to automate the process somewhat.

First of all, we need to define an enumeration of the basis

$$\{e_{i_1} \wedge e_{i_2} \wedge \cdots \wedge e_{i_n} \mid 1 \leq i_1 < i_2 < \cdots < i_n \leq 2n\}.$$

In particular, we can define a bijective map

$$\phi : \{e_{i_1} \wedge e_{i_2} \wedge \cdots \wedge e_{i_n} | 1 \leq i_1 < i_2 < \cdots < i_n \leq 2n\} \to \left\{1, 2, \ldots, \binom{2n}{n}\right\}$$

given by

$$\begin{aligned}&\phi\left(e_{i_1}\wedge e_{i_2}\wedge\cdots\wedge e_{i_n}\right)\\&\quad=\binom{2n-i_n}{n}+\binom{2n-i_{n-1}}{n-1}+\binom{2n-i_{n-2}}{n-2}+\ldots+\binom{2n-i_2}{2}+\binom{2n-i_1}{1}+1.\end{aligned}$$

This is equivalent to the usual ordering of the associated binary sequences of $2n$ elements. The basis n-form $e_{i_1}\wedge e_{i_2}\wedge\cdots\wedge e_{i_n}$ is associated with a $2n$ digit binary number with 1's in the positions $i_1, i_2, \ldots i_n$ and a 0's elsewhere. Counting only the binary sequences with an equal number of zeros and ones yields the function ϕ given above. This characterization makes it clear that if $\phi(e_{i_1}\wedge e_{i_2}\wedge\cdots\wedge e_{i_n})=i$, then the complementary n-form (spanned by the n remaining 1-forms) is numbered as $\binom{2n}{n}-i+1$.

For the evolution of the unstable subspace $E^u(\lambda,x)$ from $x=-\infty$, we need the space spanned by the eigenvectors associated to all of the eigenvalues of A_0 of positive real part. For any given value of λ, these are the eigenvalues $\mu_1(\lambda),\ldots,\mu_n(\lambda)$ with associated eigenvectors $v_1(\lambda),\ldots,v_n(\lambda)$. If these vectors are considered as the columns of a $2n\times n$ matrix $V(\lambda)$, then the initial condition for the coefficient of the basis vector $e_{i_1}\wedge e_{i_2}\wedge\cdots\wedge e_{i_n}$ will be given by computing the determinant of the $n\times n$ matrix derived by including only the rows $i_1, i_2, \ldots, i_n$ of V. So

$$\lim_{x\to-\infty} Y^+_{\phi(e_{i_1}\wedge e_{i_2}\wedge\cdots\wedge e_{i_n})}(\lambda,x)=\det\begin{bmatrix} v_1^{i_1} & v_2^{i_1} & \cdots & v_n^{i_1}\\ v_1^{i_2} & v_2^{i_2} & \cdots & v_n^{i_2}\\ \vdots & \vdots & \ddots & \vdots\\ v_1^{i_n} & v_2^{i_n} & \cdots & v_n^{i_n}\end{bmatrix}.$$

The initial conditions at $x = +\infty$ corresponding to $E^s(\lambda, x)$ are computed analogously using the eigenvalues of negative real part and their associated eigenvectors.

Step 3: Evolving forward and backward in wedge space.

The numerical method will not be implemented on the whole real line $\mathbf{R}$, but on a sufficiently large interval $[-M, M]$. The limit M is chosen large enough so that the transient matrix $R(\lambda, \pm M)$ is sufficiently small and therefore the initial conditions computed for the asymptotic systems offer a reasonable approximation to the stable and unstable subspaces. Also, because the spaces we wish to track numerically are the stable and unstable subspaces themselves, these nearby approximations will converge to the desired subspaces at a rate proportional to the spectral gap. Therefore, to increase the accuracy of our computation, one can simply increase the value M.

We evolve the initial conditions via the $\binom{2n}{n}$ dimensional equation derived earlier. Because the space of interest is the eigenspace associated with the largest positive eigenvalue, the size of the coefficients initially grows at a rate of $\mu^+ = \mu_1(\lambda) + \cdots + \mu_n(\lambda)$. To ease in the computation, we augment the differential equation as follows:

$$Y' = \left(\tilde{A}(\lambda, x) - \mu^+ I\right) Y.$$

The asymptotic system for this augmented ODE has a single zero eigenvalue and $\binom{2n}{n} - 1$ negative eigenvalues, and we are tracing the solution which is asymptotic to the null eigenvector. This also highlights the property that nearby approximations will converge down to the desired solution $E^u(\lambda, x)$. This now remains nearly constant for as long as μ^+ remains a reasonable approximation to the leading eigenvalue of $\tilde{A}$. This has the added

benefit that the asymptotic conditions can be defined in a consistent manner even before invoking linearity, in particular, the scale of the solution $E^u(\lambda, x)$ evaluated at $x = 0$ is independent of M.

Step 4: Calculating the Evans function $E(\lambda)$ at $x = 0$.

Once $E^u(\lambda, 0)$ and $E^s(\lambda, 0)$ have been calculated, it remains simply to calculate

$$E(\lambda) = E^u(\lambda, 0) \wedge E^s(\lambda, 0).$$

Because of the antisymmetry property and the enumeration scheme, this calculation can be reduced to a particularly simple form:

$$\begin{aligned}
E(\lambda) &= E^u(\lambda, 0) \wedge E^s(\lambda, 0) \\
&= \left(\sum_{1 \le i_1 < i_2 < \cdots < i_n \le 2n} y^+_{\phi(e_{i_1} \wedge e_{i_2} \wedge \cdots \wedge e_{i_n})}(\lambda, 0)\ e_{i_1} \wedge e_{i_2} \wedge \cdots \wedge e_{i_n} \right) \\
&\qquad \wedge \left(\sum_{1 \le i_1 < i_2 < \cdots < i_n \le 2n} y^-_{\phi(e_{i_1} \wedge e_{i_2} \wedge \cdots \wedge e_{i_n})}(\lambda, 0)\ e_{i_1} \wedge e_{i_2} \wedge \cdots \wedge e_{i_n} \right) \\
&= \sum_{1 \le i_1 < i_2 < \cdots < i_n \le 2n} y^+_{\phi(e_{i_1} \wedge e_{i_2} \wedge \cdots \wedge e_{i_n})}(\lambda, 0) y^-_{\binom{2n}{n} + 1 - \phi(e_{i_1} \wedge e_{i_2} \wedge \cdots \wedge e_{i_n})}(\lambda, 0) \\
&\qquad e_{i_1} \wedge e_{i_2} \wedge \cdots \wedge e_{i_n} \wedge \phi^{-1}\left(\binom{2n}{n} + 1 - \phi(e_{i_1} \wedge e_{i_2} \wedge \cdots \wedge e_{i_n}) \right) \\
&= \sum_{j=1}^{\binom{2n}{n}} y^+_j(\lambda, 0) y^-_{\binom{2n}{n}+1-j}(\lambda, 0)\ \phi^{-1}(j) \wedge \phi^{-1}\left(\binom{2n}{n} + 1 - j \right) \\
&= \sum_{j=1}^{\binom{2n}{n}} y^+_j(\lambda, 0) y^-_{\binom{2n}{n}+1-j}(\lambda, 0)\ \sigma(j)\ e_1 \wedge e_2 \wedge \cdots \wedge e_{2n}
\end{aligned}$$

where

$$\sigma(j) = \begin{cases} 1 & \text{if the number of transpositions of successive elements taking} \\ & \phi^{-1}(j) \wedge \phi^{-1}(\binom{2n}{n} - j + 1) \text{ to } e_1 \wedge e_2 \wedge \cdots \wedge e_n \text{ is even} \\ -1 & \text{if the number of transpositions of successive elements taking} \\ & \phi^{-1}(j) \wedge \phi^{-1}(\binom{2n}{n} - j + 1) \text{ to } e_1 \wedge e_2 \wedge \cdots \wedge e_n \text{ is odd.} \end{cases}$$

With this technology now at our disposal, we will first use the Evans function to explore eigenvalues bifurcating from the essential spectrum in a toy example. We will then see what can be said, both numerically and theoretically, about the full problem of pulses in coupled Schrödinger equations.

3.3 A motivating example

Numerical work by Ostrovskaya et al. [7] has shown eigenvalues bifurcating out of the essential spectrum for multi–component solutions of the coupled Schrödinger equations. In order to better understand the mechanism for the creation of these eigenvalues, we propose to study a much simpler eigenvalue problem given by

$$Y' = \left(\begin{bmatrix} 0 & 1 \\ \lambda & 0 \end{bmatrix} + \begin{bmatrix} 0 & 0 \\ -\chi_{[-\mu,0]}(t) & 0 \end{bmatrix} \right) Y.$$

This example is intended to convey a similar flavor to actual systems, but should not be thought of as the linearization about a pulse in any actual system. In this example, we can locate eigenvalues by explicitly calculating the Evans function. We know from a simple Sturm–Liouville analysis that the spectrum is composed entirely of

- essential spectrum consisting of the entire negative real axis
- point spectrum consisting of a finite number of real eigenvalues between zero and one.

In fact, as the parameter μ is increased, eigenvalues bifurcate out of the branch point at the right hand end of the essential spectrum and accumulate at $\lambda = 1$. Of special interest is understanding the origin of these bifurcating eigenvalues. Using the Evans function extended through the essential spectrum, we will locate and track these zeros of the Evans function.

We will follow the steps detailed in the previous section regarding the calculation of the Evans function.

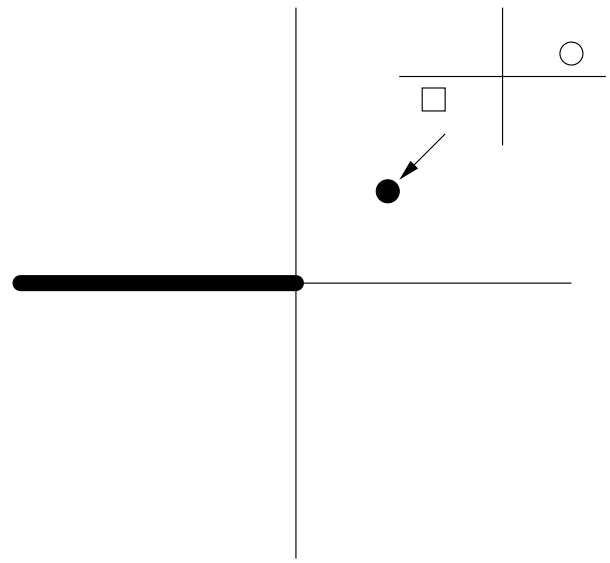

Figure 3.1: For any potential eigenvalue λ outside of the essential spectrum, the eigenvalues of the associated asymptotic system are given by $\sqrt{\lambda}$ and $-\sqrt{\lambda}$. The eigenvalue associated with the asymptotic condition at $-\infty$ is marked with a box, while the condition for $+\infty$ is marked with a circle.

Step 1: Choice of the asymptotic conditions.

For any value of λ outside of the essential spectrum, the eigenvalue/eigenvector pairs that determine the asymptotic conditions are

- $\sqrt{\lambda}$, $(1, \sqrt{\lambda})^T$
- $-\sqrt{\lambda}$, $(1, -\sqrt{\lambda})^T$.

One can quickly verify that $\sqrt{\lambda}$ and $-\sqrt{\lambda}$ are purely imaginary only within the set $\{\lambda \in \mathbb{C} \mid \operatorname{Re}\lambda \leq 0, \operatorname{Im}\lambda = 0\}$, and hence this set represents the essential spectrum. Choosing the usual branch of the function $\sqrt{\cdot}$, we use the eigenvector associated with the eigenvalue with positive real part ($\sqrt{\lambda}$) as the "initial condition" at $t = -\infty$. Likewise, we choose the eigenvector associated with the eigenvalue $-\sqrt{\lambda}$ as the "initial condition" at $t = +\infty$.

Step 2: Translation into wedge space.

Because the stable and unstable eigenspaces in the asymptotic system are both one–dimensional, the translation to the space of 1–forms is simply the identity.

Step 3: Evolution.

The evolution of these 1–forms (vectors) can be explicitly computed. Recall that we rescale the system as

$$Y' = \left(\begin{bmatrix} 0 & 1 \\ \lambda & 0 \end{bmatrix} + \begin{bmatrix} 0 & 0 \\ -\chi_{[-\mu,0]}(t) & 0 \end{bmatrix} - \begin{bmatrix} \sqrt{\lambda} & 0 \\ 0 & \sqrt{\lambda} \end{bmatrix} \right) Y.$$

Then the solution Y^u which is asymptotic to $(1, \sqrt{\lambda})^T$ also has $Y^u(-\mu) = (1, \sqrt{\lambda})^T$. Similarly, $Y^s(0) = (1, \sqrt{\lambda})^T$. All that remains is to evolve Y^u from $t = -\mu$ to $t = 0$ via the transient system.

Between $t = -\mu$ and $t = 0$, this rescaled system reduces to the autonomous system

$$Y' = \begin{bmatrix} -\sqrt{\lambda} & 1 \\ \lambda - 1 & -\sqrt{\lambda} \end{bmatrix} Y$$

with eigenvalue / eigenvector pairs given by

- $\sqrt{\lambda} - 1$, $(1, \sqrt{\lambda - 1})^T$
- $-\sqrt{\lambda} - 1$, $(1, -\sqrt{\lambda - 1})^T$.

The initial condition $(1, \sqrt{\lambda})^T$ can be written as

$$\begin{bmatrix} 1 \\ \sqrt{\lambda} \end{bmatrix} = \frac{1}{2}\left(1 + \frac{\sqrt{\lambda}}{\sqrt{\lambda-1}}\right)\begin{bmatrix} 1 \\ \sqrt{\lambda-1} \end{bmatrix} + \frac{1}{2}\left(1 - \frac{\sqrt{\lambda}}{\sqrt{\lambda-1}}\right)\begin{bmatrix} 1 \\ -\sqrt{\lambda-1} \end{bmatrix}.$$

Hence

$$Y^u(0) = \begin{bmatrix} \frac{1}{2} + \frac{1}{2}\frac{\sqrt{\lambda}}{\sqrt{\lambda-1}} \\ \frac{1}{2}\sqrt{\lambda-1} + \frac{1}{2}\sqrt{\lambda} \end{bmatrix} e^{(\sqrt{\lambda-1}-\sqrt{\lambda})\mu} + \begin{bmatrix} \frac{1}{2} - \frac{1}{2}\frac{\sqrt{\lambda}}{\sqrt{\lambda-1}} \\ -\frac{1}{2}\sqrt{\lambda-1} + \frac{1}{2}\sqrt{\lambda} \end{bmatrix} e^{(-\sqrt{\lambda-1}-\sqrt{\lambda})\mu}.$$

4. Calculation of the Evans function $E(\lambda)$.

The Evans function is now given by taking the wedge product of the forward solution $Y^u(0)$ and the backward solution $Y^s(0)$.

$$\begin{aligned}
E(\lambda) &= Y^u(0) \wedge Y^s(0) \\
&= \left(\begin{bmatrix} \frac{1}{2} + \frac{1}{2}\frac{\sqrt{\lambda}}{\sqrt{\lambda-1}} \\ \frac{1}{2}\sqrt{\lambda-1} + \frac{1}{2}\sqrt{\lambda} \end{bmatrix} e^{(\sqrt{\lambda-1}-\sqrt{\lambda})\mu} + \begin{bmatrix} \frac{1}{2} - \frac{1}{2}\frac{\sqrt{\lambda}}{\sqrt{\lambda-1}} \\ -\frac{1}{2}\sqrt{\lambda-1} + \frac{1}{2}\sqrt{\lambda} \end{bmatrix} e^{(-\sqrt{\lambda-1}-\sqrt{\lambda})\mu} \right) \\
&\quad \wedge \begin{bmatrix} 1 \\ -\sqrt{\lambda} \end{bmatrix} \\
&= \frac{1}{2}\left(-2\sqrt{\lambda} - \frac{2\lambda-1}{\sqrt{\lambda-1}}\right) e^{(\sqrt{\lambda-1}-\sqrt{\lambda})\mu} + \frac{1}{2}\left(-2\sqrt{\lambda} + \frac{2\lambda-1}{\sqrt{\lambda-1}}\right) e^{(-\sqrt{\lambda-1}-\sqrt{\lambda})\mu} \\
&= e^{-\sqrt{\lambda}\mu}\left(-2\sqrt{\lambda}\cosh\sqrt{\lambda-1}\,\mu - \frac{2\lambda-1}{\sqrt{\lambda-1}}\sinh\sqrt{\lambda-1}\,\mu\right).
\end{aligned}$$

See Figure 3.2. For the critical values of λ on the real axis between zero and one, we have

$$E(\lambda) = e^{-\sqrt{\lambda}\,\mu}\left(-2\sqrt{\lambda}\cos\sqrt{1-\lambda}\,\mu - \frac{2\lambda-1}{\sqrt{1-\lambda}}\sin\sqrt{1-\lambda}\,\mu\right).$$

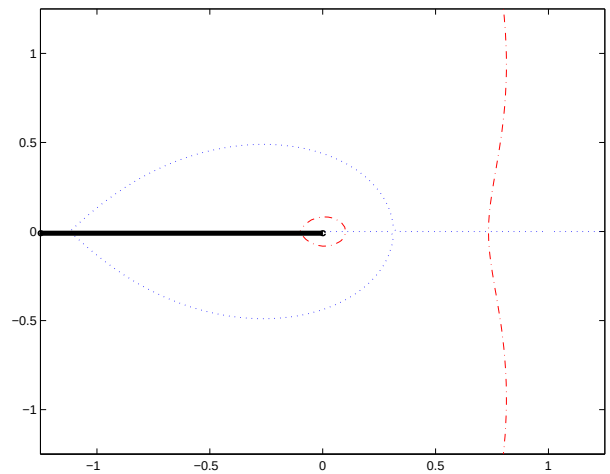

Figure 3.2: The Evans function $E(\lambda)$ in a neighborhood of the origin for $\mu = 4$. The thick black line is the essential spectrum, where the Evans function is undefined. The imaginary part of E is zero along the blue dashed curves, while the real part of E is zero along the red dash–dotted curves. For this value of μ, there are two real eigenvalues.

Since $e^{-\sqrt{\lambda}\mu} \neq 0$, for $\lambda \neq 0.5$, $E(\lambda) = 0$ if and only if

$$\frac{1}{\sqrt{1-\lambda}}\left(\tan^{-1}\left(\frac{-2\sqrt{\lambda(1-\lambda)}}{2\lambda-1}\right) - k\pi\right) = \mu$$

for some integer k. The remaining value $\lambda = 0.5$ is an eigenvalue if and only if $\mu = \sqrt{2}(0.5\pi + k\pi)$ for some integer k. The eigenvalues in the interval $(0, 1)$ are then located as in Figure 3.3. Note in particular that as μ varies, eigenvalues bifurcate from the branch point at $\lambda = 0$ exactly when

$$\mu = k\pi.$$

Extension of the Evans function.

To better understand the origin of these bifurcating eigenvalues, we must extend the Evans function through the essential spectrum. Within the essential spectrum, there are

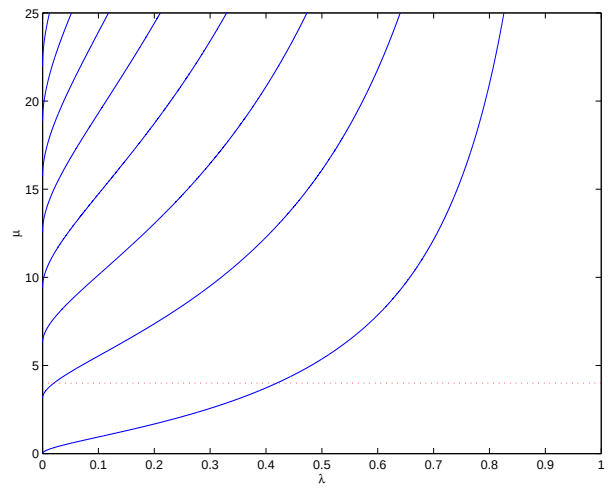

Figure 3.3: Zeros of the Evans function $E(\lambda)$ vary as μ is increased. In this example, eigenvalues bifurcate from the essential spectrum when the parameter μ passes through multiples of π.

two possible extensions for the Evans function, corresponding to choosing the asymptotic conditions continuously from either above or below, see Figure 3.4. By extending this assignment of asymptotic conditions through the essential spectrum and into the lower (or upper) half plane, we have an analytically extended Evans function whose zeros no longer necessarily correspond to eigenvalues of our system, as the associated "eigenvectors" are not guaranteed to decay. However, as the parameter μ varies, it is possible that the location of these zeros will change and that they may move into a region where the Evans function has not been artificially extended, where they will represent actual eigenvalues.

Of particular note is that there are no eigenvalues embedded within the essential spectrum itself. Indeed, for values of λ in the essential spectrum, the two possible extensions

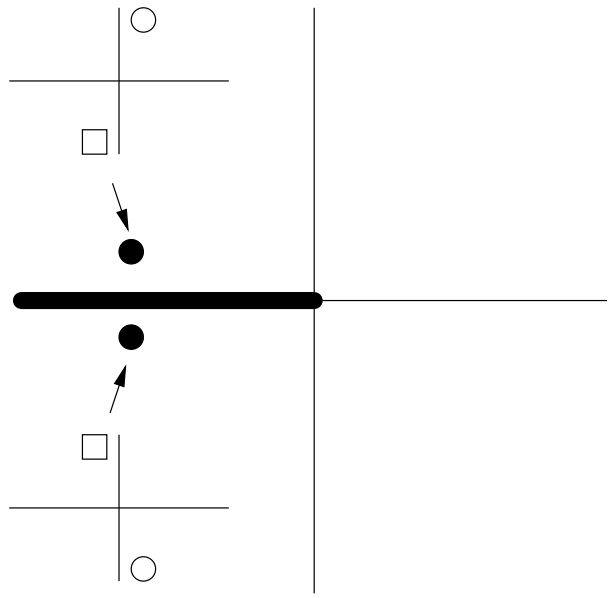

Figure 3.4: The asymptotic conditions are chosen in a different manner on opposite sides of the essential spectrum.

of the Evans function reduce to

$$\begin{aligned} E(\lambda) &= e^{\pm i\sqrt{-\lambda}\mu}\left(\mp 2i\sqrt{-\lambda}\cos\sqrt{1-\lambda}\,\mu - \frac{-1+2\lambda}{\sqrt{1-\lambda}}\sin\sqrt{1-\lambda}\,\mu\right) \\ &= \left(\cos(\sqrt{-\lambda}\,\mu) \pm i\sin(\sqrt{-\lambda}\,\mu)\right)\left(\mp 2i\sqrt{-\lambda}\cos\sqrt{1-\lambda}\,\mu - \frac{-1+2\lambda}{\sqrt{1-\lambda}}\sin\sqrt{1-\lambda}\,\mu\right). \end{aligned}$$

Since $\sin(\cdot)$ and $\cos(\cdot)$ are never simultaneously zero and all of the coefficients are nonzero for $\lambda < 0$, $E(\lambda) \neq 0$ within the essential spectrum.

We can extend the Evans function not only to the essential spectrum, but through it. One simple way to understand this extension is by making the substitution $\gamma^2 = \lambda$. Then the eigenvalue / eigenvector pairs for the asymptotic system are given by

- $\gamma, \ \ (1, \gamma)$
- $-\gamma, \ \ (1, -\gamma)$.

For any γ in the complex plane, we then choose $(1, \gamma)$ as the asymptotic condition at $x = -\infty$ and $(1, -\gamma)$ as the condition at $x = +\infty$. For γ in the right half plane, the associated function $E(\gamma)$ is related to the true Evans function. For γ in the left half plane, the asymptotic conditions have been reversed so that the computed subspaces grow rather than decay — this is the regime of the extended Evans function. We have unfolded the branch point $\lambda = 0$, and have extended the Evans function to an analytic function on a two–sheeted Riemann surface, see Figure 3.5.

As previously mentioned, "eigenvalues" move through zero and onto the positive real γ–axis when μ passes through multiples of π. Now we can see the origin of these eigenvalues. In the left half plane, there is an infinite family of zeros of the extended Evans function $E(\cdot)$ located along a vertical curve. As μ increases, the locations of these zeros move pairwise toward the real axis. When a conjugate pair meets on the negative real axis, they separate moving right and left. The left–moving zero approaches $\gamma = -1$ as $\mu \to \infty$, and the right–moving zero passes through $\gamma = 0$ and onto the positive real axis (where it now represents a true eigenvalue), going to $\gamma = +1$ as $\mu \to \infty$.

This example has demonstrated a mechanism by which eigenvalues may emerge from the essential spectrum as a parameter is varied. We will relate the mechanism shown here with a possible mechanism for eigenvalue creation in the coupled Schrödinger model in the next section.

Remark 3.2. In retrospect, it is not surprising that resonant poles accumulate at $\lambda = 1$ on the second Riemann sheet concurrently with eigenvalues accumulating at $\lambda = 1$ on the first. Consider the winding argument that counts the eigenvalues on the positive real λ–axis on the first sheet. The monotonicity of the eigenvalues with respect to λ is based

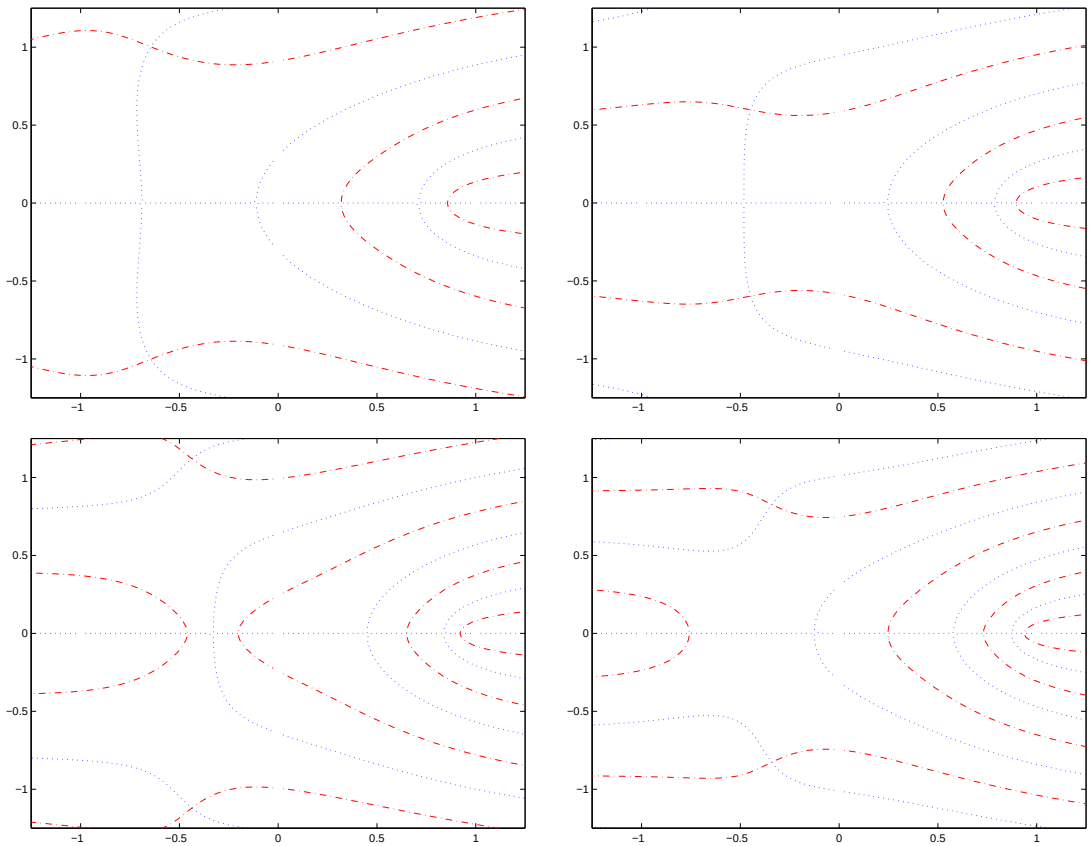

Figure 3.5: The Evans function $E(\gamma)$ extended to the two–sheeted Riemann surface using the map $\gamma^2 = \lambda$, for $\mu = 4, 5, 6$ and 7. For $\mu = 4$, we still see the two true eigenvalues (in the right half plane) as before. The positive and negative imaginary axis now correspond to the two different extensions of the Evans function to the essential spectrum. In this extension for $\mu = 4$, we also see a pair of complex valued resonance poles – zeros of the extended Evans function in the left half plane. As μ is increased, these poles meet on the negative γ axis (corresponding to the positive real axis on the second Riemann sheet), and one then moves through zero and becomes an eigenvalue as μ passes through 2π.

upon two factors: first, as λ increases, the speed of the winding decreases, until eventually the transient system is hyperbolic and there is no winding at all; second, as λ increases, the asymptotic states that provide the shooting values move apart. On the second sheet, the winding is the same, but now the roles of the asymptotic states have been reversed, so that, as λ increases, they are moving closer together. Since the winding is the dominant effect for large values of μ, zeros of the extended Evans function accumulate at $\lambda = 1$ on the second sheet just as they do on the first. However, because the monotonicity property no longer holds, there is the possibility of pairs of eigenvalues appearing in the interval $(0, 1)$ on the second sheet that would not be counted in a winding argument.

3.4 The single–component pulse $q_u(x)$

We are now prepared to begin our search for eigenvalues for pulses in the coupled nonlinear Schrödinger equations. For the stationary wave $q_u(x) = (U(x), 0)$ with trivial w-component, the eigenvalue equation (3.1) decouples into a pair of 4×4 systems

$$\begin{bmatrix} v_1 \\ v_2 \\ v_5 \\ v_6 \end{bmatrix}' = \left[\begin{array}{cc|cc} 0 & 0 & 1 & 0 \\ 0 & 0 & 0 & 1 \\ \hline 2(1 - h_1(\cdot) - 2U^2 D_1 h_1(\cdot)) & 2\lambda & 0 & 0 \\ -2\lambda & 2(1 - h_1(\cdot)) & 0 & 0 \end{array}\right] \begin{bmatrix} v_1 \\ v_2 \\ v_5 \\ v_6 \end{bmatrix} \tag{3.2}$$

and

$$\begin{bmatrix} v_3 \\ v_4 \\ v_7 \\ v_8 \end{bmatrix}' = \left[\begin{array}{cc|cc} 0 & 0 & 1 & 0 \\ 0 & 0 & 0 & 1 \\ \hline 2(r - h_2(\cdot)) & 2\lambda & 0 & 0 \\ -2\lambda & 2(r - h_2(\cdot)) & 0 & 0 \end{array}\right] \begin{bmatrix} v_3 \\ v_4 \\ v_7 \\ v_8 \end{bmatrix}. \tag{3.3}$$

The spectrum of the stationary wave will then be the union of the spectra of these two individual systems. These two contributions to the spectrum are described in the following two lemmas.

Lemma 3.3. For the first subsystem (3.2), the essential spectrum is purely imaginary encompassing the entire imaginary axis except for an open gap between $-i$ and i, in particular, $\sigma_e = \{x + iy \mid x = 0, |y| \geq 1\}$. There is an eigenvalue at the origin which has geometric multiplicity 2 and algebraic multiplicity 4. For the saturable nonlinearity of

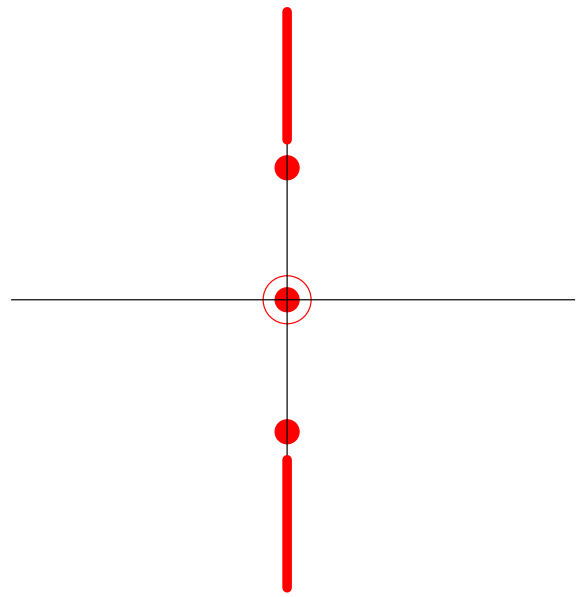

Figure 3.6: The spectrum of the first subsystem (3.2).

the Ostrovskaya–Kivshar problem, there are also a pair of eigenvalues in the gap on the imaginary axis near the branch points of the essential spectrum. See Figure 3.6.

The first system (3.2) is the usual Schrödinger equation with an intensity–dependent nonlinearity and the spectrum is well known. The essential spectrum is defined à la Henry [27], and contains the set of points at which the asymptotic matrix has eigenvalues on the imaginary axis. It is a quick calculation that the asymptotic matrix has eigenvalues $\pm\sqrt{2(r \pm i\lambda)}$ and hence λ is in the essential spectrum if and only if either $r+i\lambda$ or $r-i\lambda$ is a non-positive real number. The point spectrum at zero is determined by the symmetries present in the system. There is an eigenfunction $(U'(x), 0, U''(x), 0)$ associated with the translation invariance of the solution; i.e. if $U(x)$ is a solution then so is $U(x+\epsilon)$ for any ϵ. Similarly, there is an eigenfunction $(0, U(x), 0, U'(x))$ stemming from the phase invariance; given a solution $U(x)$, $U(x)e^{i\epsilon}$ is also a solution for any ϵ.

Depending upon the specific form of the function $h_1(\cdot)$ there may be other point

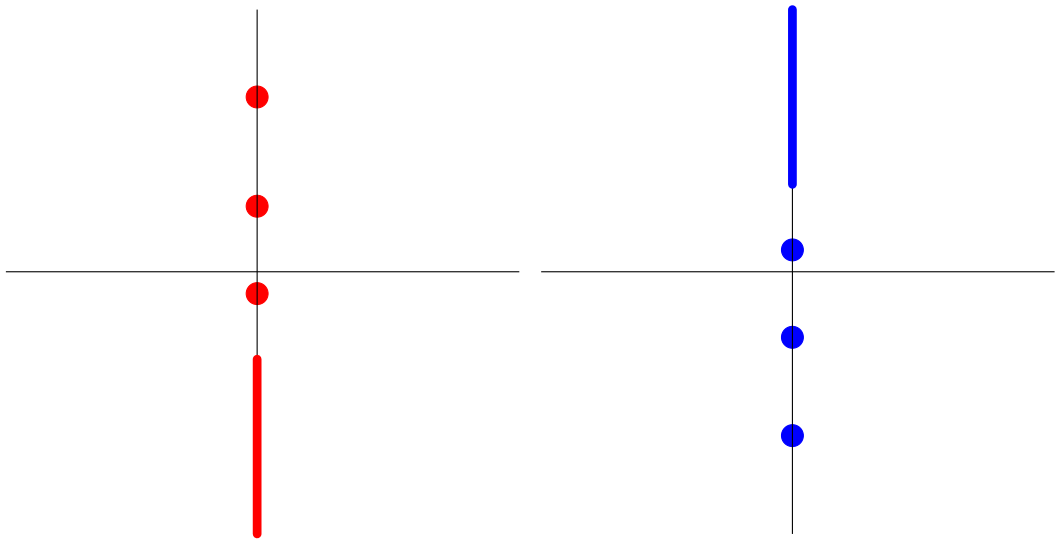

Figure 3.7: The spectrum of the second subsystem (3.3) is the union of two reflected components.

spectrum as well. For instance, with the saturable nonlinearity used by Ostrovskaya and Kivshar, with saturability parameter s, there will be a pair of eigenvalues in the gap, one at a distance $O(s^2)$ from each branch point, see Kapitula and Sandstede [28].

Lemma 3.4. For the second subsystem (3.3), the essential spectrum is purely imaginary encompassing the entire imaginary axis except for an open gap between $-ir$ and ir, in particular, $\sigma_e = \{x + iy \mid x = 0, |y| \geq r\}$. There are also a finite number of eigenvalues on the imaginary axis, whose distance from one branch point or the other are independent of r. Particularly, there is a positive descending sequence $a_1, a_2, \ldots, a_k$ such that $i(r - a_j)$ and $-i(r - a_j)$ are eigenvalues. Depending upon the parameter r, these values may be either in the gap or embedded within the essential spectrum. See Figure 3.7.

To more readily visualize the spectrum associated with the second system (3.3), we

make the substitutions $\tilde{\lambda} = -i\lambda$ and $\tilde{v_4} = -iv_4$. This yields the system

$$\begin{aligned} v_3'' &= 2(r - h_2(\cdot))\ v_3 - 2\tilde{\lambda}\ \tilde{v}_4 \\ \tilde{v_4}'' &= -2\tilde{\lambda}\ v_3 + 2(r - h_2(\cdot))\ \tilde{v}_4. \end{aligned}$$

We then consider eigenfunctions with the special form $\tilde{v}_4 = v_3$, and find the Sturm–Liouville problem

$$v_3'' = 2(r - \tilde{\lambda})\ v_3 - 2h_2(\cdot)\ v_3.$$

Letting $\tilde{r} = r - \tilde{\lambda}$, we arrive at the same equation which was used in the existence section to identify the points of degeneracy of this same pulse. In particular, it is a Sturm–Liouville problem and has essential spectrum where $\tilde{r} < 0$, along with a finite number of eigenvalues $\tilde{r}_1, \ldots, \tilde{r}_k$ corresponding to eigenfunctions with, respectively, $0, 1, \ldots, k-1$ zeros. Returning to the original variables, the second subsystem has essential spectrum $\sigma_e = \{x + iy \mid x = 0, y \geq r\}$ and eigenvalues given by $i(r - \tilde{r}_1), i(r - \tilde{r}_2), \ldots, i(r - \tilde{r}_k)$.

Similarly, if we look for eigenfunctions of the form $\tilde{v}_4 = -v_3$, we find the problem

$$v_3'' = 2(r + \tilde{\lambda})\ v_3 - 2h_2(\cdot)\ v_3.$$

This provides the other component of the essential spectrum $\sigma_e = \{x + iy \mid x = 0, y \leq -r\}$ and eigenvalues given by $-i(r - \tilde{r}_1), -i(r - \tilde{r}_2), \ldots - i(r - \tilde{r}_k)$.

The full spectrum of the second subsystem is made up of these two reflected pieces.

Remark 3.5. Considering the parallels between the simple example in the previous section and the Sturm–Liouville problem here, there are two distinct mechanisms present that

may produce eigenvalues emerging from the essential spectrum as we follow the bifurcating multi–component pulses. Suppose we follow the multi–component pulse $q_{|0,i\rangle}(x)$ associated with a bifurcation of the ith mode. First, the point spectrum that is originally either embedded in the essential spectrum or already in the gap (particularly, the eigenvalues associated with modes $0, \ldots, k-1$) may enter the gap. Additionally, motivated by the toy problem in the previous section, we might expect resonance poles representing potential modes of order greater than k to emerge from the branch point as true eigenvalues.

Remark 3.6. It is clear from the analysis above that the degeneracy of the elementary pulse $q_u(x)$ corresponds to a conjugate pair of eigenvalues meeting at zero when $r = r_1, r_2, \ldots, r_k$. If we continue to follow the elementary pulse $q_u(x)$ through one of these values of the parameter r, these eigenvalues pull through each other and continue along the imaginary axis – indicating that the pulse $q_u(x)$ is stable for all r. However, accounting for these near zero eigenvalues as we follow the symmetric bifurcating pulses $q_{|0,i\rangle}(x)$, $i = i_1, \ldots, i_k$ is of paramount importance in determining the stability properties of $q_{|0,i\rangle}(x)$ in a neighborhood of r_i. This study will be undertaken in the next section.

3.5 The bifurcating pulse $q_{|0,i\rangle}(x)$.

In this section, we consider the stability properties of the bifurcating pulse $q_{|0,i\rangle}(x)$.

The initial stability of $q_{|0,i\rangle}(x)$.

At the bifurcation point r_i, there are two additional eigenvalues at the origin. Following the elementary pulse $q_u(x)$ through this bifurcation value, these eigenvalues pass through each other. The next lemma specifies the location of these two eigenvalues if we instead follow the bifurcating multi–component pulse $q_{|0,i\rangle}(x)$.

Lemma 3.7. For $r > r_i$, the bifurcating multi–component pulse $q_{|0,i\rangle}(x)$ has a zero eigenvalue of geometric multiplicity 3 and algebraic multiplicity 6.

Proof. Recall that the elementary pulse generally, i.e. away from the bifurcation point, has an eigenvalue at the origin with geometric multiplicity 2 and algebraic multiplicity 4. These correspond to the translation and phase invariances. Because of the form of the nonlinearity, the pulse $q_{|0,i\rangle}(x)$ has a phase invariance associated with *each* nonzero pulse component. Therefore, the two new eigenvalues are locked at zero in order to account for the nontrivial phase invariance of the now nonzero w–component of $q_{|0,i\rangle}(x)$. □

This provides the somewhat surprising result that, near the bifurcation value $r = r_i$, *both* the elementary pulse $q_u(x)$ and the bifurcating pulse $q_{|0,i\rangle}(x)$ are stable, as the near zero eigenvalues move along the imaginary axis for $q_u(x)$ and are locked at zero for $q_{|0,i\rangle}(x)$. In neither case do they move onto the real axis, away from zero.

We recall from the first section that – farther from the bifurcation value $r = r_i$ where $q_u(x)$ becomes degenerate and the pulse $q_{|0,i\rangle}(x)$ bifurcates from it – it is possible for the

pulse $q_{|0,i\rangle}(x)$ itself to become degenerate. Beyond this degeneracy, there are a pair of nonsymmetric pulses bifurcating from $q_{|0,i\rangle}(x)$. At the point of degeneracy itself, there are again two additional eigenvalues at $\lambda = 0$. And again, determining the fate of these eigenvalues is the primary issue in determining the stability of either $q_{|0,i\rangle}(x)$ or the bifurcating nonsymmetric pulses.

The instability criterion of Jones and Grillakis.

Recall that the eigenvalue equation can be written as

$$\begin{bmatrix} 0_{2\times 2} & -L_- \\ L_+ & 0_{2\times 2} \end{bmatrix} \begin{bmatrix} p_1 \\ p_2 \\ q_1 \\ q_2 \end{bmatrix} = \lambda \begin{bmatrix} p_1 \\ p_2 \\ q_1 \\ q_2 \end{bmatrix}$$

where

$$\begin{aligned} L_- &= \tfrac{1}{2}\tfrac{d^2}{dx^2} + \begin{bmatrix} h_1(\cdot) & 0 \\ 0 & h_2(\cdot) \end{bmatrix} + \begin{bmatrix} 1 & 0 \\ 0 & r \end{bmatrix} \\ L_+ &= \tfrac{1}{2}\tfrac{d^2}{dx^2} + \begin{bmatrix} h_1(\cdot) & 0 \\ 0 & h_2(\cdot) \end{bmatrix} + \begin{bmatrix} 2U^2 D_1 h_1(\cdot) & 2UWD_2 h_1(\cdot) \\ 2UWD_1 h_2(\cdot) & 2W^2 D_2 h_2(\cdot) \end{bmatrix} + \begin{bmatrix} 1 & 0 \\ 0 & r \end{bmatrix}. \end{aligned}$$

Both Grillakis [10] and Jones [9] provide a criterion relating the spectrum of the operators L_+ and L_- with the spectrum of the operator

$$N = \begin{bmatrix} 0_{2\times 2} & -L_- \\ L_+ & 0_{2\times 2} \end{bmatrix}.$$

The operators L_+ and L_- are both self–adjoint and hence the spectrum of each will be contained entirely within the real axis. The spectrum of N will not be real; as we have seen already, much of it will lie upon the imaginary axis. We define

$$\begin{aligned} n(L_+) &= \text{the number of positive eigenvalues of } L_+ \\ n(L_-) &= \text{the number of positive eigenvalues of } L_- \\ z(L_-) &= \text{the number of zero eigenvalues of } L_- \end{aligned}$$

where the eigenvalues are counted including multiplicity. In the case that L_+ and L_- are scalar operators, Jones [9] provides an instability criterion, namely, that if $n(L_+) - n(L_-) \neq 0, 1$, then N has a real positive eigenvalue. The proof is geometric in nature, and involves a shooting argument in the space of Lagrangian planes $\Lambda(2)$. For higher dimensional systems, Grillakis [10] provides a generalized criterion using a functional analytic approach. In particular, if we write

$$Y = [\ker(L_+) \cup \ker(L_-)]^{\perp}$$

and let

$$\begin{aligned} \hat{L}_+ &= \text{the restriction of } L_+ \text{ to } Y \\ \hat{L}_-^{-1} &= \text{the restriction of } L_-^{-1} \text{ to } Y \end{aligned}$$

then Grillakis' theorem states that there are exactly

$$\max\{n(\hat{L}_+), n(\hat{L}_-^{-1})\} - \dim(C(\hat{L}_+) \cap C(\hat{L}_-^{-1}))$$

positive real eigenvalues. Here, $C(L) = \{y \in Y \mid \langle Ly, y\rangle < 0\}$ denotes the negative cone of an operator L. We use Grillakis' theorem to derive a generalization of Jones' criterion

suitable for our purposes. This derivation parallels the work of Yew [18].

Lemma 3.8. If $n(L_+) - z(L_-) - n(L_-) > 0$, then N has a real positive eigenvalue.

Proof. To prove this criterion, we must bound the quantities present in Grillakis' theorem. In particular, to estimate the quantities $n(\hat{L}_+)$ and $n(\hat{L}_-^{-1})$ we must consider how projection onto the subspace Y affects the indices. Because L_+ is self–adjoint, the negative eigenspace of L_+ is orthogonal to its kernel $\ker(L_+)$, and hence is influenced only by projection off of $\ker(L_-)$. At worst, projection off of $\ker(L_-)$ reduces the dimension of the negative eigenspace of L_+ by $\dim(\ker(L_-)) = z(L_-)$ and hence

$$\begin{aligned} \max\{n(\hat{L}_+), n(\hat{L}_-^{-1})\} &= n(\hat{L}_+) \\ &\geq n(L_+) - z(L_-). \end{aligned}$$

Likewise, at best, projection off of $\ker(L_+)$ leaves the dimension of the negative eigenspace of L_- unchanged. Therefore

$$\begin{aligned} \dim(C(\hat{L}_+) \cap C(\hat{L}_-^{-1})) &\leq \min\{\dim(C(\hat{L}_+)), \dim(C(\hat{L}_-^{-1}))\} \\ &\leq \min\{n(\hat{L}_+), n(\hat{L}_-^{-1})\} \\ &= n(\hat{L}_-^{-1}) \\ &\leq n(L_-) \end{aligned}$$

and it follows that

$$\max\{n(\hat{L}_+), n(\hat{L}_-^{-1})\} - \dim(C(\hat{L}_+) \cap C(\hat{L}_-^{-1})) \geq n(L_+) - z(L_-) - n(L_-).$$

Applying the theorem of Grillakis, the lemma follows immediately. □

This lemma provides a useful criterion for the instability of a pulse, but does not imply stability in the case that $n(L_+) - z(L_-) - n(L_-) \leq 0$.

We will use this condition to examine the (in)stability of the symmetric multi–component pulses $q_{|0,i\rangle}(x)$ and the asymmetric pulses bifurcating from them.

Remark 3.9. As an exercise, we can check this criterion for the single component pulse $q_u(x)$ considered in the previous section. For this pulse, both of the operators L^+ and L^- decouple further. L^+ is given by

$$L_+ = \frac{1}{2}\frac{d^2}{dx^2} + \begin{bmatrix} h_1(\cdot) & 0 \\ 0 & h_2(\cdot) \end{bmatrix} + \begin{bmatrix} 2U^2 D_1 h_1(\cdot) & 0 \\ 0 & 0 \end{bmatrix} - \begin{bmatrix} 1 & 0 \\ 0 & r \end{bmatrix}.$$

Hence L_+ can be broken into scalar operators with spectrum that can be determined by a Sturm–Liouville argument. The first operator

$$L_+^1 = \frac{1}{2}\frac{d^2}{dx^2} + h_1(\cdot) + 2U^2 D_1 h_1(\cdot) - 1$$

has a zero eigenvalue reflecting the translation invariance of the single component pulse. Moreover, since the eigenfunction $(U', 0, U'', 0)$ has one zero, there is exactly one positive eigenvalue of this operator. The second operator

$$L_+^2 = \frac{1}{2}\frac{d^2}{dx^2} + h_2(\cdot) - r$$

has a non–negative number $j(r)$ of positive eigenvalues depending upon the value of r. In particular, if $r_{i+1} \leq r < r_i$, then $j(r) = i + 1$. So $n(L_+) = 1 + j(r)$. The operator L_- is

given by

$$L_- = \frac{1}{2}\frac{d^2}{dx^2} + \begin{bmatrix} h_1(\cdot) & 0 \\ 0 & h_2(\cdot) \end{bmatrix} - \begin{bmatrix} 1 & 0 \\ 0 & r \end{bmatrix}$$

and can also be broken into two scalar operators. The first,

$$L_-^1 = \frac{1}{2}\frac{d^2}{dx^2} + h_1(\cdot) - 1,$$

has a zero eigenvalue associated with the phase invariance of the wave and hence $z(L_-^1) = 1$. Since the eigenfunction $(U, 0, U', 0)$ has no zeros in the first component, there are no positive eigenvalues of this operator, i.e. $n(L_-^1) = 0$. The second operator,

$$L_-^2 = \frac{1}{2}\frac{d^2}{dx^2} + h_2(\cdot) - r,$$

is the same as L_+^2 in this case and has the same non–negative number $j(r)$ of positive eigenvalues. L_-^2 has a zero eigenvalue only when the pulse solution $q_u(x)$ is degenerate, so $n(L_-^2) = 1$ if $r \in \{r_1, \ldots, r_k\}$ and $n(L_-^2) = 0$ otherwise.

So, $n(L_+) = 1 + j(r)$, $z(L_-) = 1$ or 2 and $n(L_-) = j(r)$. Hence $n(L_+) - z(L_-) - n(L_-) = -1, 0$. Therefore, we do not *a priori* expect an instability in this stationary wave (which is a good sign, as we proved this wave to be stable).

Remark 3.10. For both the symmetric and nonsymmetric multi–component pulses, the values $n(L_-)$ and $z(L_-)$ are easy to compute. As in the case for the elementary pulse

$q_u(x)$, the operator L_- decouples as

$$L_- = \frac{1}{2}\frac{d^2}{dx^2} + \begin{bmatrix} h_1(\cdot) & 0 \\ 0 & h_2(\cdot) \end{bmatrix} - \begin{bmatrix} 1 & 0 \\ 0 & r \end{bmatrix}.$$

The two resulting scalar operators each have a zero eigenvalue associated with the phase invariance of the two individual components of the solution, hence $z(L_-) = 2$. The value of $n(L_-)$ is then determined by the number of zeros of the two pulse components themselves. So for the pulse $q_{|0,i\rangle}(x)$ and any asymmetric pulses bifurcating from it, we have $n(L_-) = 0 + i = i$. The application of the instability criterion then depends upon the more complicated calculation of $n(L_+)$.

Winding and the calculation of $n(L_+)$.

We can use the Maslov index to count the number of real positive eigenvalues of L_+. Recall that the eigenvalue problem for L_+ can be written as

$$v' = \left[\begin{array}{cc|c} \multicolumn{2}{c|}{0_{2\times 2}} & I_{2\times 2} \\ \hline 2(1+\lambda) - f_u(\cdot) & -f_c(\cdot) & \\ & & 0_{2\times 2} \\ -f_c(\cdot) & 2(r+\lambda) - f_w(\cdot) & \end{array}\right] v. \tag{3.4}$$

In order to follow the two–dimensional unstable subspace, we can once again move to

Plücker coordinates:

$$
\begin{aligned}
P'_{12} &= P_{14} - P_{23} \\
P'_{13} &= -f_c(\cdot)P_{12} \\
P'_{24} &= f_c(\cdot)P_{12} \\
P'_{14} &= P_{34} + (2(r+\lambda) - f_w(\cdot))P_{12} \\
P'_{23} &= -P_{34} - (2(1+\lambda) - f_u(\cdot))P_{12} \\
P'_{34} &= (2(1+\lambda) - f_u(\cdot))P_{14} - (2(r+\lambda) - f_w(\cdot))P_{23} + f_c(\cdot)\left(P_{13} - P_{24}\right).
\end{aligned}
\tag{3.5}
$$

This equation preserves both the Grassmannian condition (2.9) and the Lagrangian condition (2.10) — and so we can consider a flow on the space of Lagrangian two–dimensional planes in $\mathbf{R}^4$, $\Lambda(2)$. Because $\Lambda(2)$ is a 3–dimensional manifold, a concrete visualization can be given. In particular, $\Lambda(2)$ can be seen as $S^2 \times [-1, +1]$ where the spheres at $+1$ and -1 are identified via the antipodal map (see Jones [9]). Specifically, $\Lambda(2)$ is a fiber bundle over S^1 with fiber S^2 and clutching function the antipodal map. The fundamental group is $\mathbb{Z}$ and the projection onto S^1 gives the winding — this winding is the Maslov index. In order to exploit this winding, it is natural to use the covering space of $\Lambda(2)$ — this covering space is $S^2 \times \mathbf{R}$ and will be denoted $C(2)$.

The eigenvalue problem can then be reformulated as a shooting problem in $\Lambda(2)$. Before detailing this shooting problem, we require the notion of the train of a point $\psi \in \Lambda^2$.

Definition 3.11. The *train of* ψ, denoted $D(\psi)$ is the set of all $\phi \in \Lambda(2)$ that have a nontrivial intersection with ψ, where ψ and ϕ are considered as two–dimensional subspaces of $\mathbf{R}^4$.

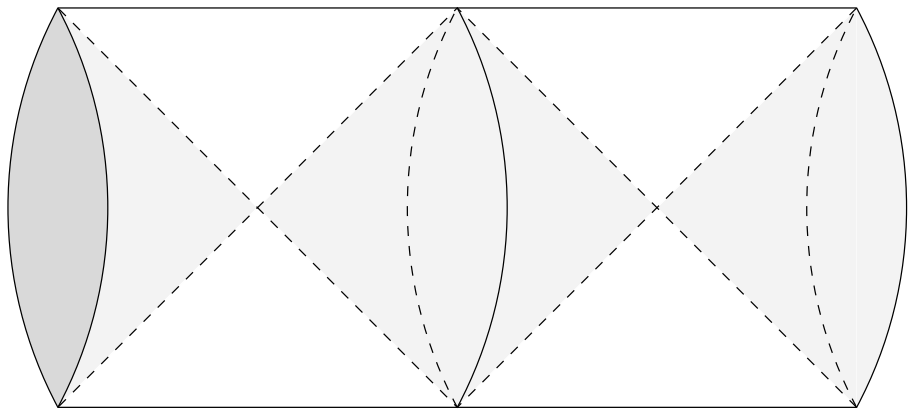

Figure 3.8: The covering space $C(2)$ for the space of Lagrangian planes $\Lambda(2)$.

For any $\phi \in \Lambda(2)$, the train $D(\psi)$ can be lifted to $\hat{D}(\psi)$ in the covering space $C(2)$. In $C(2)$, $\hat{D}(\psi)$ has the appearance of the union of infinitely many cones, joined base to base and vertex to vertex. Each vertical slice is a disk and the fiber S^2 is obtained by identifying the boundary of S^2 to a single point. $\hat{D}(\psi)$ partitions $C(2)$ into an infinite number of components, see Figure 3.8.

For a fixed train $\hat{D}(\beta)$, any curve in $\Lambda(2)$ starting at a point α and ending at a point β' can then be lifted $C(2)$. We can then define the Maslov Index.

Definition 3.12. The *Maslov index* of a path starting at a point α and ending at β', $\alpha \notin \hat{D}(\beta)$ is, by definition, either

1. the index of intersection of this path with $\hat{D}(\beta)$ if $\beta \neq \beta'$, or

2. $1 +$ the index of intersection of this path with $\hat{D}(\beta)$ if $\beta = \beta'$.

We are required to distinguish between paths ending at the vertex β and paths ending at other points because the intersection of a path with the vertex is two dimensional, whereas intersections with other parts of the train are one dimensional.

The shooting argument is then clear. For a fixed $\lambda \in \mathbf{R}$, we can identify the two points $W_-^u \in \Lambda(2)$ associated with the unstable subspace of the asymptotic system and $W_+^s \in \Lambda(2)$ which is associated with the stable subspace. Lifting W_-^u to a point $\hat{W}_-^u$ in the covering space, λ is an eigenvalue if and only if there is a connecting orbit between $\hat{W}_-^u$ and $\hat{D}(W_+^s)$.

Letting $I(\lambda)$ denote the Maslov index of the path in $C(2)$ with α-limit set $\hat{W}_-^u$ for a particular λ, we have the following lemmas.

Lemma 3.13. If $\lambda_1 < \lambda_2$, then the number of eigenvalues $\lambda \in [\lambda_1, \lambda_2)$ equals $I(\lambda_1) - I(\lambda_2)$.

Lemma 3.14. The number of eigenvalues $\lambda \in [\lambda_1, \infty)$ equals $I(\lambda_1)$.

The fact that $I(\lambda_1) - I(\lambda_2)$ provides a lower bound for the number of eigenvalues is clear. Equality requires a monotonicity argument – we defer to Deng [29] in this matter. The second lemma is once more a result of the loss of ellipticity of the transient system for λ large.

The Maslov index is related to the horizontal distance traveled by a path in $C(2)$ projected onto $\mathbf{R}$ (the covering space of the fiber bundle S^1). However, some information is lost in this projection, as two points in the same fiber may be in separate components of $C(2)$ (they may lie on opposite sides of the train) and the Maslov index of paths ending at these two points will differ by 1. However, because the equation for L_+ reduces to the equation of variations when $\lambda = 0$, we know *a priori* that $\lambda = 0$ is an eigenvalue (this eigenvalue is associated with the translation invariance of the stationary wave). Therefore, the orbit with α-limit $\hat{W}_-^u$ connects exactly with the train $\hat{D}(W_+^s)$. In particular, we can

compute the Maslov index $I(0)$ exactly using only the angular information associated with the aforementioned projection onto $\mathbf{R}$. And $n(L_+) = I(0) - 1$.

Remark 3.15. When the pulse $q_{|0,i\rangle}(x)$ becomes degenerate, the associated orbit in $C(2)$ will intersect the vertex of the train. On opposite sides of the degeneracy then, we expect this orbit to have different values of the Maslov index $I(0)$ and hence different values for $n(L_+)$. For the single–component pulse $q_u(x)$, this change was offset by a corresponding change in $n(L_-)$. For multi–component pulses like $q_{|0,i\rangle}(x)$, however, $n(L_-)$ is fixed by the phase invariances of the two components. Hence an increase in $I(0)$ (and therefore $n(L_+)$) will likely trigger an instability in this case.

The space of Lagrangian planes $\Lambda(2)$ can be represented as a homogeneous space: $\Lambda(2) \cong U(2)/O(2)$, where $U(2)$ is the group of unitary matrices and $O(2)$ is the subgroup of real orthogonal matrices (see Arnol'd [30]). With this view, the projection onto S^1 is achieved via the map $\mathrm{Det}^{\,2}(\cdot)$. The angular equation associated with the map $\mathrm{Det}^{\,2}(\cdot)$ is then

$$\kappa = \tan^{-1} \frac{\mathrm{Im}\,\mathrm{Det}^{\,2}(\cdot)}{\mathrm{Re}\,\mathrm{Det}^{\,2}(\cdot)}.$$

In Bose and Jones [31], this formulation is used to derive formulae for κ and κ' in Plücker coordinates:

$$\kappa = \tan^{-1} \frac{2(P_{14} - P_{23})(P_{12} - P_{34})}{(P_{14} - P_{23})^2 - (P_{12} - P_{34})^2}$$

and

$$\kappa' = \tan^{-1} \frac{2(P'_{12} - P'_{34})(P_{14} - P_{23}) - (P'_{14} - P'_{23})(P_{12} - P_{34})}{(P_{14} - P_{23})^2 + (P_{12} - P_{34})^2}.$$

We use these expressions for κ in order to numerically evaluate $I(\lambda)$ and therefore $n(L_+)$

for various incarnations of the stationary wave. First of all:

Lemma 3.16. For r near $r = r_i$, where the multi–component wave $q_{|0,i\rangle}(x)$ originates, $q_{|0,i\rangle}(x)$ has $I(0) = i+2$ or $i+3$, and therefore $n(L_+) = i+1$ or $i+2$. Because $n(L_-) = i$ and $z(L_-) = 2$, it is clear that $n(L+) - z(L_-) - n(L_-)$ is either -1 or 0, and we do not necessarily expect the pulse to be unstable.

Proof. At the parameter value r increases through $r = r_i$, the one–component pulse $q_u(x)$ passes through a degeneracy. The associated orbit in $C(2)$ terminates at the vertex of the train for this value of r. Because L_+ decouples into two smaller systems in this case, we easily calculate that $n(L_+)$ drops from $i+2$ to $i+1$ at this same point. Because the associated orbit of the bifurcating pulse $q_{|0,i\rangle}(x)$ originates at this same point, for small changes of r, the terminal point of the associated orbit in $C(2)$ can only move to one of the two components of the train which meet at this vertex. These have $I(0) = i+2, i+3$ and the lemma follows. □

Remark 3.17. We numerically observe that the terminus of the orbit in $C(2)$ for the bifurcating pulse $q_{|0,i\rangle}(x)$ moves in the opposite direction from that of the single component pulse $q_u(x)$ with increasing r and has $I(0) = i+3$.

For the sake of specificity, we lay down the following lemma.

Lemma 3.18. If the stationary wave $q_{|0,i\rangle}(x)$ itself becomes degenerate, and passage through this degeneracy is associated with an increase in the Maslov index $I(0)$ from $i+3$ to $i+4$, then beyond this degeneracy, the pulse $q_{|0,i\rangle}(x)$ is unstable.

Proof. This is clear, as we then have $n(L_+) - z(L_-) - n(L_-) = i+3-2-i = 1$. The instability criterion is then satisfied. □

We will now compute these values in three cases for the Ostrovskaya–Kivshar problem with saturability parameter $s = 0.8$.

1. For r between the bifurcation value $r_2 \approx 0.20$ and the parameter value for which $q_{|0,2\rangle}(x)$ becomes degenerate $r \approx 0.48$, the pulse $q_{|0,2\rangle}(x)$ has $I(0) = 5$, $n(L_+) - z(L_-) - n(L_-) = 4 - 2 - 2 = 0$ and is not necessarily unstable, as seen in Lemma 3.16. See Figure 3.9.

2. For r beyond the parameter value for which $q_{|0,2\rangle}(x)$ becomes degenerate $r \approx 0.48$, the pulse $q_{|0,2\rangle}(x)$ has $I(0) = 6$, and hence $n(L_+) - z(L_-) - n(L_-) = 5 - 2 - 2 > 0$ and is unstable as in Lemma 3.18. See Figure 3.10.

3. For r beyond the parameter value for which $q_{|0,i\rangle}(x)$ becomes degenerate $r \approx 0.48$, the bifurcating non–symmetric pulse has $I(0) = 5$, $n(L_+) - z(L_-) - n(L_-) = 4 - 2 - 2 = 0$ and may actually be stable. See Figure 3.11.

Remarks concerning stability.

Remark 3.19. We should be able to count eigenvalues on the imaginary axis as well as those on the real axis. For λ in the gap of the imaginary axis, we can make the transformations $\lambda \to i\tilde{\lambda}$ and $q = (q_1, q_2) \to i\tilde{q}$. Then the operator N can be written as a real operator, and the eigenvalues of L_+ and L_- should again tell us something about the eigenvalues of N. A potential difficulty comes from the fact that the equivalent "λ large" limit is not available in this case. Perhaps some extension into the essential spectrum (or onto another Riemann sheet) is possible that would help us to bound the number of eigenvalues that might enter into play through the branch points.

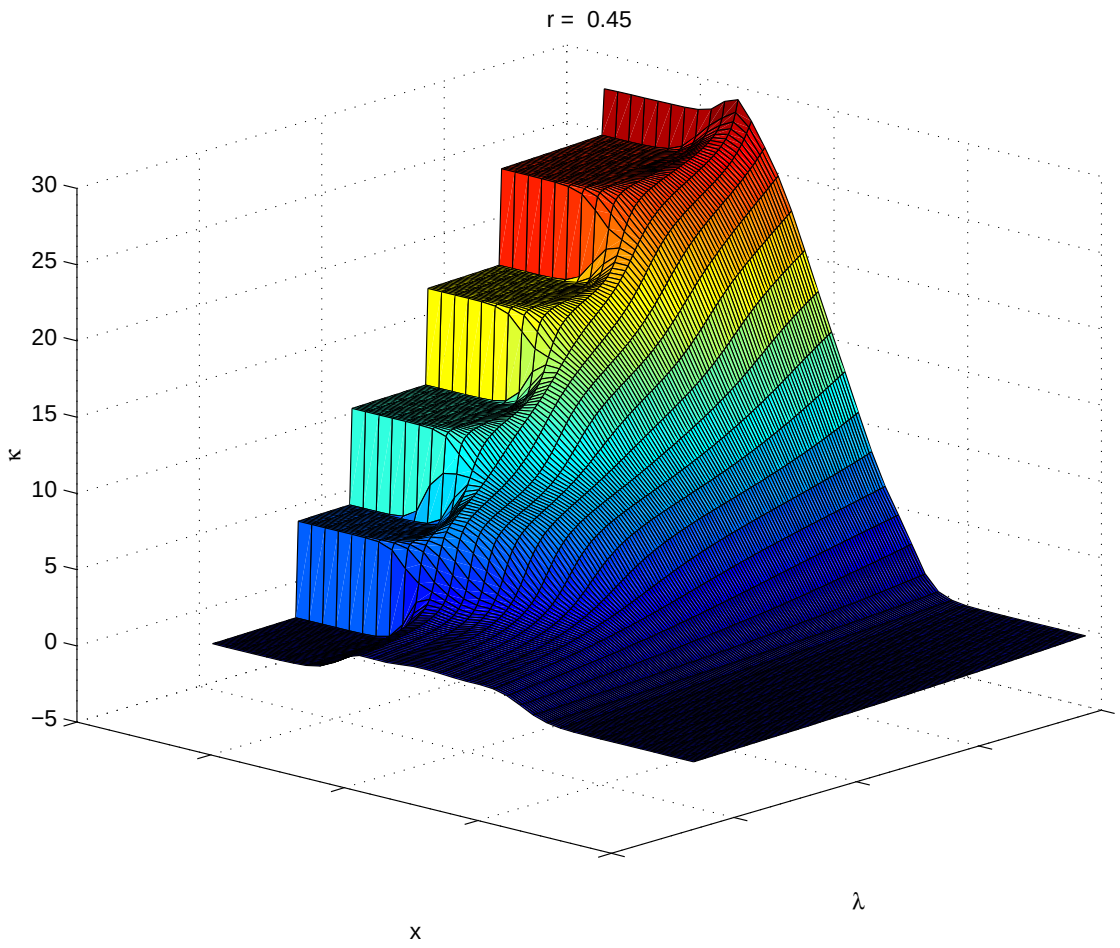

Figure 3.9: Calculation of $n(L_+)$ for the pulse $q_{|0,2\rangle}(x)$ at $r = 0.45$, before the degeneracy. The angular variable $\kappa(x)$ is shown for increasing values of the eigenvalue parameter λ. λ values for which λ is an eigenvalue are seen as steps – for λ values on either side of these steps, the orbit in $C(2)$ goes to different components of the train. The highest "half–step" is associated with the eigenvalue $\lambda = 0$. Here $I(0) = 5$, and hence $n(L_+) - z(L_-) - n(L_-) = 4 - 2 - 2 = 0$ and the pulse may be stable.

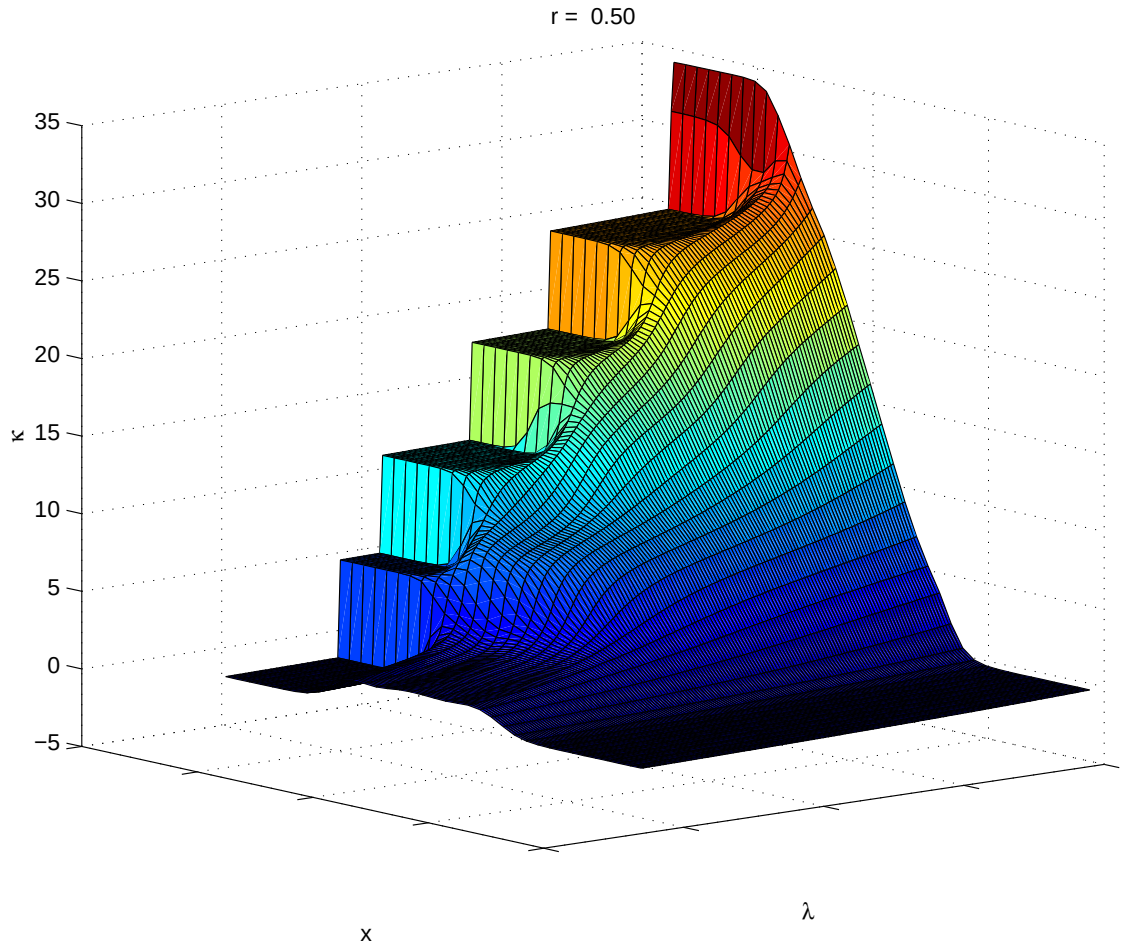

Figure 3.10: Calculation of $n(L_+)$ for the pulse $q_{|0,2\rangle}(x)$ at $r = 0.50$, after the degeneracy. The angular variable $\kappa(x)$ is shown for increasing values of the eigenvalue parameter λ. λ values for which λ is an eigenvalue are seen as steps – for λ values on either side of these steps, the orbit in $C(2)$ goes to different components of the train. The highest "half–step" is associated with the eigenvalue $\lambda = 0$. Here a new eigenvalue has appeared with λ small. Now $I(0) = 6$, and hence $n(L_+) - z(L_-) - n(L_-) = 5 - 2 - 2 = 1$ and the pulse is unstable.

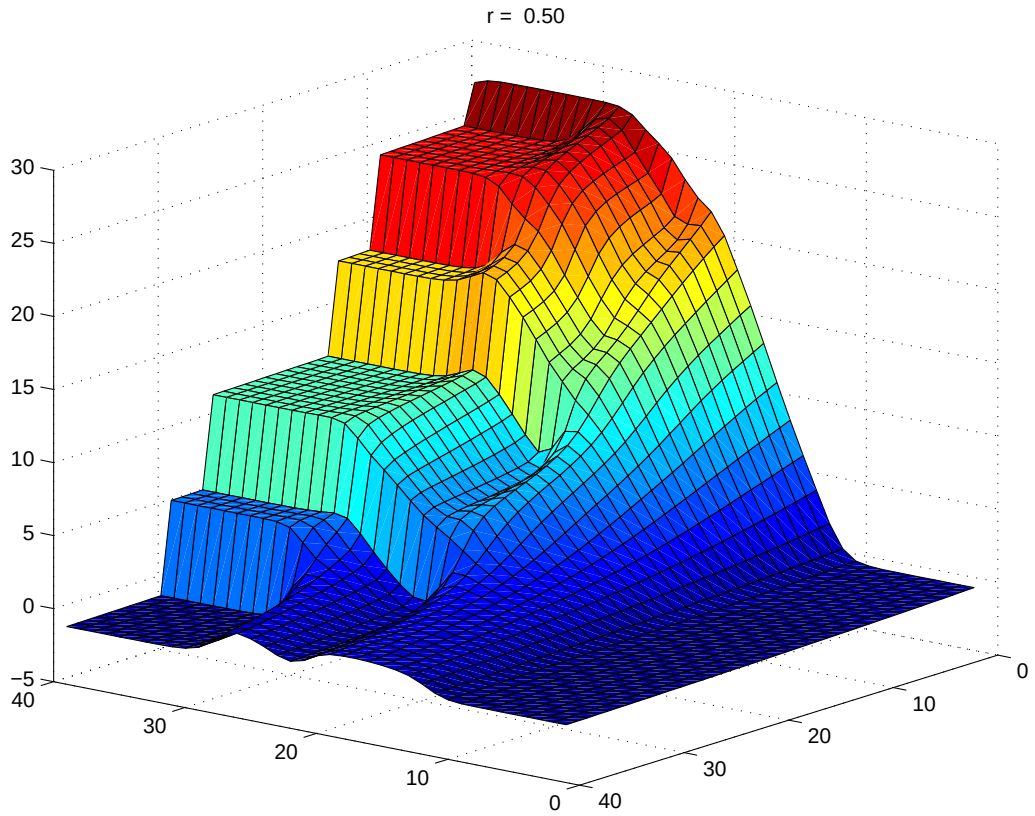

Figure 3.11: Calculation of $n(L_+)$ for the bifurcating nonsymmetric pulse at $r = 0.50$, after the degeneracy. The angular variable $\kappa(x)$ is shown for increasing values of the eigenvalue parameter λ. λ values for which λ is an eigenvalue are seen as steps – for λ values on either side of these steps, the orbit in $C(2)$ goes to different components of the train. The highest "half–step" is associated with the eigenvalue $\lambda = 0$. Here we still have $I(0) = 5$, and hence $n(L_+) - z(L_-) - n(L_-) = 4 - 2 - 2 = 0$. The nonsymmetric bifurcating pulse may indeed be stable!

3.6 N–pulses

The criterion of Grillakis and Jones also applies to the multi–pulses that bifurcate from the single–component pulse $q_u(x)$ as it passes through degeneracy for $r = r_i$. The primary complication for determining the stability of multi–pulses is the issue of eigenvalue multiplication. If the pulse $q_{|0,i\rangle}(x)$ has k eigenvalues near a point, then an N–pulse that looks like $q_{|0,i\rangle}(x)$ concatenated with itself N times, will have Nk eigenvalues near that same point. For instance, the pulse $q_u(x)$ has an eigenvalue with algebraic multiplicity 8 at the origin at the bifurcation point $r = r_i$. For an N–pulse created at this bifurcation, only 6 of the $8N$ eigenvalues are guaranteed to remain at the origin. The primary issue in the study of stability is determining whether any of these $8N - 6$ eigenvalues move into the positive half–plane, generating an instability.

The manner in which the multi–pulses are "glued" together is often a critical factor in determining the motion of eigenvalues following the bifurcation. This is of course true in this case as well, but here there is a simplification which eases the following conclusion:

Lemma 3.20. For r near a bifurcation value r_i, all N–pulses which look like concatenations of the bifurcating pulse $q_{|0,i\rangle}(x)$ are unstable. In particular, they have *at least* $N - 1$ positive eigenvalues.

Proof. This follows from Remark 3.17. In particular, as the pulse $q_u(x)$ passes through degeneracy increasing r through the value r_i, the Maslov index $I(0)$ of the pulse $q_u(x)$ decreases to $i + 2$, while the bifurcating pulse $q_{|0,i\rangle}(x)$ has Maslov index $I(0) = i + 3$. Therefore the operator L_+ for the pulse $q_{|0,i\rangle}(x)$ has $i + 2$ positive eigenvalues, including the small positive eigenvalue that bifurcates from zero for $r > r_i$. The N–pulse then has

N eigenvalues exponentially close to each of these $i+2$ positive eigenvalues, in particular $n(L_+) \geq (i+2)N$.

Because any N–pulse is required to alternate in exactly one of its components between successive pulses, the N–pulse has $n(L_-) = iN + (N-1)$. Additionally, we still have $z(L_-) = 2$.

Hence,

$$\begin{aligned} n(L_+) - z(L_-) - n(L_-) &\geq (i+2)N - 2 - (iN + (N-1)) \\ &= N - 1. \end{aligned}$$

So, by way of the proof of Lemma 3.8, any N–pulse has at least $N-1$ positive eigenvalues.

□

Remark 3.21. The inherent instability of N–pulses is due to the multiplication of the near–zero, but positive, eigenvalue of L_+ for the pulse $q_{|0,i\rangle}(x)$ that appears at bifurcation. This multiplication produces $N-1$ positive (and also $N-1$ negative) eigenvalues for the full composite operator. Of course, there may be additional instabilities present once we account for the other $6N-6$ near zero eigenvalues.

We make the following conjecture, and numerically verify it only in the case $N = 2$.

Conjecture 3.22. Consider a sequence of N binary digits given by $j_1, j_2, \ldots, j_N$ and let $q_{\{j_1,\ldots,j_N\}}(x)$ be an N–pulse in which the u–component of the ith pulse is positive if $j_i = 0$ and negative if $j_i = 1$. We conjecture that $q_{\{j_1,\ldots,j_N\}}(x)$ has exactly

$$N - 1 \; + \; \sum_{i=1}^{N-1} \left(1 - (j_{i+1} - j_i)^2\right)$$

positive real eigenvalues.

Remark 3.23. This conjecture says that the alternating N–pulses constructed in Section 2.2 are, in some sense, as stable as possible, with only the $N-1$ positive eigenvalues specified above. At the other extreme, the N–pulses in which the u–component does not alternate at all has $2N-2$ positive eigenvalues.

Both the alternating and the non–alternating 2–pulse near the bifurcation point $r = r_1$ are shown in Figure 3.12. In Figure 3.13, we see the numerical calculation of the Maslov index and the location of the positive eigenvalues for L_+ of the alternating 2–pulse $q_{\{1,0\}}(x)$. The operator L_+ for this pulse has $2(i+2) = 6$ positive eigenvalues. Since $n(L_-) = 3$ and $z(L_-) = 2$, this pulse has at least one real positive eigenvalue and is unstable. Likewise, in Figure 3.13, we see the numerical calculation of the Maslov index and the location of the positive eigenvalues of L_+ of the non–alternating 2–pulse $q_{\{1,1\}}(x)$. Here, L_+ has an additional near–zero eigenvalue, so that $n(L_+) = 7$. It follows that this pulse is unstable and has at least 2 positive eigenvalues.

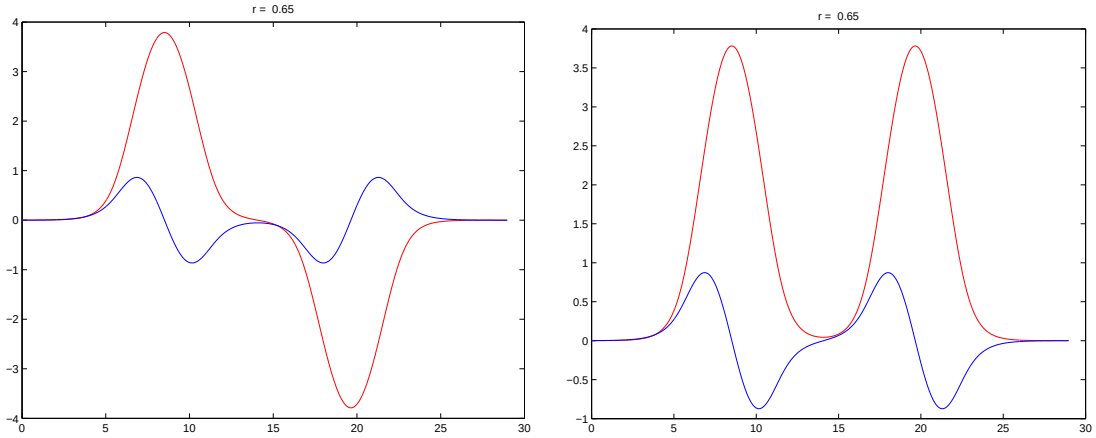

Figure 3.12: Two different 2–pulses are found for $r = 0.65$ near the bifurcation point $r = r_1$. The first is alternating in the first component while the second is not.

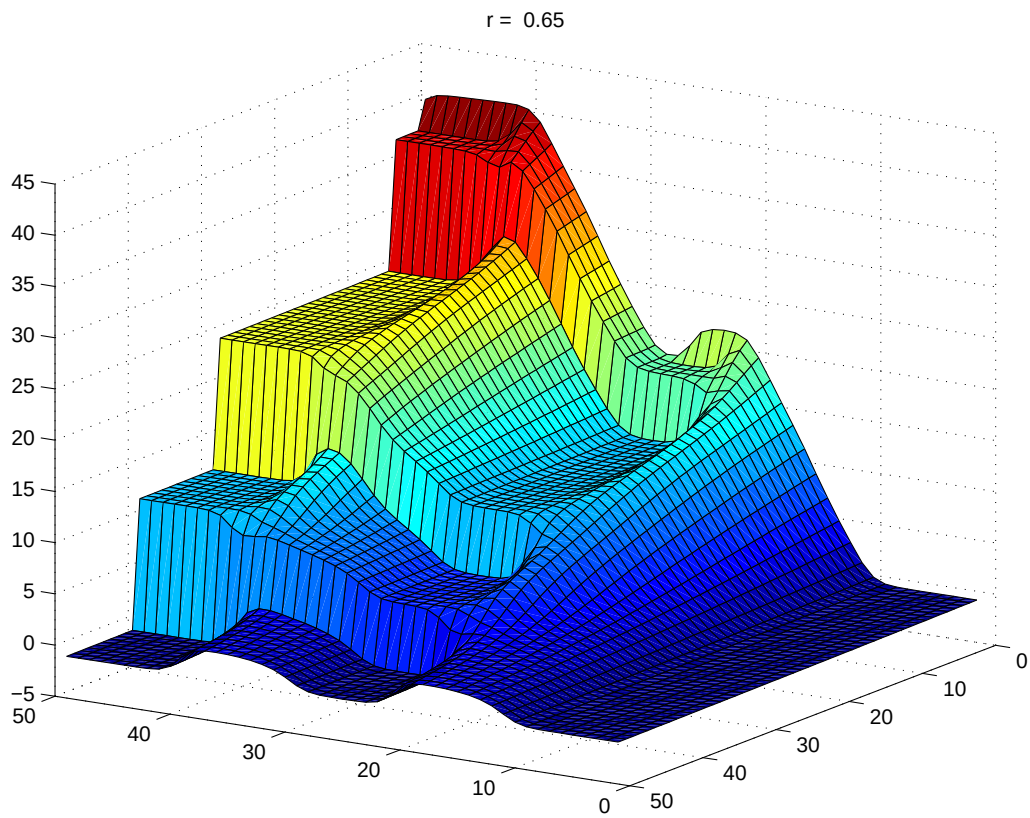

Figure 3.13: Calculation of $n(L_+)$ for the alternating 2–pulse at $r = 0.65$ near the degeneracy $r = r_1$. There are two eigenvalues near each λ value at which the 1–pulse $q_{|0,1\rangle}(x)$ has a single eigenvalue. The angular variable $\kappa(x)$ is shown for increasing values of the eigenvalue parameter λ. Zero is a simple eigenvalue here and there are no eigenvalues exponentially close to zero. Now $I(0) = 7$, and hence $n(L_+) - z(L_-) - n(L_-) = 6 - 3 - 2 = 1$ and the pulse is unstable.

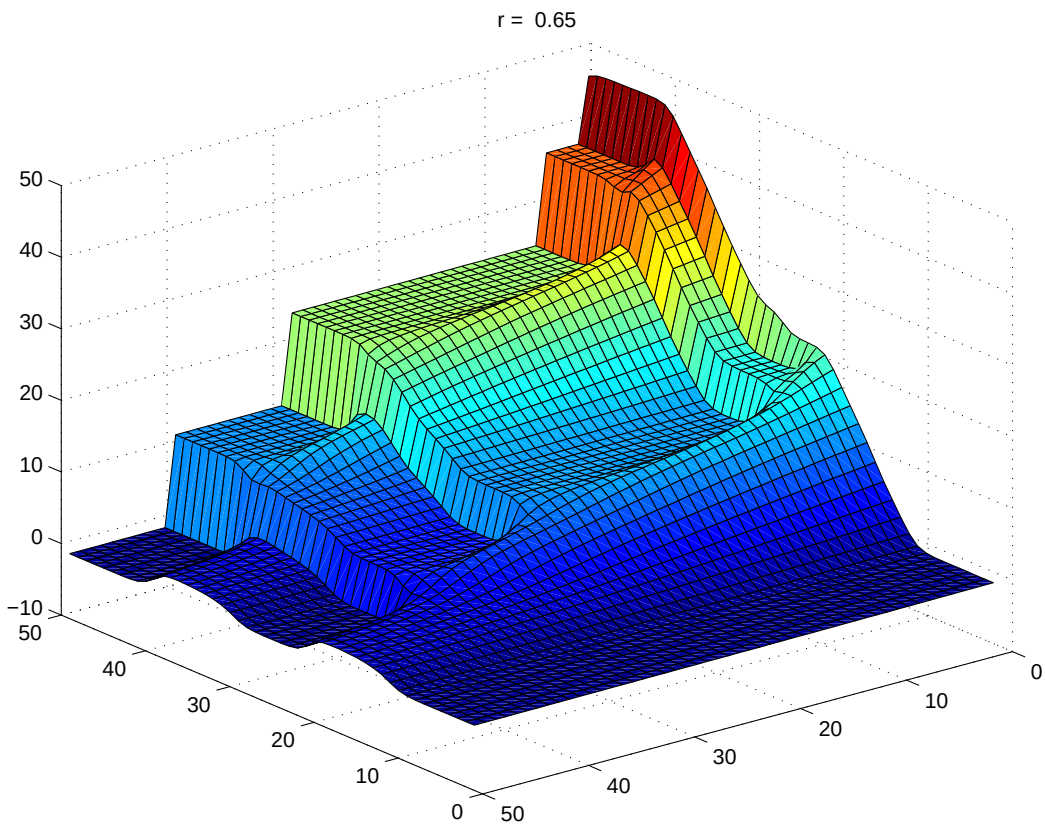

Figure 3.14: Calculation of $n(L_+)$ for the non–alternating 2–pulse at $r = 0.65$ near the degeneracy $r = r_1$. There are two eigenvalues near each λ value at which the 1–pulse $q_{|0,1\rangle}(x)$ has a single eigenvalue. The angular variable $\kappa(x)$ is shown for increasing values of the eigenvalue parameter λ. Zero is a simple eigenvalue here, and there is a positive eigenvalue exponentially close to zero. Now $I(0) = 8$, and hence $n(L_+) - z(L_-) - n(L_-) = 7 - 3 - 2 = 2$. The pulse is unstable and has at least two positive eigenvalues.

Part II

Pulses in the Gabitov–Turitsyn Equation

Chapter 4

Introduction

Within the last decade, dispersion management has become an important principle in the field of fiber optic communication. As we described in the first part, the nonlinear Schrödinger equation provides a model for pulse propagation in optical fibers, incorporating the effects of chromatic dispersion, as well as the nonlinearity of the material properties. Under the right circumstances, the broadening due to dispersion can be counteracted exactly by this nonlinearity and a *soliton* can be formed. Unfortunately, much of the world's optical fiber was installed without this balance in mind, and for the most part, the effects of nonlinearity were ignored. In these fibers, dispersion is so large that the power required in order to achieve the nonlinear balance is prohibitive. However, it is possible to manufacture fiber that has a dispersion coefficient of opposite sign at the usual operating wavelength. By alternating lengths of this "dispersion managed" fiber with the usual fiber, we reach a regime in which the average dispersion is small and the nonlinearity can again play an important role.

Pulse propagation in the regime of strong dispersion management is described by the

following nonlinear Schrödinger equation:

$$iu_z + d(z)u_{tt} + \epsilon(|u|^2 u + \alpha u_{tt}) = 0. \tag{4.1}$$

This models the situation described above in which there is a large periodically varying dispersion term $d(z)$ (with $\langle d \rangle = 0$) but where the effects of nonlinearity and the residual dispersion are both small. A natural step in the analysis of this equation would be to use an averaging procedure to remove the periodic dispersion term $d(z)$, and in so doing, we derive the Gabitov–Turitsyn equation

$$iv_z + \alpha v_{tt} + \frac{1}{4}\int_{-1}^{1} (T^{-1}\left(|T(z)v|^2 T(z)v\right) dz = 0. \tag{4.2}$$

We call a stationary solution of this equation a *dispersion managed (DM) soliton.*

Rapid development in the theory of the DM soliton has been driven by its practical importance as well as its somewhat intriguing properties. One of these properties is the persistence of the DM soliton when the residual dispersion α is zero or even slightly negative; the corresponding nonlinear Schrödinger equation has no pulse–like solutions in this regime. A typical explanation for this behavior is based on Lagrangian averaging over a Gaussian ansatz. This reduction produces an effective finite dimensional system with a corresponding potential. When the residual dispersion α is positive, this potential well has a global minimum that corresponds to the DM soliton. This global minimum persists for the case of zero residual dispersion, and when the residual dispersion is slightly negative, there is still a local minimum. However, as the residual dispersion is decreased further,

this local minimum is destroyed in a saddle–node bifurcation. This was described by Pelinovsky [32].

The DM soliton can be understood as the ground state for the averaged Hamiltonian associated with equation (4.2). Recently, it was shown by Zharnitsky et al. [33] that the ground state for the averaged Hamiltonian could be found by carrying out a minimization procedure. That approach was also used to show that a critical point could not be a minimum if the residual dispersion were negative [33], see also related work by Pelinovsky [32].

In this thesis, we numerically implement such a minimization procedure using a basis of Hermite–Gaussian functions. In studying stationary waves of the equation (4.2), we consider a constrained variational principle, as introduced by Zakharov in the context of the nonlinear Schrödinger equation, see [3]. (For an interesting historical discussion of the use of variational principle for stability analysis, see [34].) Any finite collection of elements from this Hermite–Gaussian basis spans a finite dimensional space; and minima of the Hamiltonian restricted to this space may be expected to approximate nearby critical points of the infinite–dimensional Hamiltonian. Locating such local minima then gives us information about the form of the standing waves of equation (4.2).

Using the Hermite–Gaussian functions as a basis, we approximate the profile of the DM soliton for positive and mean–zero residual dispersion and even into the negative residual dispersion regime. We explore the destruction of the DM soliton as residual dispersion is decreased and note that our minimization technique yields an approximation for the DM soliton into the regime where the Gaussian ansatz fails to do so. Additionally, the better approximations of the DM soliton in the Hermite–Gaussian basis propagate in all regimes

with far less noise than their Gaussian counterparts. Furthermore, the increased accuracy in the tails provides for far better modeling of well–separated pulse interactions than a Gaussian ansatz allows.

Finally, as we increase the number of Hermite–Gaussian functions in the approximation, it is possible to find local minima that do not correspond to a single DM soliton. In fact, we find a local minimum that corresponds to a pulse with the appearance of two widely spaced DM solitons, we call this solution a bisoliton. Such a solution (first found in Maruta et al. [35]) suggests an ideal pulse spacing for DM solitons or even advanced coding systems for information transmission.

Chapter 5

Approximate pulses via a variational principle

5.1 Governing equations and the numerical method

Pulse propagation in the regime of strong dispersion management is described by a nonlinear Schrödinger equation with periodically varying dispersion, see Lakoba and Kaup [36]. This is written

$$iu_z + d(z)u_{tt} + \epsilon(|u|^2 u + \alpha u_{tt}) = 0,$$

where $d(z)$ is a periodically varying group velocity dispersion with $\langle d \rangle = 0$ (see Figure 5.1), $\epsilon\alpha$ is the residual dispersion, and z and t correspond to the distance along the fiber and the retarded time, respectively.

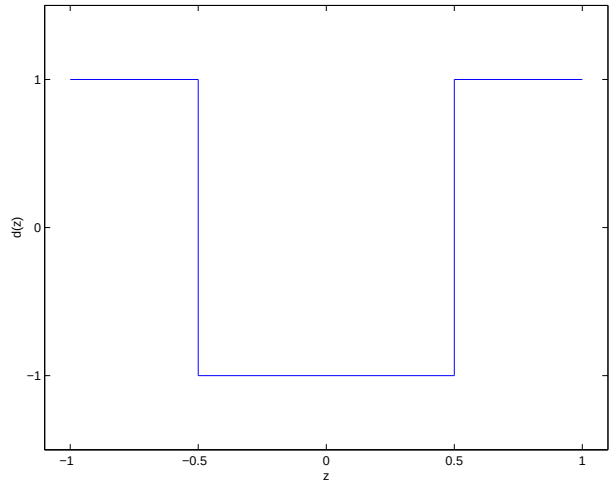

Figure 5.1: The symmetric dispersion map.

This is a Hamiltonian equation, and the Hamiltonian is given by

$$H(u) = \int_{-\infty}^{+\infty} d(z)|u_t|^2 + \epsilon \left(\alpha |u_t|^2 - \frac{1}{2}|u|^4 \right) dt.$$

To remove fast oscillations induced by the strong dispersion $d(z)$, we make a linear canonical transformation $u = T(z)v$ and $\bar{u} = T^-(z)\bar{v}$, where T is the solution operator of $iu_z + d(z)u_{tt} = 0$ and T^- is the solution operator of $iu_z - d(z)u_{tt} = 0$. This change of variables provides an equivalent formulation for the Hamiltonian:

$$H(v) = \alpha \int_{-\infty}^{+\infty} |v_t|^2 \, dt - \frac{1}{2} \int_{-\infty}^{+\infty} \left[T(z)v\right]^2 \left[T^-(z)\bar{v}\right]^2 \, dt.$$

And because $T^-(z)\bar{v} = \overline{T(z)v}$, we can rewrite this Hamiltonian in the more convenient form

$$H(v) = \int_{-\infty}^{+\infty} \left(\alpha |v_t|^2 - \frac{1}{2}|T(z)v|^4 \right) \, dt.$$

Finally, we average over a single period of the dispersion map to obtain

$$\langle H\rangle(v) = \alpha \int_{-\infty}^{+\infty} |v_t|^2 dt - \frac{1}{4}\int_{-\infty}^{+\infty}\int_{-1}^{1} |T(z)v|^4 \; dz \; dt \tag{5.1}$$

with the corresponding averaged equation

$$iv_z + \alpha v_{tt} + \frac{1}{4}\int_{-1}^{1} T^{-1}\left(|T(z)v|^2 T(z)v\right) \; dz = 0. \tag{5.2}$$

The constrained variational principle takes the form

$$H_E = \inf\left\{\langle H\rangle(v) \;\mid\; \int_{-\infty}^{+\infty} |v_t|^2 \; dt < \infty, \int_{-\infty}^{+\infty} |v|^2 \; dt = E\right\}.$$

A solution of this variational principle corresponds to a standing wave in the averaged equation (5.2). Indeed, a constrained minimizer $V(t) \in H^2(\mathbf{R})$ must satisfy the relationship

$$\frac{\partial\langle H\rangle}{\partial\overline{V}} = \omega V,$$

for some $\omega \in \mathbf{R}$ and hence the solution $v(t,z) = e^{i\omega z}V(t)$ satisfies the averaged equation (5.2).

The averaged equation (5.2), as well as the associated variational principle, were obtained by Gabitov et al. in [37]. When the residual dispersion α is positive, this variational principle has been shown to possess a ground state [33]. Even when the residual dispersion α is zero, a similar result can be demonstrated, see Kunze [38]. This ground state

corresponds to the dispersion managed soliton.

The numerical procedure.

In this thesis, we locate minimizers numerically using the following procedure.

Reduction to a finite dimensional space.

We approximate the Sobolev space $H^1(\mathbf{R})$ by introducing a finite–dimensional Galerkin approximation for $V(t)$ in the basis of Hermite–Gaussian functions. A similar reduction was carried out in [36] and [39]. The set of Hermite–Gaussian functions is given by

$$\left\{ \frac{1}{\sqrt{2^n n! \sqrt{\pi}}} H_n(t) e^{-\frac{t^2}{2}} \mid n = 0, 1, 2, \dots \right\}$$

where the terms $H_0(t), H_1(t), \dots, H_N(t)$ are the Hermite polynomials. The Hermite polynomials themselves can be computed recursively using $H_0(t) = 1$, $H_1(t) = 2t$ and the relation

$$H_{n+1}(t) = 2tH_n(t) - 2nH_{n-1}(t).$$

The Hermite–Gaussian functions can be shown to be eigenfunctions of the differential equation

$$y'' - t^2 y = 0$$

and are thus mutually orthogonal; the coefficient $\sqrt{2^n n! \sqrt{\pi}}$ is required to insure that the set of Hermite–Gaussians are orthonormal.

In order to better make use of this basis, we insert a width parameter σ and use the

renormalized basis

$$\left\{ \frac{A_1}{\sqrt{2^n n! \sqrt{\pi}}} H_n\left(\frac{t}{A_2}\right) e^{-\frac{t^2}{2\sigma}} \mid n = 0, 1, 2, \ldots \right\},$$

where

$$A_1^2 = \frac{\sqrt{|\mathrm{Re}\,\sigma|}}{|\sigma|} \qquad A_2 = \frac{|\sigma|}{\sqrt{|\mathrm{Re}\,\sigma|}}$$

are defined so that this orthonormality is preserved in the presence of the variable σ. The parameter σ allows a more natural scaling of the Hermite–Gaussian functions appropriate for the system at hand; hence fewer terms are necessary to produce more accurate pulse approximations. Our approximation for $V(t)$ then takes the form

$$V(t) = \sum_{k=0}^{N} a_k \left(\frac{A_1}{\sqrt{2^k (k)! \sqrt{\pi}}} H_k\left(\frac{t}{A_2}\right) \right) e^{-\frac{t^2}{2\sigma}}, \tag{5.3}$$

where σ and $a_0, a_2, \ldots, a_{2N}$ are complex numbers; these will serve as the variables in our minimization procedure.

The minimization procedure.

We wish to find critical points of the functional $\langle H \rangle(V)$ given in (5.1) within a finite dimensional space of functions of the form (5.3) restricted to the energy surface

$$\int_{-\infty}^{+\infty} |v|^2 dt = E$$

for a fixed value of E.

The function $\langle H \rangle(V)$.

For a fixed value of N, it is tempting to derive a closed form for $\langle H\rangle(V)$ in terms of σ, $a_0, a_1, \ldots, a_N$. This is possible, as the operator $T(z)$ takes Hermite–Gaussian functions to combinations of other Hermite–Gaussian functions, and the integrals of products of such functions can be explicitly computed. However, this becomes extremely unpleasant (in large part because of the nonlinear term) and is not especially elucidating beyond one–dimension. We will make this calculation for the Gaussian (one–dimensional) ansatz, but for all higher dimensional spaces, we will approximate $\langle H\rangle(V)$ numerically.

First of all, we can reduce the scale of the computation by exploiting the structure of the operator $|T(z)V|$. Indeed, because of the symmetric structure of the dispersion map, we know that for $z \in [0, 1/2]$,

$$T(z)V = T(1-z)V = \bar{T}(1+z)V = \bar{T}(2-z)V.$$

In particular then

$$\langle H\rangle(V) = \alpha \int_{-\infty}^{+\infty} |V_t|^2 dt - \int_{-\infty}^{+\infty} \int_0^{1/2} |T(z)V|^4 \, dz \, dt.$$

For any particular realization of V specified by the coefficients σ, $a_0, a_1, \ldots, a_N$, we use the Fast Fourier Transform (FFT) to numerically compute both V_t and $T(z)V$, for a finite grid of values for z. The integration is also carried out numerically.

Constrained minimization of $\langle H\rangle(V)$.

Because of the orthogonality of the Hermite–Gaussian basis, the energy constraint

$\int_{-\infty}^{+\infty} |v|^2 dt = E$ takes the simple form

$$|a_0|^2 + |a_1|^2 + ... + |a_N|^2 = E. \tag{5.4}$$

The constraint $\int_{-\infty}^{+\infty} |V_t|^2 dt < \infty$ holds automatically.

In order to find minima of $\langle H \rangle(V)$ restricted to this set, we use the function fmincon() found in Matlab's Optimization Toolbox. fmincon() finds local minima using a sequential quadratic programming (SQP) method.

We make several additional simplifications to aid in our search. First, we expect that minimizers will display an even symmetry (see Turitsyn et al. [40]) – the evolution equation (5.2) also respects this symmetry. Therefore, we will restrict our basis to only the even Hermite–Gaussian functions, i.e., we will set the odd coefficients $a_1, a_3, a_5, \ldots$ all to zero.

Additionally, because we have specified the dispersion map $d(z)$ in a symmetric manner, we expect that a minimizer will be real (again, see Turitsyn et al. [40]). In this way, our minimization problem can be considered on $\mathbf{R}^+ \times S^N$, where $\sigma \in \mathbf{R}^+$ and $a_0^2 + a_2^2 + \ldots + a_{2N}^2 = E$.

5.2 The dispersion managed soliton

In this section we give a description of the dispersion managed soliton using the minimization procedure described in the previous chapter. For the Gaussian case, where $V(t) = a_0\ \pi^{-1/4}\ \sigma^{-1/4}\ e^{-t^2/2\sigma}$, we derive an analytical expression for the functional $\langle H\rangle(V)$. This gives us a good first approximation for the dispersion managed soliton, and can be used as a first verification for our numerical method. For higher dimensional approximations including increasing numbers of elements from the Hermite–Gaussian basis, we search for minimizers numerically using the routine described in the previous section.

The Gaussian case, $N = 0$.

Lemma 5.1. For the initial profile $V(t) = a_0\ \pi^{-1/4}\ \sigma^{-1/4}\ e^{-t^2/2\sigma}$, we have

$$\langle H\rangle(V) = \frac{1}{2}\ \alpha\ a_0^2\ \frac{1}{\sigma} - \frac{1}{2^{3/2}}\ \frac{a_0^4}{\pi^{1/2}}\ \sigma^{1/2}\ \sinh^{-1}\left(\frac{1}{\sigma}\right).$$

Proof. The proof is by computation – and most of this computation is simply using the tools of integration. The only exception is that we are required to compute the evolution $|T(z)V|$ where $T(z)$ is the solution operator of $iu_z + d(z)u_{tt} = 0$. This can be done by moving to Fourier space, where the linear Schrödinger equation becomes a simpler parameter–dependent ODE. We perform this calculation first.

To begin, we must translate the initial condition $V(t)$ into Fourier space:

$$\begin{aligned}
\hat{V}_0(\xi) &= \tfrac{1}{\sqrt{2\pi}} \int_{-\infty}^{+\infty} V(t) e^{-it\xi}\ dt \\
&= \tfrac{1}{\sqrt{2\pi}} \int_{-\infty}^{+\infty} a_0\ \pi^{-\frac{1}{4}}\ \sigma^{-\frac{1}{4}}\ e^{-\frac{t^2}{2\sigma}}\ e^{-it\xi}\ dt \\
&= \tfrac{1}{\pi^{\frac{3}{4}} 2^{\frac{1}{2}}}\ a_0\ \sigma^{-\frac{1}{4}} \int_{-\infty}^{+\infty} e^{-\frac{t^2}{2\sigma} - it\xi}\ dt \\
&= \tfrac{1}{\pi^{\frac{3}{4}} 2^{\frac{1}{2}}}\ a_0\ \sigma^{-\frac{1}{4}}\ e^{-\frac{1}{2}\sigma\xi^2} \int_{-\infty}^{+\infty} e^{-\frac{1}{2}\left(\frac{1}{\sqrt{\sigma}}t + i\sqrt{\sigma}\xi\right)^2}\ dt \\
&= \tfrac{1}{\pi^{\frac{3}{4}} 2^{\frac{1}{2}}}\ a_0\ \sigma^{-\frac{1}{4}}\ e^{-\frac{1}{2}\sigma\xi^2}\ \sqrt{\sigma}\ \sqrt{2\pi} \\
&= a_0\ \pi^{-\frac{1}{4}}\ \sigma^{\frac{1}{4}}\ e^{-\frac{1}{2}\sigma\xi^2}.
\end{aligned}$$

The evolution equation $iV_z + V_{tt} = 0$ itself becomes

$$\hat{V}_z = -i\xi^2 \hat{V}.$$

This is a simple ODE and is solved by

$$\hat{V}(\xi, z) = \hat{V}_0(\xi) e^{-i\xi^2 z}.$$

It then remains to return $\hat{V}_0 e^{-i\xi^2 z}$ from Fourier space to the original variables. This is a

simple calculation:

$$
\begin{aligned}
V(t,z) &= \tfrac{1}{\sqrt{2\pi}} \int_{-\infty}^{+\infty} \hat{V}(\xi,z)\ e^{it\xi}\ d\xi \\
&= \tfrac{1}{\sqrt{2\pi}} \int_{-\infty}^{+\infty} \hat{V}_0(\xi)\ e^{-i\xi^2 z}\ e^{it\xi}\ d\xi \\
&= \tfrac{a_0 \sigma^{\frac{1}{4}}}{\pi^{\frac{3}{4}} 2^{\frac{1}{2}}} \int_{-\infty}^{+\infty}\ e^{-\frac{1}{2}\sigma\xi^2}\ e^{-i\xi^2 z}\ e^{it\xi}\ d\xi \\
&= \tfrac{a_0\ \sigma^{\frac{1}{4}}}{\pi^{\frac{3}{4}} 2^{\frac{1}{2}}} \int_{-\infty}^{+\infty} e^{-\frac{1}{2}((\sigma+2iz)\xi^2 - 2it\xi)}\ d\xi \\
&= \tfrac{a_0\ \sigma^{\frac{1}{4}}}{\pi^{\frac{3}{4}} 2^{\frac{1}{2}}}\ e^{-\frac{1}{2}\frac{t^2}{\sigma+2iz}} \int_{-\infty}^{+\infty} e^{-\frac{1}{2}\left(\sqrt{\sigma+2iz}\,\xi - \frac{it}{2\sqrt{\sigma+2iz}}\right)^2} d\xi \\
&= \tfrac{a_0\ \sigma^{\frac{1}{4}}}{\pi^{\frac{3}{4}} 2^{\frac{1}{2}}}\ e^{-\frac{1}{2}\frac{t^2}{\sigma+2iz}}\ \tfrac{1}{\sqrt{\sigma+2iz}}\ \sqrt{2\pi} \\
&= \tfrac{a_0\ \sigma^{\frac{1}{4}}}{\pi^{\frac{1}{4}}\ (\sigma+2iz)^{\frac{1}{2}}}\ e^{-\frac{1}{2}\frac{t^2}{\sigma+2iz}}.
\end{aligned}
$$

Now that we have the solution $T(z)V$, the evaluation of $\langle H\rangle(V)$ is merely an exercise in integration. Because

$$
\begin{aligned}
|V_t|^2 &= \left| \frac{d}{dt}\ a_0\ \pi^{-\frac{1}{4}}\ \sigma^{-\frac{1}{4}}\ e^{-\frac{t^2}{2\sigma}} \right|^2 \\
&= \left| a_0\ \pi^{-\frac{1}{4}}\ \sigma^{-\frac{1}{4}}\ \frac{-2t}{2\sigma}\ e^{-\frac{t^2}{2\sigma}} \right|^2 \\
&= \left| -a_0\ \pi^{-\frac{1}{4}}\ t\ \sigma^{-\frac{5}{4}}\ e^{-\frac{t^2}{2\sigma}} \right|^2 \\
&= a_0^2\ \pi^{-\frac{1}{2}}\ t^2\ \sigma^{-\frac{5}{2}}\ e^{-\frac{t^2}{\sigma}},
\end{aligned}
$$

the first term of $\langle H \rangle(V)$ is simply:

$$
\begin{aligned}
\alpha \int_{-\infty}^{+\infty} |V_t|^2 \, dt \\
&= \alpha \; a_0^2 \; \pi^{-\frac{1}{2}} \; \sigma^{-5/2} \int_{-\infty}^{+\infty} t^2 \; e^{\frac{-t^2}{\sigma}} \; dt \\
&= \alpha \; a_0^2 \; \pi^{-\frac{1}{2}} \; \sigma^{-5/2} \int_{-\infty}^{+\infty} \frac{\sigma}{2} \; s^2 \; e^{-\frac{s^2}{2}} \; \frac{\sqrt{\sigma}}{\sqrt{2}} \; ds \\
&= \alpha \; a_0^2 \; \pi^{-\frac{1}{2}} \; \sigma^{-1} \; 2^{-3/2} \; \left(- \int_{-\infty}^{+\infty} s \; \left(-s \; e^{-\frac{s^2}{2}} \right) \; ds \right) \\
&= \alpha \; a_0^2 \; \pi^{-\frac{1}{2}} \; \sigma^{-1} \; 2^{-3/2} \int_{-\infty}^{+\infty} e^{-\frac{s^2}{2}} \; ds \\
&= \alpha \; a_0^2 \; \pi^{-\frac{1}{2}} \; \sigma^{-1} \; 2^{-3/2} \; (2\pi)^{1/2} \\
&= \frac{1}{2} \; \alpha \; a_0^2 \; \sigma^{-1}.
\end{aligned}
$$

The second term is calculated in a similar manner:

$$
\begin{aligned}
&\int_{-\infty}^{\infty}\int_{0}^{1/2} |T(z)V|^4 \; dz \; dt \\
&\quad = \int_{-\infty}^{\infty}\int_{0}^{1/2} \frac{a_0^4 \; \sigma}{\pi} \; \frac{1}{\sigma + 2iz} \; \frac{1}{\sigma - 2iz} \; e^{-\frac{t^2}{\sigma+2iz}} \; e^{-\frac{t^2}{\sigma-2iz}} \; dz \; dt \\
&\quad = \frac{a_0^4 \; \sigma}{\pi} \int_{-\infty}^{\infty}\int_{0}^{1/2} \frac{1}{\sigma^2 + 4z^2} \; e^{-\frac{t^2 \; (\sigma+2iz) + t^2 \; (\sigma-2iz)}{\sigma^2+4z^2}} \; dz \; dt \\
&\quad = \frac{a_0^4 \; \sigma}{\pi} \int_{-\infty}^{\infty}\int_{0}^{1/2} \frac{1}{\sigma^2 + 4z^2} \; e^{-\frac{2\sigma t^2}{\sigma^2+4z^2}} \; dz \; dt \\
&\quad = \frac{a_0^4 \; \sigma}{\pi} \int_{0}^{1/2} \frac{1}{\sigma^2 + 4z^2} \; \int_{-\infty}^{\infty} e^{-\frac{2\sigma t^2}{\sigma^2+4z^2}} \; dt \; dz \\
&\quad = \frac{a_0^4 \; \sigma}{\pi} \int_{0}^{1/2} \frac{1}{\sigma^2 + 4z^2} \; \left(\frac{\sqrt{\sigma^2 + 4z^2}}{2\sqrt{\sigma}} \sqrt{2\pi} \right) \; dz \\
&\quad = \frac{a_0^4 \; \sigma^{1/2}}{2^{1/2} \; \pi^{1/2}} \int_{0}^{1/2} \frac{1}{\sqrt{\sigma^2 + 4z^2}} \; dz \\
&\quad = \frac{a_0^4 \; \sigma^{1/2}}{2^{3/2} \; \pi^{1/2}} \int_{0}^{1} \frac{1}{\sqrt{\sigma^2 + s^2}} \; ds \\
&\quad = \frac{a_0^4 \; \sigma^{1/2}}{2^{3/2} \; \pi^{1/2}} \; \sinh^{-1}\left(\frac{1}{\sigma}\right).
\end{aligned}
$$

Combining these two terms, we arrive at the promised expression

$$
\langle H \rangle (V) = \frac{1}{2} \; \alpha \; a_0^2 \; \frac{1}{\sigma} - \frac{1}{2^{3/2}} \; \frac{a_0^4}{\pi^{1/2}} \; \sigma^{1/2} \; \sinh^{-1}\left(\frac{1}{\sigma}\right).
$$

□

The coefficient a_0 in the formula above is fixed by the energy constraint; in particular, $E = a_0^2$. So, for any particular value of the dispersion parameter α, $\langle H \rangle$ can be considered as function of the single variable σ, where σ controls the width of the pulse.

In Figure 5.2, we show the reduced Hamiltonian for different values of residual dispersion α. For all values of α, $\langle H \rangle$ approaches zero from below as $\sigma \to \infty$. As $\sigma \to 0$, however, the first term, which is inversely proportional to σ, dominates. When $\alpha > 0$, $\langle H \rangle \to +\infty$ as $\sigma \to 0$. Conversely, when $\alpha < 0$, $\langle H \rangle \to -\infty$ as $\sigma \to 0$. And when $\alpha = 0$, $\langle H \rangle \to 0$.

One can see that for positive and zero values of α, the Hamiltonian function has a unique global minimum. When α is only slightly negative, the function possesses a local minimum and a local maximum – these extrema disappear in a saddle-node bifurcation as α is decreased further.

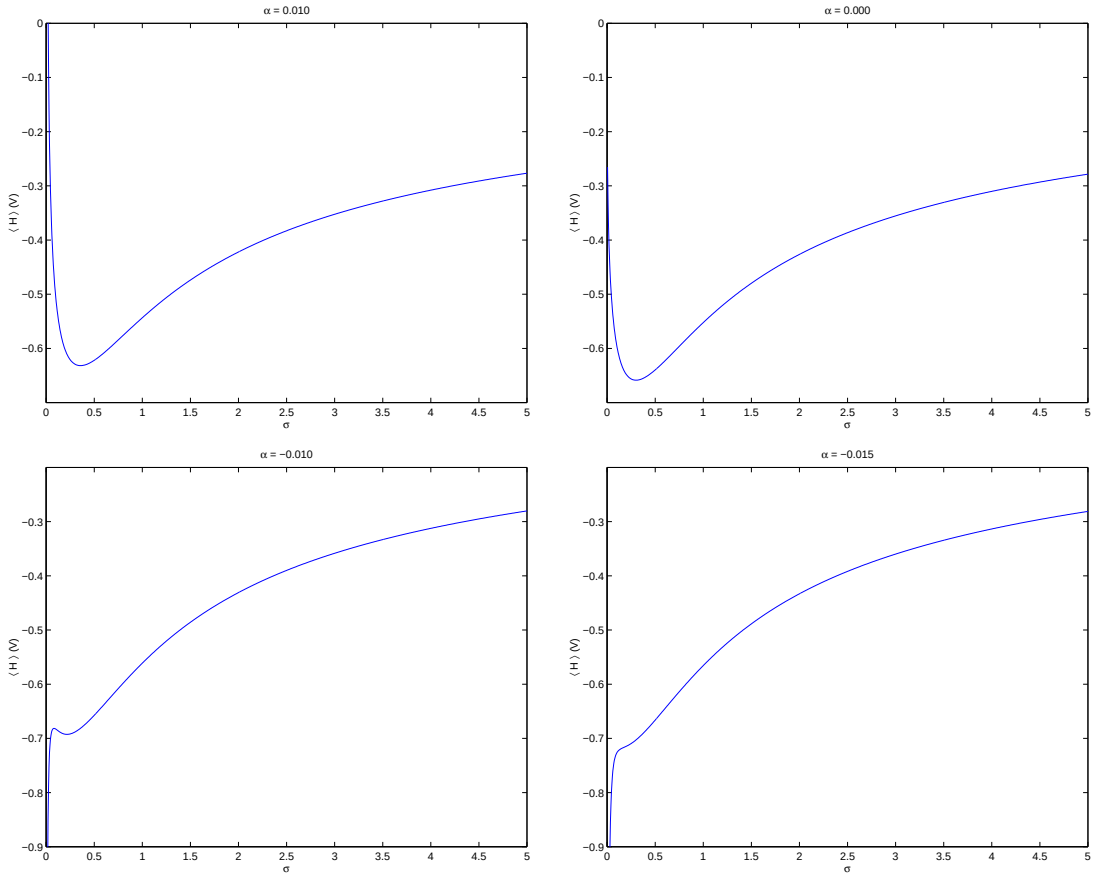

Figure 5.2: The reduced Hamiltonian for the Gaussian pulse.

Hermite–Gaussian case, $N = 1$.

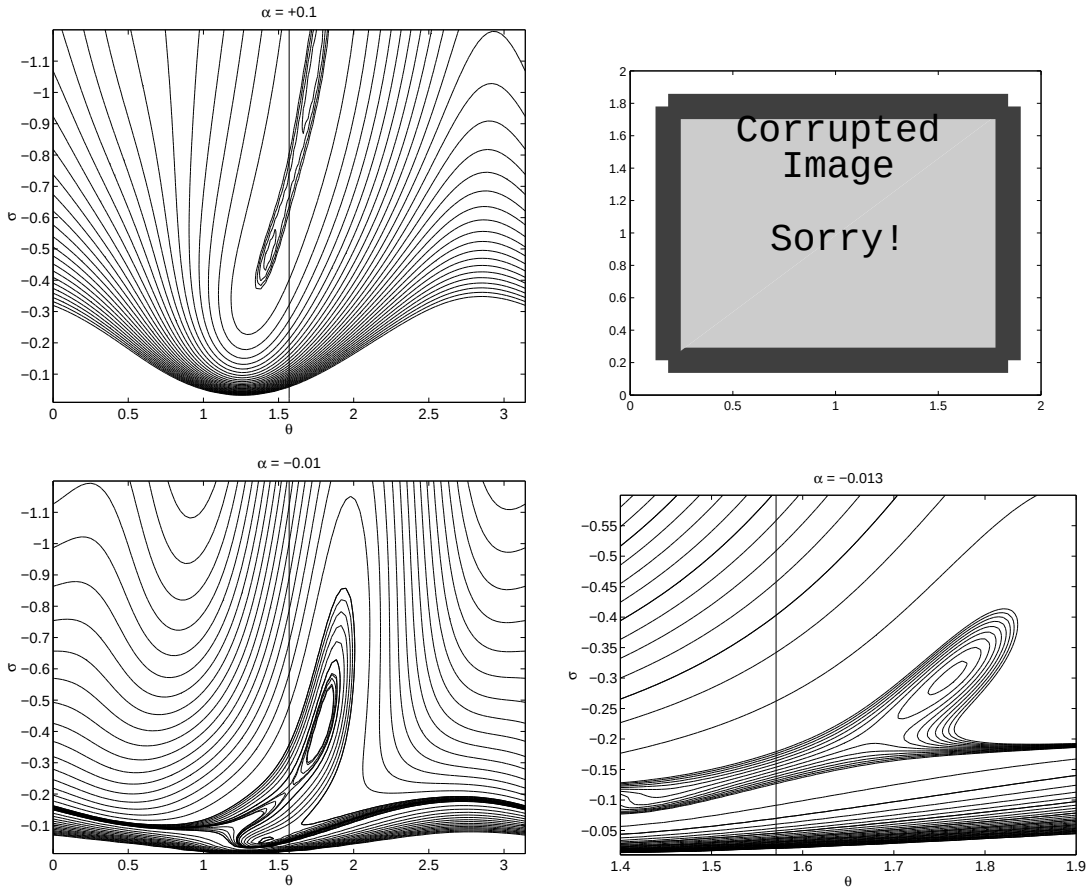

Figure 5.3: Reduced Hamiltonian for the two mode pulse. $a_0 = \sin(\theta)$ and $a_2 = \cos(\theta)$. For $\alpha \geq 0$, there are two minima corresponding to refinements of the DM soliton with zero and one oscillation. As α is decreased, the non–oscillating pulse is destroyed first. The singly–oscillating pulse persists slightly into the regime where the Gaussian ansatz has no minimum before being destroyed.

In this section, we look for minima of the Hamiltonian $\langle H \rangle$ where two Hermite–Gaussian modes are considered. This analysis reduces to a search for critical points on a cylinder $S^1 \times R^+$, since the width σ must be positive and the coefficients a_0 and a_2 satisfy $a_0^2 + a_2^2 = E$. In particular, critical points can still be seen visually on a two–dimensional plot. This cylinder is shown in Figure 5.3, where the cylinder is cut open along the curve

$a_0 = 0$. The curve $a_2 = 0$ corresponds to the Gaussian approximation of the previous section. We view the level curves of the Hamiltonian $\langle H \rangle$ for various values of α: $\alpha = +0.1$, $\alpha = 0.0$, $\alpha = -0.01$ and $\alpha = -0.013$. As one can see, for $\alpha \geq 0$, the minimum from the Gaussian approximation has opened up as a saddle in the higher dimensional space and there are now two local minima on either side of the curve $a_2 = 0$. These two nearby local minima provide various approximations to the ground state — they differ in the number of oscillations in their tails. These different approximations to what we believe to be the unique DM soliton seem to be an artifact of the imposed finite–dimensionality, much like the Peierls–Nabarro barrier in discretized systems. It is important to be aware of this multiplicity of minima as we look into the structure of the DM soliton.

For $\alpha < 0$, there is no longer a global minimum because $\langle H \rangle \to -\infty$ as $\sigma \to 0$. However, for α close enough to zero the bow tie structure persists and we still find two approximations to the DM soliton. As α becomes more negative, the loop of the bow tie in the two mode approximation with σ closer to zero is "untied" and its corresponding local minimum disappears. At this point the non–oscillating approximation to the ground state no longer exists, however the saddle and the oscillating minimum are still present. As α is decreased further, this remaining minimum and the saddle are simultaneously washed out in a saddle node bifurcation. However, it is interesting to note that this minimum persists slightly into the regime where the original Gaussian guess fails to produce any local minima at all. This can be seen in Figure 5.3; when $\alpha = -0.013$, the Hamiltonian decreases monotonically to $-\infty$ along the line $\theta = \pi/2$ as $\sigma \to 0$, while the saddle and the oscillating minimum can still be seen in the region $\theta > \pi/2$. This suggests that the oscillating approximations better reflect the structure of the DM soliton than the non–

oscillating ones.

Hermite–Gaussian case, $N \geq 2$.

As we increase the number of Hermite–Gaussian modes in our expansion, we find better and better approximations to the dispersion managed pulse. We summarize the results up to $N = 20$ in Figure 5.4 and choose the approximation in which a_{2k} and a_{2k+2} are of opposite sign for all $0 \leq k \leq 20$. When the residual dispersion is positive, the Hamiltonian quickly approaches a minimizing value as the number of modes increases. In particular, the first three modes are enough to get a reasonable approximation to the minimizing value. This provides confirmation that our minimization process is actually converging to a ground state. Further evidence is provided in the next plot where the weight of the modes for the $N = 20$ pulse is shown. Most of the weight is in the low order modes, and the weights can be seen to steadily decay on a logarithmic scale.

Similar results are obtained for the mean–zero case and even in the case where the residual dispersion is negative and small. As α decreases, the pulse narrows and tail oscillations become more pronounced, as found in earlier works, see Ablowitz and Biondini [41] for example.

Recall that when residual dispersion is negative, the constrained variational principle has no minima [42]. A global minimum is not expected, of course, since the Hamiltonian functional is unbounded from below. What is more, there are no local minima. A heuristic explanation is that the negative gradient term becomes dominant for high frequency harmonics even if their amplitudes are small. It is then possible to construct a sequence of pulses converging to a hypothetical minimizer, having the same energy, but with lower

Hamiltonian values. This shows that there can be no minima in the negative case, however it does not prove the instability of a hypothetical critical point.

However, using our numerical algorithm we have found local minima in each reduced finite–dimensional function space even for the case of small negative dispersion. An explanation for this may be that our control over the parameter σ allows us to "smooth out" the higher frequencies by increasing σ simultaneously with the increase in the number of modes. Even as the number of modes is increased, this affords the opportunity of finding local minima in the finite dimensional approximations that may approximate saddle points of the full system.

It is possible, however, to choose reduced spaces strategically which have no local minima. For instance, in Figure 5.5, we show a higher dimensional analogue of the reduced Hamiltonian using only the coefficients a_0, corresponding to the Gaussian mode and a_{20}, a rapidly oscillating mode. The local minimum which was present in the one dimensional approximation when only the Gaussian mode was present (recall Figure 5.2) has become a saddle in this higher dimensional system. The maximum in Figure 5.5 corresponds to the maximum in Gaussian case (Figure 5.2) and it is known to be unstable [32]. No local minima exist in this subspace. Similarly, we expect that any minimum of a higher dimensional reduced Hamiltonian in the case of negative residual dispersion can be made into a saddle by adding a sufficiently oscillatory mode.

One way to answer the question of which of the family of minima is the most pertinent is to actually compare how far these various approximations are from being actual solutions

of the nonlinear eigenvalue problem. To this end we write

$$\mathrm{Res}(v) = -\omega v \ + \ \alpha v_{tt} \ + \ \int_{-1/2}^{1/2} T^{-1}(\xi) \left[T(\xi)v \ T(\xi)v \ \overline{T(\xi)v} \right] d\xi.$$

If v were actually a critical point of the average variational principle, then $\mathrm{Res}(v)$ would be identically zero. So we can calculate the mismatch

$$Res = \int_{-\infty}^{\infty} |\mathrm{Res}(v)|^2 \ dt$$

as a measure of the error in our approximate solutions. A table of these errors follows, see Figure 5.2.

Reading across the rows, we observe that the error for improving approximations with a fixed number of oscillations appears small but seems to saturate rather than approaching 0. Moving down the table, it appears that increasing the number of oscillations reduces this saturating value — the approximations with an increasing number of oscillations as we increase N provide the most accurate solutions.

Another method for determining which pulse profiles are the most relevant can be given by numerically evolving these approximate pulse shapes using a Fourier split–step scheme. All of these approximations evolve without significant disruption for at least one hundred periods of the dispersion map.

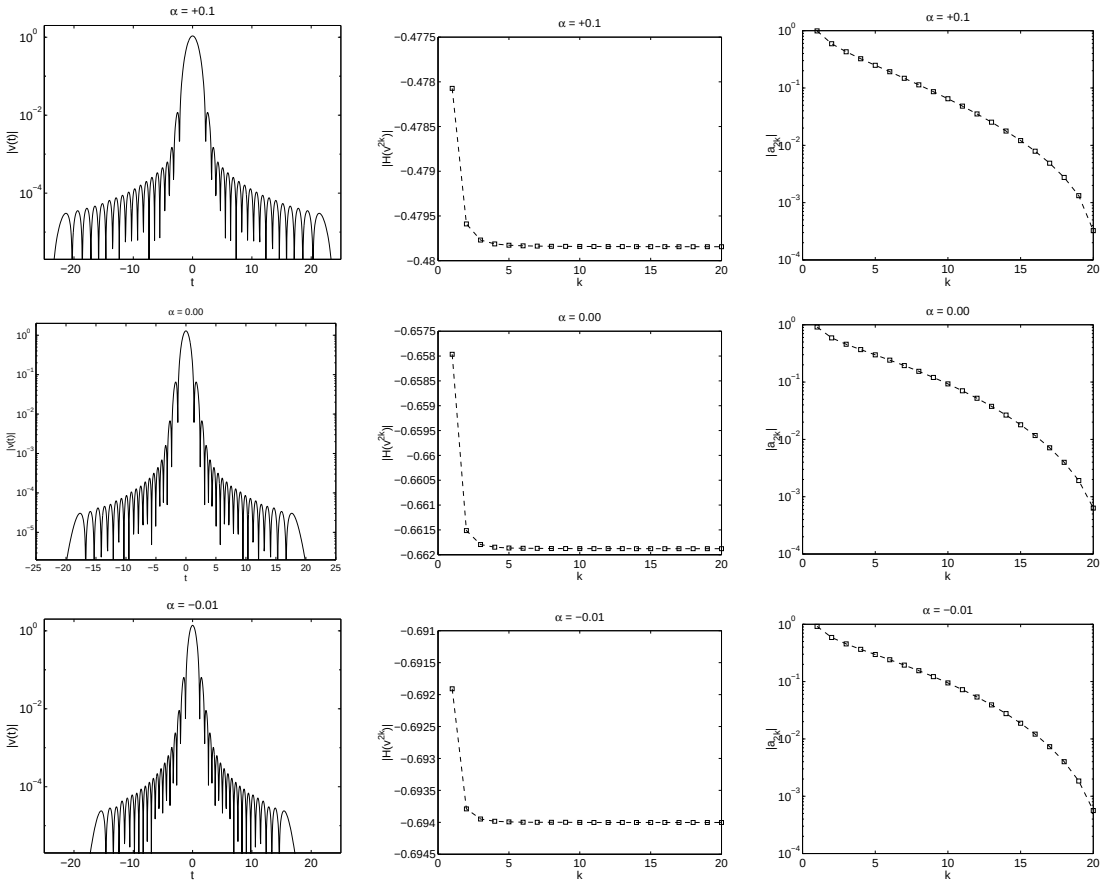

Figure 5.4: The results of the minimization procedure with a Hermite-Gaussian approximation. For $\alpha = +0.1$, 0.0 and -0.01 the following are plotted from left to right: (a) the minimizing pulse for $k = 20$; (b) the Hamiltonian value of the minimizing pulse as k is increased; and (c) the decay of the coefficients in the Galerkin expansion for the 20–mode pulse.

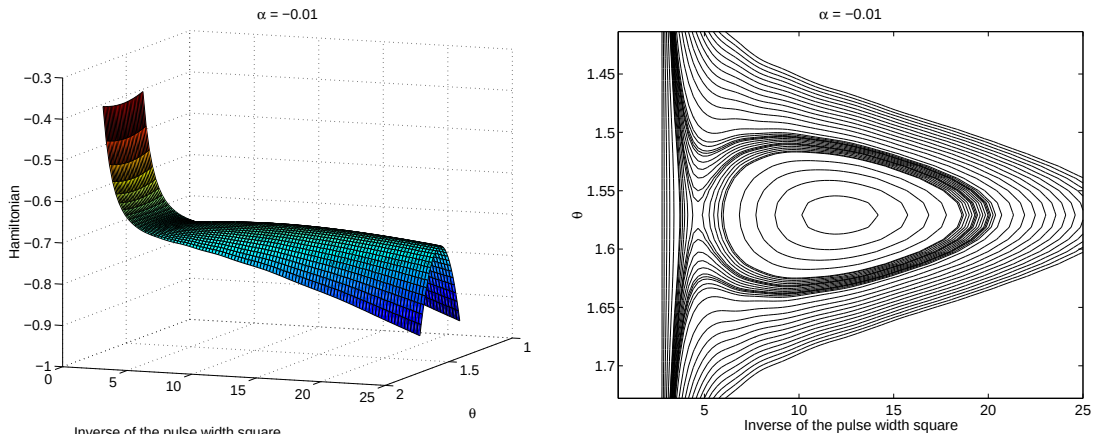

Figure 5.5: Reduced Hamiltonian for modes H_0 and H_{20}. $a_0 = \sin(\theta)$ and $a_{20} = \cos(\theta)$. The maximum from the Gaussian approximation ($\theta = \pi/2$) persists, but the minimum from that approximation has now become a saddle and no other minima are present.

	1-mode	2-mode	3-mode	4-mode	5-mode
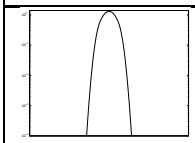	$1.446 * 10^{-3}$	$9.076 * 10^{-4}$	$8.080 * 10^{-4}$	$7.406 * 10^{-4}$	$7.405 * 10^{-4}$
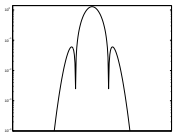	—	$1.499 * 10^{-4}$	$4.637 * 10^{-5}$	$2.391 * 10^{-5}$	$2.396 * 10^{-5}$
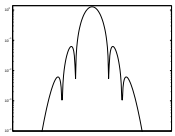	—	—	$3.483 * 10^{-5}$	$6.835 * 10^{-6}$	$5.996 * 10^{-6}$
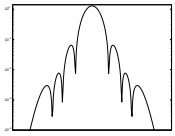	—	—	—	$1.376 * 10^{-5}$	$7.075 * 10^{-6}$
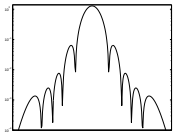	—	—	—	—	$6.281 * 10^{-6}$

Figure 5.6: Errors for the various approximations to the DM soliton with $\alpha = +0.1$. Increasing the number of Galerkin modes (reading across) or considering minima with more oscillations (reading down) decreases the error of the approximate solutions.

5.3 The bisoliton

In this section, we continue to explore the global structure of the reduced Hamiltonian. Making use of the finite dimensional approximation (5.3), we search this reduced space for local minima (and other critical points) of the constrained variational principle – these minima may correspond to stable pulse solutions in the averaged DM system. Not only does finding such minima give us important insight into the structure of the DM soliton and its region of existence, as in the previous section, but it is also possible (and in fact required via topological considerations) that other critical points exist in this finite dimensional space, and these may correspond to different pulse solutions. In fact, when the number of modes $N \geq 5$, we observe a bisoliton, found earlier by [35] using different techniques.

On the cylinder representing the phase space for the two mode approximation, as in the previous section, there are several prominent features (see Figure 5.7). First of all, a pair of local minima separated by a saddle can be seen in the lima bean shaped region along the line $\theta = \pi/2$, where the pulse is approximately Gaussian; these are a family of approximations of the DM soliton. Additionally, however, there is another critical point of $\langle H \rangle$ far from this near–Gaussian pulse. Near the line $\theta = 0$ in Figure 5.7 (corresponding to a solution in which the Gaussian mode is not present) is a saddle. As the number of modes is increased, this saddle spawns a separatrix, organizing the phase space, and provides the foundation for another local minimum which corresponds to a two-humped pulse. The Hamiltonian value of this pulse is not nearly as low as that of the single pulse at the same energy value but, as could be expected, is approximately twice that of the

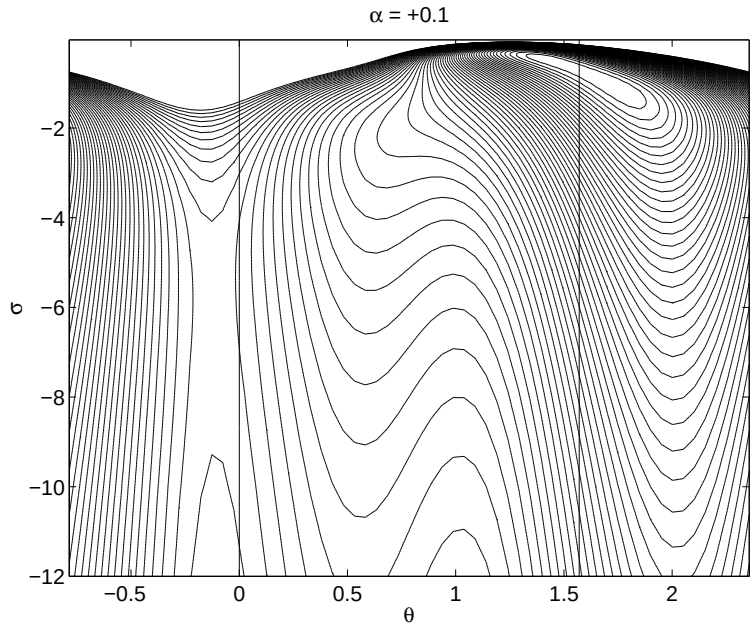

Figure 5.7: The phase space in the two mode approximation. $a_0 = \sin(\theta)$ and $a_2 = \cos(\theta)$. The phase space a near–Gaussian global minimum as well as a saddle which organizes the structure in higher dimensions.

single pulse of half the energy. Following Maruta et.al. [35], we call this pulse a bisoliton and show this pulse in Figure 5.8. Using a Fourier split–step scheme, this bisoliton is seen to evolve stably in the averaged equation (5.2).

Approximation of the bisoliton in other bases.

We now address a practically important question: whether or not this bisoliton can be well approximated by two separated Gaussians.

A first attempt.

One way to answer this question is to look for local minima in the expansion

$$V(t) = A\left(e^{-t^2/2\sigma} \; + \; e^{-(t-t_0)^2/2\sigma}\right),$$

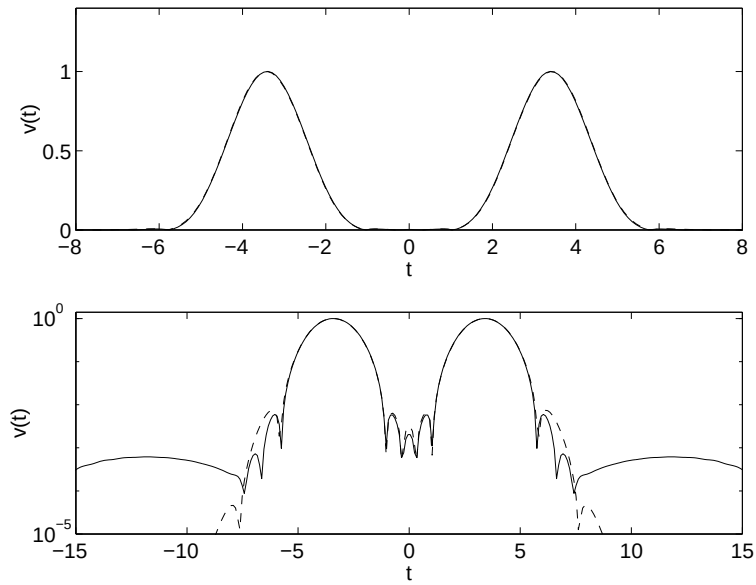

Figure 5.8: The bisoliton. $\alpha = +0.1$ and $E = \pi$. The dashed line shows the ten term approximation to the bisoliton, while the solid line traces its evolution after seventy–five periods. This is shown on both a linear and a logarithmic scale.

where σ and t_0 are variable and $A(\sigma, t_0)$ is chosen to fix the energy of the double pulse at a specified level. Interestingly enough, for some energy levels there is a minimum corresponding to a double pulse in this approximation. In the phase space, there is a symmetric bow tie around $t_0 = 0$, once again providing a small correction to the Gaussian approximation of the DM soliton. Additionally, there is a small loop down at the value of σ corresponding to the ideal pulse width for a pulse of half the energy. This loop and the minimum it contains give a suggestion of a preferred stable pulse spacing in the system. However, perhaps because the Gaussian approximation gives such a poor approximation of the tails where the pulses interact, this minimum corresponds to a pulse spacing less than that of the bisoliton found in the Galerkin approximation and does not evolve stably. This is shown in Figure 5.9.

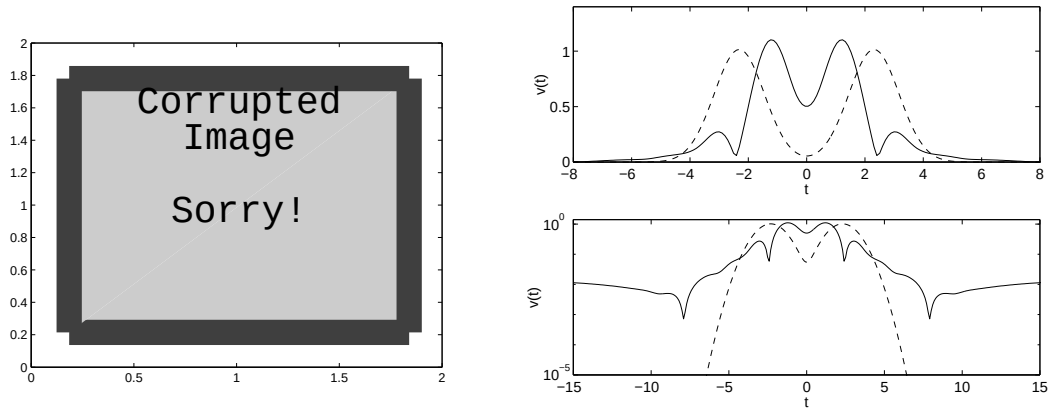

Figure 5.9: Two separated Gaussians — take 1. On the left are the level curves for two separated Gaussians. There is a global minimum which is a correction to the Gaussian pulse and a local minimum which looks like two separated Gaussians, each with half the energy of the original pulse. On the right is the evolution of this local minimizer on its way to being destroyed after seventy–five periods.

A second attempt.

Another more practical answer to this question of approximating this bisoliton is to simply fit two Gaussians to the bisoliton as well as possible. To this end, we choose σ and t_0 to minimize the value

$$\int |V_{\text{galerkin}}(t) - V_{\text{gaussian}}(t)|^2 dt,$$

where V_{galerkin} is the approximation to the bisoliton found in the Hermite–Gaussian basis and V_{gaussian} is an approximation using two separated Gaussian pulses. This best value of (σ, t_0) is marked with an 'o' in phase space, with a note that its Hamiltonian value is greater than the nearby local minimum. The initial condition $V_{\text{gaussian}}(t)$ corresponding to the best–fitting parameter values evolves stably under the averaged PDE (5.2), see Figure 5.10.

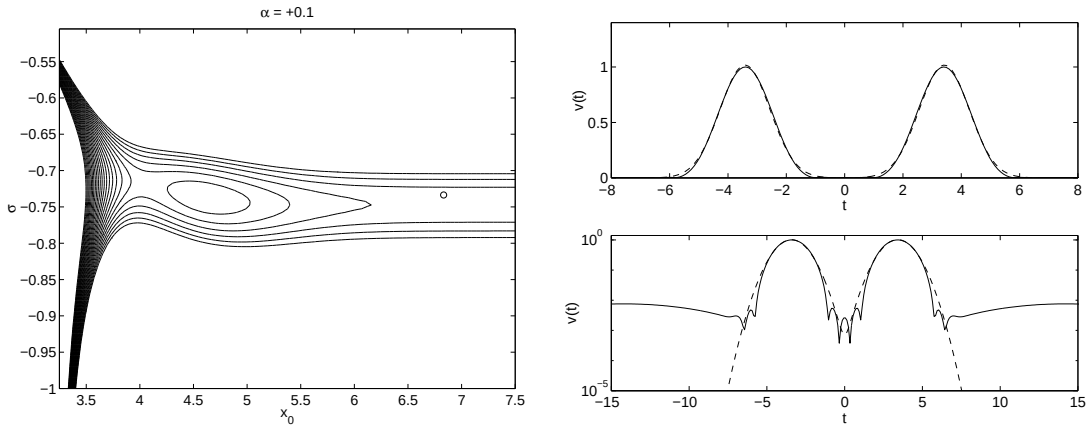

Figure 5.10: Two separated Gaussians — take 2. On the left is a closer view of the loop and local minimum for two separated Gaussians and their relationship with the best approximation of the bisoliton, marked with an 'o'. On the right is this Gaussian approximation and its evolution after seventy–five periods.

Changing the spacing between Gaussians.

A follow up question to approximating the bisoliton using a pair of Gaussians is this: what happens if we increase or decrease the pulse spacing? As we have seen, if too small a spacing is specified, the two pulses will collapse into one another. This is shown again in Figure 5.11, where the pulse separation is one unit less than that of the best approximation to the bisoliton.

Increasing the pulse spacing one unit from ideal, we see little effect. After one hundred periods of the dispersion map, the centers of the two humps have not moved in either direction. The spacing present in the bisoliton then seems to yield a threshold, beyond which the interpulse interactions are less important.

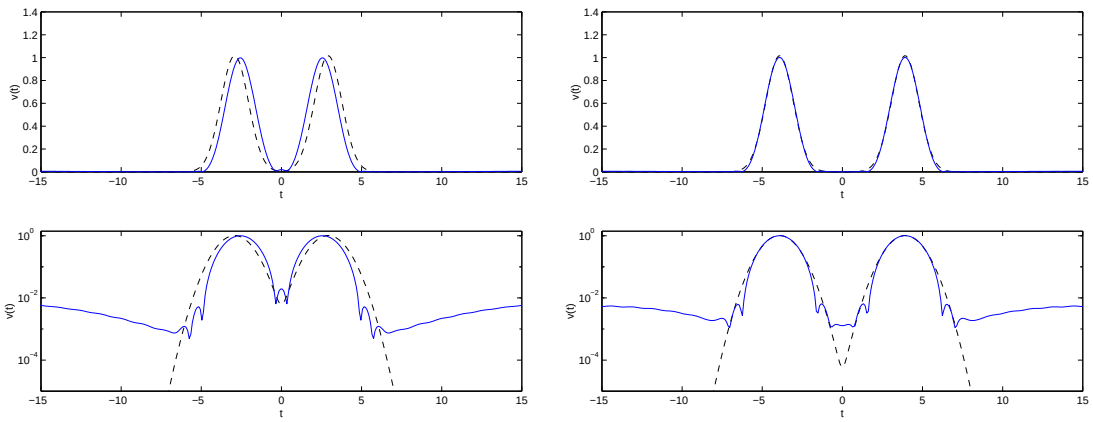

Figure 5.11: Changing the separation distance. If the initial spacing between Gaussian pulses is less than that of the bisoliton, the pulses attract each other. On the left is an initial condition one unit closer than the spacing of the bisoliton ('dashed') and the evolution after 100 periods of the dispersion map ('solid'). Pulses in which the separation is larger seem to have little or no interaction. This is shown in the figure on the right, in which an initial condition with spacing one unit greater than that of the bisoliton evolves for 100 periods.

Bibliography

[1] V. E. Zakharov and A. B. Shabat, *Exact theory of two dimensional self–focusing and one dimensional self–modulation of waves in nonlinear media,* Sov. Phys. JETP **34** (1972), 62–69.

[2] M. J. Ablowitz and H. Segur, *Solitons and the inverse scattering transform,* SIAM, Philadelphia, Pa., 1981.

[3] A. Hasegawa and Y. Kodama, *Solitons in optical communications,* Oxford University Press, New York, 1995.

[4] M. Haelterman and A. Sheppard, *Bifurcation phenomena and multiple soliton–bound states in isotropic Kerr media,* Phys. Rev. E **49** (1994), 3376–3381.

[5] E. A. Ostrovskaya and Y. S. Kivshar, *Multihump optical solitons in a saturable medium,* J. Opt. B **1** (1999), 77–83.

[6] A. C. Yew, B. Sandstede and C. K. R. T. Jones, *Instability of multiple pulses in coupled nonlinear Schrödinger equations,* Phys. Rev. E **61** (2000), 5886–5892.

[7] E. A. Ostrovskaya, Y. S. Kivshar, D. V. Scryabin and W. J. Firth, *Stability of multihump optical solitons,* Phys. Rev. Lett. **83** (1999), 296–299.

[8] M. I. Weinstein, *Lyapunov stability of ground states of nonlinear dispersive evolution equations,* Comm. Pure Appl. Math. **39** (1986), 51–67.

[9] C. K. R. T. Jones, *Instability of standing waves for non–linear Schrödinger–type equations,* Ergodic Theory Dynam. Systems **8** (1988), 119–138.

[10] M. Grillakis, *Analysis of the linearization around a critical point of an infinite-dimensional Hamiltonian system,* Comm. Pure Appl. Math. **43** (1990), 299–333.

[11] B. Sandstede, *Center manifolds for homoclinic solutions,* J. Dynam. Differential Equations **12** (2000), 449–510.

[12] S.–N. Chow, W. Liu and Y. Yi, *Center manifolds for smooth invariant manifolds,* Trans. Amer. Math. Soc. **352** (2000), 5179–5211.

[13] J. Knobloch, *Bifurcation of degenerate homoclinic orbits in reversible and conservative systems,* J. Dynam. Differential Equations **9** (1997), 427–444.

[14] S. Nii, *N–homoclinic bifurcations for homoclinic orbits changing their twisting,* J. Dynam. Differential Equations **8** (1996), 549–572.

[15] A. J. Homburg, H. Kokubu and M. Krupa, *The cusp horseshoe and its bifurcations in the unfolding of an inclination–flip homoclinic orbit,* Ergodic Theory Dynam. Systems **14** (1994), 667–693.

[16] A. J. Homburg and B. Krauskopf, *Resonant homoclinic flip bifurcations,* J. Dynam. Differential Equations **12** (2000), 807–850.

[17] B. Sandstede, *Verzweigungstheorie homokliner Verdopplungen,* PhD thesis, University of Stuttgart, (1993).

[18] A. C. Yew, *An analytical study of solitary–waves in quadratic media*, PhD thesis, Brown University, (1998).

[19] B. Sandstede, C. K. R. T. Jones and J. C. Alexander, *Existence and stability of N–pulses on optical fibers with phase–sensitive amplifiers,* Phys. D **106** (1997), 167–206.

[20] S. A. van Gils, M. Krupa and V. Tchistiakov, *Homoclinic twist bifurcation in a system of two coupled oscillators,* J. Dynam. Differential Equations **12** (2000), 733–806.

[21] J. Moser, *On the generalization of a theorem of A. Liapounoff,* Comm. Pure Appl. Math. **11** (1958), 257–271.

[22] R. L. Devaney, *Homoclinic orbits in Hamiltonian systems,* J. Differential Equations **21** (1976), 431–438.

[23] W. H. Aschbacher, J. Frölich, G. M. Graf, K. Schnee and M. Troyer, *Symmetry breaking regime in the nonlinear Hartree Equation,* preprint (2001).

[24] J. Alexander, R. Gardner and C. Jones, *A topological invariant arising in the stability analysis of travelling waves.* J. Reine Angew. Math. **410** (1990), 167–212.

[25] L. Q. Brin, *Numerical testing of the stability of viscous shock waves*, PhD thesis, Indiana University, (1998).

[26] L. Q. Brin and K. Zumbrun, *Analytically varying eigenvectors and the stability of viscous shock waves,* preprint (2002).

[27] D. Henry, *Geometric theory of semilinear parabolic equations*, Lecture Notes in Math., 840, Springer, Berlin, 1981.

[28] T. Kapitula and B. Sandstede, *Stability of bright solitary–wave solutions to perturbed nonlinear Schrödinger equations,* Physica D **124** (1998), 58–103.

[29] J. Deng, *Instability of waves and patterns in Hamiltonian systems and the Maslov index*, PhD thesis, Brown University, (2002).

[30] V. I. Arnol'd, *On a characteristic class entering into conditions of quantization. (Russian),* Funkcional. Anal. i Priložen. **1** (1967), 1–14.

[31] A. Bose and C. K. R. T. Jones, *Stability of the in-phase travelling wave solution in a pair of coupled nerve fibers,* Indiana Univ. Math. J. **44** (1995), 189–220.

[32] D. Pelinovsky, *Instabilities of dispersion–managed solitons in the normal dispersion regime,* Phys. Rev. E **62** (2000), 4283–4293.

[33] V. Zharnitsky, E. Grenier, C. K. R. T. Jones and S. K. Turitsyn, *Stabilizing effects of dispersion management,* Physica D **152-153** (2001), 794–817.

[34] R. L. Pego and M. I. Weinstein, *Convective linear stability of solitary waves for Boussinesq equations,* Stud. in Appl. Math. **99** (1997), 311–375.

[35] A. Maruta, Y. Nonaka and T. Inoue, *Symmetric bi–soliton solution in a dispersion managed system,* post–deadline poster PD4, Nonlinear Guided Waves and their applications, OSA Technical Digest.

[36] T. I. Lakoba and D. J. Kaup, *Hermite–Gaussian expansion for pulse propagation in strongly dispersion managed fibers,* Phys. Rev. E **58** (1998), 6728–6741.

[37] I. Gabitov, E. G. Shapiro and S. K. Turitsyn, *Asymptotic breathing pulse in optical transmission systems with dispersion compensation,* Phys. Rev. E **55** (1997), 3624–3633.

[38] M. Kunze, *A variational problem with lack of compactness related to the nonlinear Schrödinger equation,* preprint (2001).

[39] S. K. Turitsyn and V. K. Mezentsev, *Dynamics of self–similar dispersion–managed soliton presented in the basis of chirped Gauss–Hermite functions,* JETP Letters **67** (1998), 640–646.

[40] S. K. Turitsyn, J. H. B. Nijhof, V. K. Mezentsev and N. J. Doran, *Symmetries, chirp–free points, and bistability in dispersion managed fiber lines,* Optics Letters **24** (1999), 1871–1873.

[41] M. J. Ablowitz and G. Biondini, *Multiscale pulse dynamics in communication systems with strong dispersion management,* Opt. Lett. **23** (1998), 1668–1670.

[42] V. Zharnitsky, E. Grenier, S. K. Turitsyn, C. K. R. T. Jones and Jan S. Hesthaven, *Ground states of dispersion–managed nonlinear Schrödinger equation*, Phys. Rev. E **62** (2000), 7358–7364.